Design and Characterization of a

Silk Fibroin Sutureless Dural Repair System

A thesis

submitted by

Kelly E. Flanagan

In partial fulfillment of the requirements

for the degree of

Master of Science

in

Biomedical Engineering

TUFTS UNIVERSITY

May 2013

Advisor: David L. Kaplan, PhD

Abstract

The dura mater, a fibrous membrane surrounding the brain and spinal column, acts as the final barrier to cerebrospinal fluid (CSF) leakage. This membrane can be resected in neurosurgery or damaged by trauma. With the resulting dural defects comes the need for watertight dural closures to prevent CSF leakage and further complications. Current dural closure techniques include suturing, tissue sealants, and dural replacement materials. These materials, however, have numerous limitations and carry large risks of postoperative complications to the patients. A novel silk fibroin sutureless dural repair system was explored in this work. This system consists of a silk adhesive and a dual layer silk composite material that has been specifically designed to both promote dural regeneration while also functioning as an impermeable barrier to CSF leakage. A series of experiments were performed to determine its morphology, mechanical characteristics, biocompatibility, biodegradability, and adhesive sealing ability. The results of experiments in this work show the potential for this system to significantly improve on currently used dural closure techniques.

Acknowledgements

Firstly, I would like to thank my advisor, Dr. David Kaplan, for the continuous guidance, support, motivation, and sincerity through my undergraduate and graduate careers. His guidance has helped me through countless steps of my Tufts career and has been an integral factor in my pursuit of biomedical engineering research.

I would also like to thank Dr. Julian Wu for the opportunity to explore the clinical side of biomedical engineering, observe surgeries, and conduct clinical research. My exposure to his work, his feedback on my designs and experiments in the lab, and his explanations of how they would contribute to neurosurgery procedures were extremely interesting and greatly motivated my work.

Additionally, I would like to thank Dr. Fiorenzo Omenetto for his guidance throughout my undergraduate and graduate careers. I would especially like to thank him for his enthusiasm and support during my undergraduate senior design project that lead to this graduate thesis work and for his contribution as a member of my thesis committee.

I wish to thank Lee Tien for his support, patience, and guidance during my senior design project. He taught me an invaluable amount in terms of the project content and about biomedical lab research in general over the last two years and always made it enjoyable. The project that I started with him led to me staying for my masters, which I am so grateful that I did.

I would also like to thank Roberto Elia for his invaluable support, guidance and enthusiasm over the last two years. He is a source of constant help and fun around the lab, is always ready and willing to give intelligent advice, and helped me immensely with my graduate work this year.

I wish to thank Amy Hopkins for her assistance with neural cell isolation and confocal imaging, Andrew Reeves for his assistance with dermal fibroblasts, Eun Seok Gil for his training and assistance on the SEM and Instron machines, Jodie Moreau for her guidance regarding *in vivo* testing, Kelly Burke for assistance with silk hydrogel testing, and Jon Kluge for his assistance with Instron testing and data analysis. Also thank you to all those at 200 Boston Ave who are always ready to help and make lab experience so enjoyable: Amanda Baryshyan, Alex Mitropoulos, Laura Domigan, Tony Dinis, Joe Brown, Christa Margossian, Rodrigo Jose, Gabe Perrone, and Rosie Friedman. And I'd like to thank the Silk Devices and Implants Mini-Group for all of their feedback and support.

Finally and most importantly, I would like to extend my sincere gratitude to my family and friends for all of their support, motivation, and unending and invaluable encouragement through this entire process.

Table of Contents

List of Tables

List of Figures

Chapter 1: Introduction

1.1 Significance

The dura mater, which is the outermost membrane surrounding the brain and spinal cord and the final barrier to cerebrospinal fluid (CSF) leakage, can be damaged through trauma or resected during neurosurgical procedures. With dural defects comes the need for a watertight dural closure in order to prevent CSF leakage, which is one of the most challenging and dangerous results of both traumatic and planned durotomies. Complications of CSF leakage include meningitis, pseudomenigoceles, impaired wound healing, and subgaleal fluid collection [Cosgrove et al., 2007]. The incidence of CSF leakages following cranial procedures can be as high as 10 to 27% when performed using infratentorial or supratentorial approaches [Cosgrove et al., 2007; Vanaclocha et al., 1997]. When studied using CT scanning instead of observation of medical symptoms, the incidence of CSF leakage was observed to be as high as 42% in one study [Dolenc et al., 1997]. The incidence of leakage is high due to the limitations of current wound closure techniques, which include implantation of dural replacements, and the use of tissue sealants in conjunction with sutures.

Currently used dural replacement materials include autografts, allografts, xenografts, and synthetic grafts. While each graft has its advantages, none satisfy all of the requirements of an ideal dural substitute, or have been proven to be complication free in large clinical studies [Moskowitz et al., 2009]. Similarly, while current tissue sealants are FDA-approved, their uses are minimal in neurosurgical applications due to limitations and complications. In fact,

commonly used tissue sealants carry the risk of viral transmission [Fattahi et al., 2004], nerve compression [Thavarajah et al., 2009], or inadequate sealing ability [Epstein, 2010].

Due to the prevalence of dural defects in trauma and neurosurgery procedures, the need for a superior dural repair system is required that can improve on current wound closure techniques. This system must provide a watertight seal from CSF leakage while also being biocompatible and limiting postoperative complications.

1.2 Research Aims

1.2.1 Clinical Review

The aim of the clinical research portion of this work is to determine the efficiency of current dural closure procedures used in spinal neurosurgery cases at a single institution, the Department of Neurosurgery at Tufts Medical Center. Specifically, dural closure techniques that included the use of DuraSeal, a leading synthetic tissue sealant for dural closure, were studied in order to understand the use of this sealant as an adjuvant to other implanted materials and sutures.

1.2.2 Silk Dural Replacement

The aim of this research is to develop a silk fibroin material with the mechanical properties, degradability, and biocompatibility to act as a successful dural replacement material. The first objective is to design a silk material that functions as an impermeable watertight barrier to CSF leakage while also promoting dural regeneration across its surface. The second objective is to

characterize the mechanical characteristics of this material in order to develop a material that mimics both the macro and micro mechanical characteristics of the natural dura, which would promote successful host tissue integration of the implanted silk material. The third objective is to determine the biocompatibility of this material in the context of cells and tissues that would be in closest contact with it as an implanted dural replacement. And the fourth objective is to determine the degradability of the material, which must be optimized to match the rate of neo-dura formation. If the material is able to match this rate, it will be able to promote dural fibroblast growth across its surface, but eventually degrade such that full dural regeneration and, therefore, complete wound healing can occur for the patient.

The motivation of the combined four objectives is to create a novel biodegradable, biocompatible silk fibroin material that will successfully function as dural replacement material and improve on currently used materials and grafts.

1.2.3 Silk Sutureless Dural Repair System

The aim of this portion of the research is to create a silk fibroin adhesive to be used in conjunction with the previously described silk fibroin dural replacement material. By creating this adhesive quality of the dural replacement, it could be used as a sutureless dural replacement that does not require the use of any other tissue sealants. The main objective is to make a silk-based adhesive and test the sealing capability of the combined silk material system. Specifically, this system must be able to seal pressures as high as 50 mm Hg, which is maximum

observed intracranial pressure [Yamada et al., 1997], and improve on the sealing ability of currently used dural tissue sealants.

The final goal of this research is the development of a sutureless silk fibroin dural replacement that can seal pressures exceedingly those of currently used technologies while also maintaining biocompatibility, biodegradability and promoting complete dural regeneration.

Chapter 2: Background

2.1 The Dura Mater

The dura mater is the outermost and most fibrous of the three layers of the meninges surrounding the brain and the spinal cord. The two other meningeal layers are the arachnoid mater and the pia mater, which is the innermost layer. Cerebrospinal fluid fills the meninges in order to cover and protect the central nervous system. Specifically, CSF fills between the pia and arachnoid maters in the subarachnoid space and the dura mater acts as the final barrier to cerebrospinal fluid leakage [Figure 1]. In fact, the dura is the toughest and thickest meninges, and its name is derived from Latin meaning “tough mother” of the brain and spinal cord.

The dura mater also works as a drainage system within the central nervous system. It functions as the thecal sac that surrounds the arachnoid mater and the cerebral sinuses and has several vein-like sinuses that drain blood back to the heart after supplying the brain with oxygen.

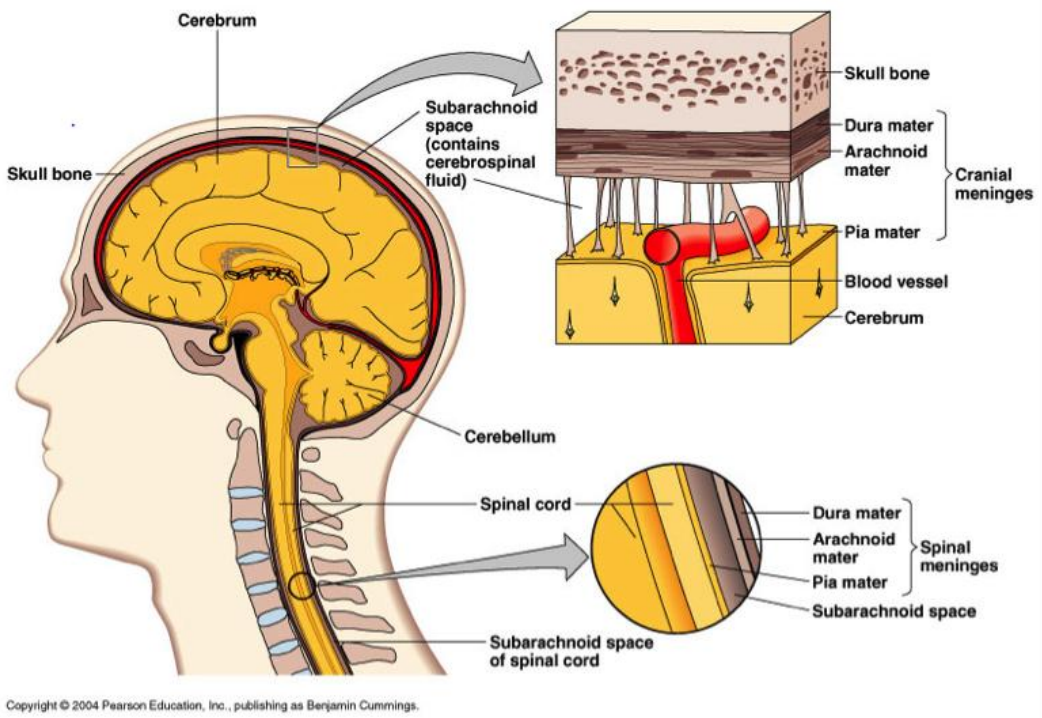

Figure 1: Schematic diagrams depicting the anatomy and function of the dura mater, which is the final barrier against CSF leakage around the brain and along the spinal cord [Marieb and Hoehn, 2013].

2.1.1 Incidence of Durotomy

Durotomies are required for nearly all cranial neurosurgery cases, in which the cortical tissues of interest are located beneath the dura mater membrane. For spinal surgeries, the majority of dural defects occur in the treatment of traumatic injury and removal of intradural tumors, such as meningiomas.

Although unintended in most types of spinal surgery that don't involve tumor removal, dural tears are often unavoidable during neurosurgery treatments of degenerative spinal conditions. Such conditions include degenerative disk disease, spondylotic radiculopathy, spinal stenosis, disk herniation, and lumbar

postlaminectomy syndrome. The incidence of durotomy during surgical treatments of these conditions is 1.8%, with the majority from disk herniation (1.5%) and spinal stenosis (1.7%) treatments [Williams et al., 2011].

For all events of dural resection or tear, dural closure techniques are required to reestablish the sealing membrane to limit CSF leakage in both spinal and cranial locations.

2.1.2 Complications of Unsuccessful Dural Repair

Complications resulting from unsuccessful dural repair and dural tears include cerebrospinal fluid leak or fistula [McCallum et al., 1975; Couture et al., 2003], meningitis [deFreitas et al., 2004], arachnoiditis [Carmouche et al., 2004], psuedomeningocele [O'Connor et al., 1998], intracranial or instraspinal hemorrhage [Lu et al., 2002; Mikawa et al., 1994], and headache [Williams et al., 2011]. Along the spinal column, spinal pseodomeningoceles and CSF fistulas, which are extradural collections of CSF, can cause back pain, headaches, and more serious events of nerve root entrapment [Couture et al., 2003]. All of these complications occur due to the inability for the dural closure to seal against CSF fluid.

Dural tears and unsuccessful dural closure following neurosurgery requires postoperative management, which usually involves flat bed rest and subarachnoid drain placement for minor CSF leak. Lumbar drains and numerous spinal taps are used in order to reduce CSF pressure, therefore reducing CSF leakage and promoting wound healing. Intravenous antibiotics are also used in order to treat and prevent infection induced by the CSF leakage [Ferroli et al.,

2012]. Despite these measures, however, some patients require surgical revisions due to complications or high risk of further complications. In general, unsuccessful dural closure results in heightened patient risk for further complications, delayed wound healing, increased hospital stay, and, therefore, increased health costs to the patient. In fact, medical costs in neurosurgery cases involving treatment of CSF leakage and its complications have been estimated to be 141% higher than in uncomplicated cases [Grotenhuis et al., 2005].

The incidence of fluid leakage is high due to the inherent limitations of current wound closure techniques, specifically the use of surgical sutures. The application of sutures inherently limits the strength and stability of the tissue and is especially hazardous in areas susceptible to large pressure changes, such as along the spinal column. The perforations produced by sutures preclude a completely watertight dural repair [Kaufman et al, 2010]. In order to avoid such risks and promote wound healing, physicians look to further wound closure techniques including various sealants and dural replacement materials.

2.2 Dural Tissue Replacements

Dural defects can vary from requiring sutures or a tissue sealant, to covering enough area to require a tissue replacement. In posterior cranial fossa or cranial base operations or following trauma or resection of dural based tumors including meningioma, for example, a dural substitute is required to prevent CSF leakage, infection, and complications of cerebral hernia [Terasaka et al., 2005].

Dural substitutes range in materials and can be classified as autografts, allografts, xenografts, and synthetic grafts. While each graft used clinically has its

advantages, none satisfy all of the requirements for an ideal dural substitute, and many have been associated with postoperative complications, including hemorrhages, development of cerebral meningeal adhesions, and inflammatory reactions [Parlato et al., 2011].

2.2.1 Autografts

Optimal closure of a durotomy includes the primary reapproximation of the dural edges. Because this is not always a possibility due to disease or large dural defects, use of autologous material, which is defined as a tissue explanted from one area of an individual's body and implanted into another location within his or her body, is a common neurosurgical practice [Moskowitz et al., 2009]. Several types of autografts are used in dural repair, the most important being temporalis fascia, pericranium, autologous fat, muscle patch, and fascia lata [Parlato et al., 2012]. A major advantage of autografts is the eliminated risks of immune-mediated host response and disease transmission. However, the dimensions and quality of autologous tissue can be inadequate to treat large dural defects [Islam et al., 2004], and they require an additional wound site and increase of surgery time for the patient. Such an increase in surgery time, increases anesthesia to the patient and hypoxia of the graft tissue can cause inflammatory responses of the underlying cortex or spinal tissue [Islam et al., 2004].

Autologous fat grafts are recommended for repair of dural defects that are inaccessible for standard suture closure techniques [Parlato et al., 2012]. For example, this tissue is often used for cranial base reconstruction, specifically for sellar packing [Kaptain et al., 2001]. Fat grafts are commonly used because they

are impervious to water, therefore allowing for water-tight closures, they do not adhere to surrounding tissues, and they naturally become revascularized [Black et al., 2010]. They do, however, carry risk of early fat necrosis and liquefaction [Hwang et al., 1996], fat dissemination in the subarachnoid space [McAllister et al., 1992] and subsequent lipoid meningitis [Ricaurte et al., 2000]. Fat liquefaction is more frequent in the presence of CSF leak, the presence of an infection, and after postoperative surgical wound irradiation [Taha et al., 2011]. In addition to being used as a dural replacement, fat grafts are often used to "plug" small dural defects before suturing or sealing. This is also done with muscle patches harvested from the patient for dural defects less than 5 mm in diameter [Ferroli et al., 2012].

Pericranium, which is a thin membrane that covers the inner surface of the skull, is another autologous graft used in cranial procedures specifically. It is easy to harvest, does not require an additional incision, and is resistant to infection. However, it is thin, fragile, and difficult to handle to the surgeon [Parlato et al., 2012]. Due to its lacking of mechanical robustness, tissue sealants, such as fibrin sealants, are generally also required to apply it to the dural defect [Ito et al., 2011]. Fascia tissues, including fascia lata and temporalis fascia, have greater thickness and mechanical strength, which makes them more usable in dural reconstruction. Fascia lata, however, must be obtained from deep tissue in the thigh and, therefore, is not often used in neurosurgery applications due to the requirement of this additional wound site. Temporalis fascia, which covers the

temporalis muscle of the head, does not require an additional skin incision and, therefore, makes for an optimal dural autograft.

2.2.2 Allografts

Allografts are defined as transplanted tissue from one individual to another. In the majority of dural closure cases, allografts have previously consisted of amniotic and placental membranes, pericranium, and cadaveric lyophilized dura mater [Parlato et al., 2012]. However, the majority of these allografts have been rejected for use as duraplasty materials due to high risks of rejection and disease transmission. Dehydrated human pericranium, however, has proven to be a valuable alternative to autologous grafts. This tissue has similar physical and mechanical properties to the dura, has demonstrated vascularization, fibroblast infiltration, and good incorporation with the host dural tissue [Caroli et al., 2004].

A commonly used allograft material used for dural closure is acellular dermis. This material, Alloderm (Life Cell Corporation, The Woodlands, TX), is made by processing cadaver skin to remove the epidermis and cells that can lead to tissue rejection and graft failure. The remaining tissue is immunologically inert, does not create adherence to surrounding tissue, creates a watertight barrier to prevent CSF leak, and it is mechanically tough, flexible, and easy to suture [Weber et al., 2002]. The internal structure of the acellular graft stimulates dural fibroblast invasion and rapid neovascularization, which results in duralization of the graft [Chaplin et al., 1999; Warren et al., 2000]. Due to its demonstrated success as a dural material, Alloderm has been suggested material for use when

autologous fascia or other tissues are not readily available or the size of the defect precludes the use of autologous tissue [Weber et al., 2002].

The acellular cadaver dermis, however, has been linked to complications and limitations. In general, studies have shown that dense collagen tissue grafts, such as Alloderm, have higher risks of postoperative complications [Vanaclocha et al., 1997]. Additionally, because sutures are required for Alloderm implantation, there is increased risk of dural tearing, CSF leakage through suture holes, and, therefore, a necessity for dural sealant use as an adjuvant to primary dural closure [Cosgrove et al., 2007]. The acellular dermis material has also been associated with atrophy or adhesion with the brain surface [Alleyene et al., 1998]. Overall, although Alloderm is widely used as a dural replacement, it carries numerous risks.

2.2.3 Xenografts

The two major types of xenografts, which are tissue products from different species, used as dural replacement materials are 1) processed whole tissue and 2) highly engineering collagen matrix, in which the collagen is animal-derived [Parlato et al., 2012].

Whole tissue xenografts used in dural closure include bovine or porcine pericardium, which are strong, easy to handle, low in cost, but require watertight suturing similar to Alloderm. Additionally, these materials have common complications including foreign body reactions, aseptic meningitis, and disease transmission [Parlato et al., 2012]. Due to such complications, surgeons look to use more controlled and engineered biological tissue.

DuraGen (Integra LifeSciences Corporation, Plainsboro, NJ) is an avascular collagen matrix specifically designed and used for dural closure. It is formed by highly purified type I collagen, which is insoluble and only weakly immunogenic [Narotam et al., 2009]. The matrix is inert, elastic, easy to handle, and serves as a scaffold to facilitate dural ingrowth. In fact, it has specifically designed porosity and degradation to allow for dural tissue integration at the same rate as material resorption [Narotam et al., 2007]. Additionally, it is an adhesive material that allows for use as a sutureless onlay [Figure 2]. The collagen matrix acts as a low-pressure absorptive surface to diffuse cerebrospinal fluid and attaches to the dural surface via surface tension. It also helps clot formation by the platelets depositing onto the collagen, which then disintegrate and release clotting factors, ultimately facilitating fibrin formation. This fibrin has an important role in holding the graft in place until fibroblasts, which are associated with blood vessels, proliferate into the graft [Parlato et al., 2012]. If a 1 cm overlap is available between the matrix and the durotomy edge, it can be used as an onlay with no additional fixation techniques; however, it can also be used with sealant systems or minimal suturing. When additional fixation techniques are required, however, there is an associated higher risk of infection and cerebrospinal leakage [Stendel et al., 2008]. When no suturing or additional fixation techniques are required, this material reduces complication risk and surgery time. Due to its advantageous qualities, DuraGen is currently considered the clinical "gold standard" of dural replacement materials [Xie et al., 2010].

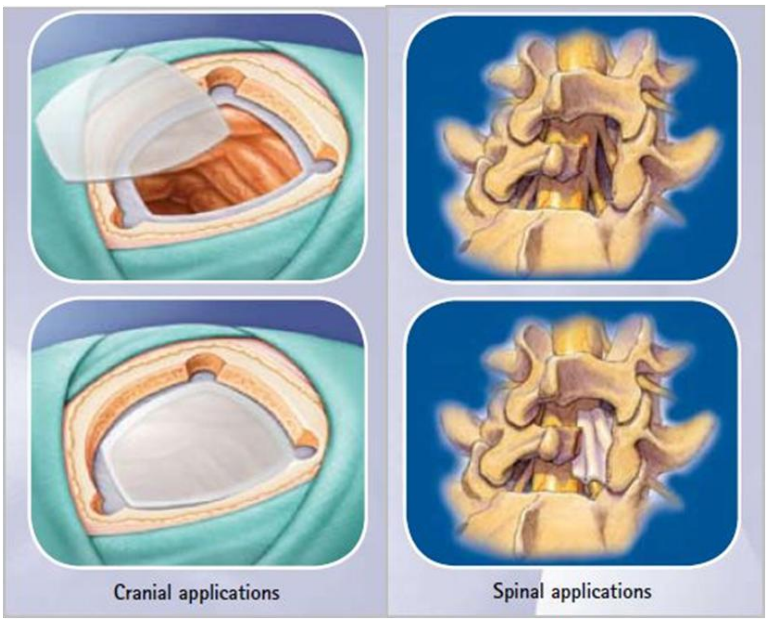

Figure 2: DuraGen applied as an onlay dural replacement in cranial and spinal applications [DuraGen-Plus Instructions for Use, Integra LifeSciences Corporation; 2003].

2.2.4 Synthetic

Synthetic grafts have recently been developed for use in neurosurgery to improve on the limitations and complications associated with biologically derived dural replacement materials. Previously studied and clinically used materials include polyester urethane and polytetrafluoroethylene. Such materials were chosen due to the ability to design their dimensions and allow for no risk of disease or infection transmission. However, because these synthetic materials are not biologically based, they lack many of the characteristics required of a tissue substitute and, specifically, a dural substitute.

As a foreign material, synthetic grafts often cause numerous inflammatory and foreign body reactions, which can cause further inflammation of surrounding tissues, graft encapsulation, cerebrospinal fluid bleeding, meningitis, scarring,

graft rejection, and delayed bleeding [Parlato et al. 2012]. Additionally, the mechanical characteristics of these materials result in rigid and brittle structures that are hard to handle and require suturing (cannot be used as conformable onlays). For example, polytetrafluoroethylene dural grafts have strong surface tension and lack of adaptability with the surrounding dural tissue. This results in frequent occurrence of friction injury with the underlying brain and spinal cord tissue, which can cause bleeding and inflammation [Islam et al., 2004]. Additionally, such synthetic grafts are only guaranteed for mechanical strength and stability for the first 2 weeks *in vivo*, after which they have been shown to cause cerebrospinal fluid leaks and inflammatory reactions [Yamada et al., 1997].

The lacking in mechanical characteristics and chemical compositions that would allow for successful integration of synthetic grafts with the dural tissue, limits their success as dural replacements. Therefore, more synthetic materials are being designed and used that better mimic the dural tissue and promote tissue interaction and regrowth. One such material is silk fibroin protein, which will be explained further.

Dural Substitute Type	Materials and Commercial Products	Advantages	Disadvantages and Associated Risks
Autografts		-No risks of host immune response or disease transmission	-Limited dimensions and quality of tissue -Additional wound site -Increase in surgery time -Graft tissue hypoxia can result in tissue inflammation
	Fat Grafts	-Water-impermeable -Limited adhesion to surrounding tissue -Naturally revascularized	*Associated Risks:* -Fat necrosis and liquefaction -Fat dissemination -Lipoid meningitis
	Pericranium	-Easy to harvest -No additional wound site -Resistant to infection	-Difficult to handle -Requires tissue sealants
	Fascia	-Adequate thickness and mechanical strength	-Fascia lata requires additional wound site in the thigh
Allografts	***Alloderm***: Acellular dermis	-Immunologically inert -Does not adhere to surrounding tissue -Suturable, watertight barrier -Mechanically robust -Promotes dural regeneration	-Requires tissue sealants *Associated Risks:* -Dural tearing by sutures -Heightened occurrence of postoperative complications including CSF leakage -Atrophy -Adhesion to brain surface
Xenografts	Whole tissue grafts	-Easy to handle -Low cost	*Associated Risks:* -Foreign body reactions -Aseptic meningitis -Disease transmission
	DuraGen: Avascular collagen matrix	-Adhesive onlay application (sutureless) -Immunologically inert -Promotes dural integration and regeneration -Promotes blood clotting	*Associated Risks:* -Infection -CSF leakage
Synthetic		-No risk of disease transmission -Designable characteristics	-Limited mechanical strength over time *in vivo* *Associate Risks:* -Foreign body & inflammatory reactions -Meningitis -CSF leakage and bleeding -Tissue friction injury

Table 1: Comparison of currently used dural replacement materials.

2.3 Tissue Sealants

Tissue sealants are used in nearly every surgical specialty due to their safety and efficacy as adhesive materials. In general, a tissue sealant is defined as a substance with characterizations that allow for polymerization and holding together of tissues and/or serving as a barrier to leakage of biological fluids [Fattahi et al., 2004]. The currently used tissue sealants can be divided into three functionalities: hemostasis, general tissue sealing, and the local delivery of exogenous substances [Reese et al., 2001]. The tissue adhesion process between tissues prevents air and fluid, such as lymphatic or cerebrospinal fluid leakages, in addition to promoting successful wound healing [Spicer and Mikos, 2010]. The tissue sealants presently available in the United States for surgical applications fit into several broad categories based on their chemical components and properties: fibrin sealants, albumin-based compounds, cyanoacrylates, hydrogels, and collagen compounds.

In terms of closure of deliberate and traumatic durotomies during neurosurgery, the dural repair systems include biological-based or synthetic sealants, specifically fibrin glues or hydrogel tissue sealants [Epstein et al., 2010].

2.3.1 Biologic Sealants

Fibrin tissue sealant is a widely used biomaterial due to its haemostatic effect, biodegradability, and induction of neither inflammatory response nor tissue necrosis at application site [Emilia et al., 2011]. It functions by mimicking the body's natural coagulation process via reaction of two biological components: thrombin and fibrinogen, which results in hemostasis and tissue adhesion [Reese

et al., 2001]. Although this formulation provides such effects, the plasma products carry the risk of disease transmission [Hino et al., 2000]. Additionally, fibrin sealants have relatively weak tensile and adhesive strengths and reduced mechanical strength in wet conditions [Sierra et al., 1992]. Therefore, they have limited success in dural closure and the sealing of cerebrospinal fluid leakages.

2.3.2 Synthetic Sealants

Due to the limitations of biologic tissue sealants, synthetic dural sealants have been developed with specifically designed mechanical and chemical characteristics. Commonly used dural synthetics sealants include polymeric hydrogels, specifically polyethylene glycol hydrogels.

2.3.2.1 Polyethylene-Glycol Hydrogels

Polyethylene glycol is a common polymer used in the hydrogel sealants, which are polymerized by such methods as photopolymerization and chemical crosslinking via spray or mixing methods [Duarte et al., 2011]. Polyethylene glycol (PEG) hydrogels have been extensively researched in biomedical applications due to the versatility of the PEG macromer chemistry in combination with its high biocompatibility [Nuttelman et al., 2008]. The hydrophilic PEG hydrogels are not only biocompatible but support cell interaction with the material, including cell adhesion, migration, and encapsulation under specific polymerization and functional group conditions [Lin et al., 2009]. PEG-based tissue sealants have been shown to gel rapidly, form adhesive bonds to tissue, and exhibit good tissue compatibility [Wallace et al., 2001]. Additionally, the chemical versatility and biocompatibility of polyethylene glycol supports the

development of PEG-based tissue sealants, which rely on crosslinking methods to produce an adhesive gel [Fu et al., 2011]. Previous research has shown that application of the PEG-based sealants successfully decrease air leaks following major thoracic surgery [Reese et al., 2007, Macchiarini et al., 1999], promote wound healing and hemostasis in cardiovascular surgery [Torchiana et al., 2003, White et al., 2000], and support dural mater tissue sealing in cranial surgery [Alleyene et al., 1998]. These hydrogels are predominantly formed *in situ* through photopolymerization, ionic interaction, or chemical cross-linking [Nguyen et al., 2002].

There are many limitations and adverse events, however, associated with currently available PEG-based tissue sealants. A leading sealant used in neurosurgical procedures is DuraSeal®, which is a synthetic absorbable sealant made of polyethylene glycol (PEG) and trilysin amine [Figure 3]. Although it is FDA-approved as a cranial and spinal surgery sealant system, DuraSeal can swell after application and is suggested for use only in addition to general wound closure protocols due to the possibility of CSF leakage [Epstein, 2010]. The DuraSeal hydrogel can swell by 50% and, is not recommended for use in locations that present a risk for neural compression, such as the spine [Thavarajah et al., 2009]. DuraSeal also carries the risk of renal compromise, inflammatory reaction, neurologic compromise, allergic reaction, and delayed wound healing (DuraSeal, Covidien, Mansfield, MA). Additionally, commercialized hydrogel sealants must be used adjunct to additional dural closure procedures, including sutures [Figure 3]. Sutures inherently diminish the strength of the dural closure

due to the small holes that preclude a watertight dural repair [Kaufman et al., 2010]. The tissue sealants, therefore, rely on dural repair procedures that increase the chance of CSF leakage, which is not ideal for physicians or patients.

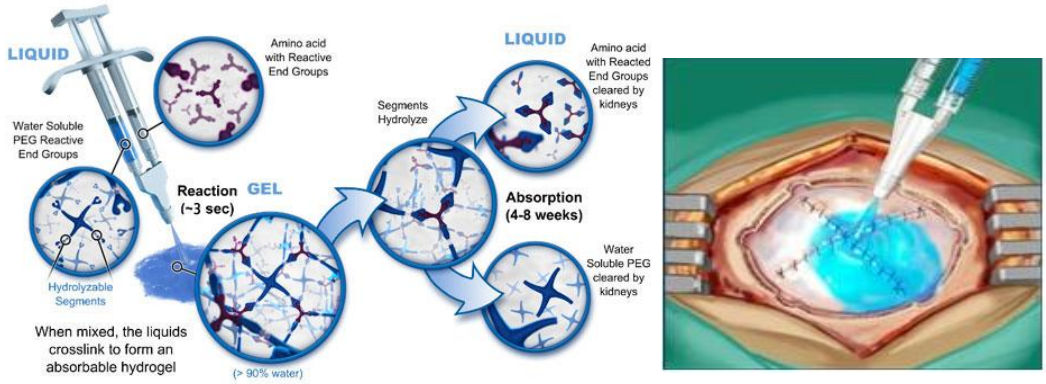

Figure 3: DuraSeal is a tissue sealant designed as an adjunct to sutured dural repair during cranial and spinal surgery to provide a watertight closure. The hydrogel is applied through a dual-barrel syringe facilitating the crosslinking of water soluble PEG reactive groups with trilysine, which is a small molecule amine with reactive linkages (DuraSeal, Covidien, Mansfield, MA).

2.3.2.2 Adhesive Membranes

While the majority of tissue sealants occur as liquids or gels, some newly designed sealant systems are membranous materials. One such material is the TissuePatch™ (Tissuemed Ltd, Leeds, UK), which is a sterile, self-adhesive, absorbable surgical sealant. It is a multi-layer sealant device comprised of alternating layers of poly(lactide-*co*-glycolide) (PLGA) and a proprietary adhesive terpolymer called TissueBond [Zhang et al., 2012]. While the PLGA provides mechanical strength for temporary wound support [Puppa et al., 2010], the adhesive layer is able to form covalent bonds to tissue through nucleophilic substitution reactions between *N*-hydroxysuccinimide and amine/thiol groups [Ferroli et al. 2012]. This active chemistry is able to form crosslinks at the site of

application, while the PLGA functions as an impermeable barrier that is largely absorbed over 70 days [Zhang et al., 2012].

While the TissuePatch has been documented as a reliable sealant for alternative or adjunctive treatment of superficial defects in lung surgery, the more specific TissuePatchDural is indicated for adjunctive prevention of CSF leakage in neurosurgery [Puppa et al., 2010]. By its design, it is to be used by being applied over regular suturing techniques both in spinal and cranial cases. Figure 4 shows TPD applied to a sutured dural defect in a cranial procedure.

In a study of its application in 119 high-risk dural closure procedures, there was a CSF leakage occurrence of only 9.2% [Zhang et al., 2012].

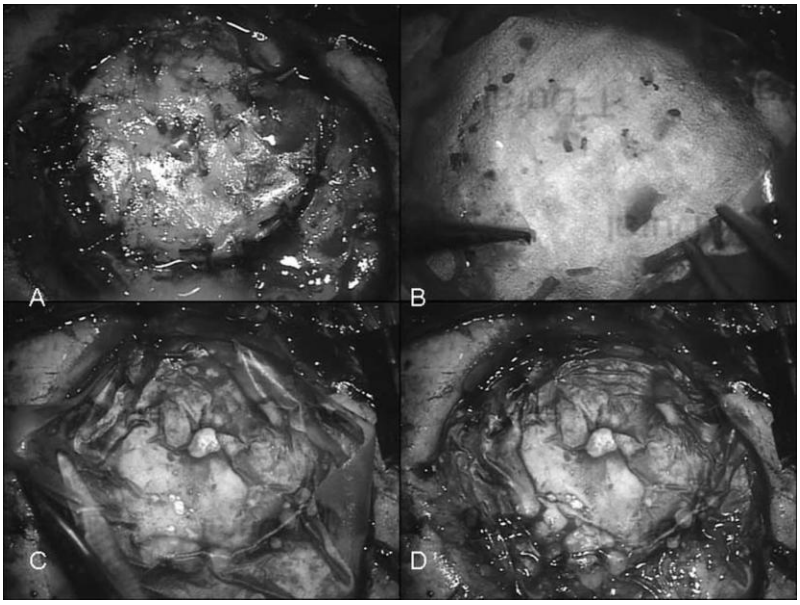

Figure 4: Cranial application of TissuePatchDural (TPD) at microscopic level. Images show the final dural defect (A), TPD application (B), TPD adhered on the dural surface (C), and the final view after cutting of extra material (D) [Ferroli et al., 2012].

Although the TissuePatchDural shows success as a dural closure device, it must be used in adjunct to suturing and carries additional other risks and

limitations. For example, the material has a documented risk of allergic reaction and local, mild inflammatory response leading to encapsulation and fibrosis around the material [Ferroli et al., 2012]. Additionally, covalent bonding system of its adhesive layer is not specific to dural tissue and, instead, could result in bonding to any tissue once activated by water or CSF. This material, therefore, must be used in addition to numerous other dural tissue closure techniques, which inherently carry their own risks, and the material increases the general risk of cortical and cerebral tissue adhesions.

Tissue Sealant Type	Commercial Products	Advantages	Disadvantages and Associated Risks
Biologic	Fibrin Sealants	-Haemostatic effect -Biodegradable -No inflammatory response	-Weak tensile and adhesive strengths -Reduced mechanical strength in wet conditions *Associated Risks:* -Disease transmission -CSF Leak
Synthetic			
PEG Hydrogels	***DuraSeal***	-Biocompatible -Support host cell interaction -Form adhesive bonds to tissue	-Requires preliminary suturing -Can swell by 50% -Not recommended for neural application *Associated Risks:* -Neurological compromise -CSF leakage -Allergic reaction -Delayed wound healing
Adhesive Membranes	***TissuePatch-Dural (TPD)***	-Self-adhesive -Absorbable	-Requires preliminary suturing *Associated Risks:* -Allergic reaction -Inflammatory response -Unwanted tissue adhesion -CSF leakage

Table 2: Comparison of currently used tissue sealants for dural closure.

2.4 Silk Fibroin as a Biomaterial for Dural Closure

While silk from the *Bombyx mori* silkworm has been used for centuries as a surgical suture material due to its mechanical strength and limited immunogenic effect, silk fibroin, the main component of the silk protein, has been established as an extremely successful and versatile biomaterial. The silk fibroin protein consists of a 1:1 ratio of two protein chains linked by a single disulfide bond when produced by the *B. mori* silkworm. The heavy chain (390 kDa) display hydrophobic properties and can form crystalline regions which the amorphous light chain (26 kDa) has hydrophilic properties [Vepari and Kaplan, 2007]. Regional interactions of the chains result in crystalline beta-sheet and other secondary structures that affect the mechanical properties of the material and its ability to interact with water [Wong et al., 2006].

The biological protein has a combination of unique attributes including high mechanical strength, excellent biocompatibility, and controllable structure and morphology. Its distinct biological properties are maintained in a wide range of silk fibroin material morphologies, including films, fibers, gels, and porous sponges [Vepari and Kaplan, 2007]. In all formats, it has good water vapor and oxygen permeability, blood compatibility, and accelerates collagen formation [Kim et al., 2011]. Additionally, the silk fibroin materials can be designed to degrade over controlled periods of time in order to facilitate host tissue interaction and eventual complete regeneration [Horan et al. 2005]. Extensive studies have explored silk fibroin as a material for tissue engineering. The material has shown

success in cell and tissue studies including bone, cartilage, ligament, blood vessel, skin and many others [Vepari and Kaplan, 2007].

The silk fibroin protein, therefore, has been demonstrated as a successful biomaterial and specifically successful in the field of tissue engineering and regeneration.

2.4.1 Silk Films

Silk fibroin films can be formed by casting of aqueous or organic solvent systems or through blending of other polymers. The mechanical characteristics and water permeability of these films can be altered by altering the crystallization levels of the silk fibroin protein. Additionally, silk films can be patterned or include microstructures in order to further control or enhance cell attachment to the films.

Silk films have shown success in human mesenchymal stem cell proliferation [Wang et al., 2005], fibroblast attachment [Minoura et al., 1995], bone formation when modified with RGD cell binding domains [Sofia et al., 2001] and when coupled with BMP-2 [Karageorgiou et al., 2004]. As implant materials, silk fibroin films successfully facilitated healing of full thickness wounds in rat models and in applications specifically for neurosurgery. In fact, Kim et al. [2011] developed a transparent dura mater derived from silk fibroin. Although only a preliminary study, silk films were implanted over craniotomy sites as dural replacements, where they showed suturability, successful impermeability against cerebrospinal fluid, and excellent biocompatibility [Figure

5]. Based on the preliminary results of this study, silk fibroin film materials appear to be safe and suitable for dural repair applications in neurosurgery.

Figure 5: Implantation of silk film dural replacement in a rat model cranial dural defect by Kim et al. [2011].

2.4.2 Electrospun Mats

Electrospun silk fibroin mats are of particular interest in tissue engineering applications due to their biocompatibility, mechanical characteristics, porous 3D structure, and nanofiber morphology.

Briefly, the electrospinning process involves the charging of a viscous liquid solution to a high electric potential in order to create nanofibers onto a grounded collector plate. As the liquid travels throw a positively charged capillary needle via a controlled syringe pump, a grounded collector plate is placed a measured distance below. The electric potential between the tip of the capillary tube and the collector plate results in a tensile force on the drop of the solution at the base of the needle. This tensile force results in nanofibers being produced from the droplet and spun down onto the collector plate [Reneker et al. 1996]. As they spin down to the grounded surface, the dry and lock in their nanofiber morphology. The resulting material on the collector plate is a nonwoven randomly

aligned nanofiber mat. Characteristics of the mat, including fiber morphology, can be tuned by controlling flow rate, electric field strength, distance between capillary tip and grounded collector, and collector design [Pham et al., 2006].

Required characteristics of successful tissue engineering scaffolds include biocompatibility, a 3-D framework that mimics the natural ECM seen by host cells, porosity with a high surface-volume ratio to allow for cell attachment and ingrowth, and degradability [Pham et al., 2006]. Silk fibroin nanofibers are biodegradable and biocompatible and the electrospun nanofibers can be made in the sub-micron range, which mimics the collagen fibrils within the ECM. Silk fibroin electrospun scaffolds, therefore, are ideal for tissue engineering applications. They have been successfully used in wound healing as functionalized electrospun silk wound dressings to induce healing processes [Scheider et al., 2008]. Additionally, they have been used in bone and cartilage regeneration [Kim et al., 2005].

2.4.3 Silk Adhesives

2.4.3.1 Silk-PEG Hydrogels

While silk hydrogels can be formed by pH control, sonication, and other chemical or physical mechanisms, chemical crosslinking has been studied for the production of an adhesive silk gel.

Polyethylene glycol (PEG) hydrogels have been extensively researched in biomedical applications due to the versatility of the PEG macromer chemistry in combination with its high biocompatibility [Nuttleman et al., 2008]. The hydrophilic PEG hydrogels are not only biocompatible but support cell interaction

with the material, including cell adhesion, migration, and encapsulation under specific polymerization and functional group conditions [Lin and Anseth, 2009]. PEG-based tissue sealants have been shown to gel rapidly, form adhesive bonds to tissue, and exhibit good tissue compatibility [Wallace et al., 2001]. Previous research has shown that application of the PEG-based sealants successfully decrease air leaks following major thoracic surgery [Reece et al., 2001; Macchiarini et al., 1999], promote wound healing and hemostasis in cardiovascular surgery [Torchiana et al., 2003; White et al., 2000], and support dural mater tissue sealing in cranial surgery [Alleyene et al., 1998]. These hydrogels are predominantly formed *in situ* through photopolymerization, ionic interaction, or chemical cross-linking [Nguyen et al., 2002]. One such chemical crosslinking uses Michael addition, which is facile reaction between nucleophiles and activated alkynes in which the nucleophile adds across a carbon-carbon double bond [Michael, 1887]. The more specific thiol-Michael addition to electron-deficient carbon-carbon double bonds, such as those in maleimides, has many advantages including requiring few catalysts, displaying rapid reaction rates in benign reaction conditions, and the absence of byproducts [Fu et al., 2011].

A silk-PEG tissue sealant was designed with PEG-maleimide and PEG-thiol in order to take advantage of the clinically relevant polymerization process of Michael addition. This gel forms by a two-step stabilization process. The gel was tested using varying silk concentrations [Figure 6] in order to control the mechanical stability and adhesive strength via PEG crosslinking and ß-sheet formation. The gels of higher concentration showed greater adhesive abilities as

did those with increase beta-sheet content via ethanol exposure. The hydrophobic domains of the silk fibroin were facilitated to organize into ß-sheet structures while also interacting with the highly hydrophilic PEG molecules, which resulted in a more mechanically robust and adhesive gel. When tested on steel, the PEG-based silk tissue sealant had comparable adhesive strengths to clinically used PEG-based tissue sealants [Serban et al., 2011].

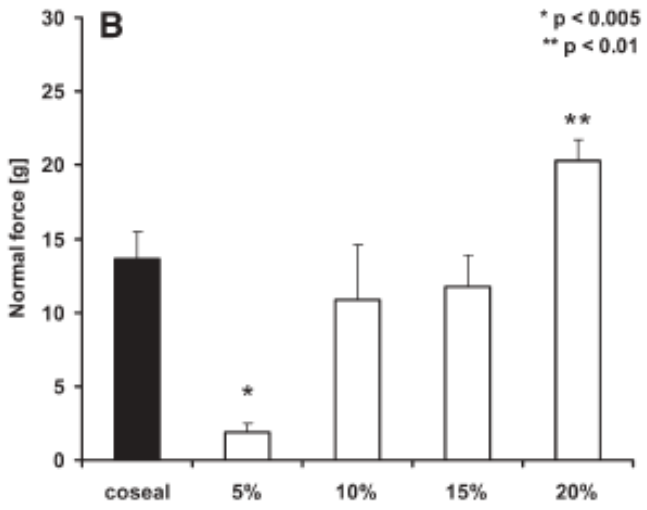

Figure 6: DMA measurements of adhesion to determine silk concentration dependence as compared to a commercial tissue sealant, CoSeal (n=3, p=0.00002) [Serban et al., 2011].

2.4.3.2 Electrogelated Silk (E-Gels)

Electrogelated silk, or e-gels, is a novel, electrically mediated adhesive gel formed from silk fibroin. This unique, reversible protein adhesive is formed by electrolysis. Specifically, when aqueous silk solutions are exposed to low direct current (DC) voltages, gelation occurs at the positive electrode. Since silk (6-8% w/v) has a high water content, the applied voltage and current through the solution results in electrolysis. Bubbles occur on the positive electrode, reflecting the

generation of oxygen gas, while hydrogen gas bubbles form at the negative electrode. As this process progresses, a thick gel forms on the cathode. This gelation state is stable after electric field has been removed, but can be reversed by reversing the electrical field applied [Leisk et al., 2010].

While the majority of silk hydrogels, including pH and sonicated silk hydrogels, are formed by beta-sheet structures [Kim et al., 2004], electrogelated silk relies on intermediate conformations rather than beta-sheet formation. In fact, the electrogelation process results in an increase in turns, a decrease in random coil content, and no significant change in beta-sheet content when compared to the original aqueous silk solution [Lu et al., 2011].

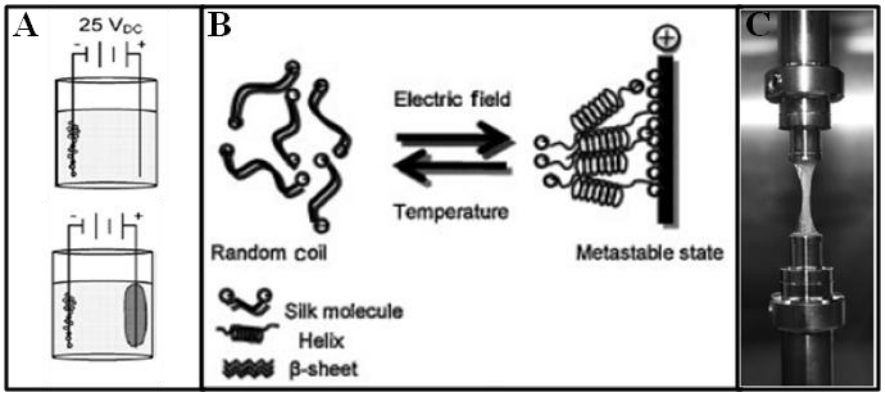

Figure 7: Schematic of e-gel process when 25 V is applied to aqueous silk solution (A) and the resulting conformational change of silk fibroin from the random coil to helical state (B). The resulting gel is mechanically robust and adhesive, as displayed on steel (C) [Leisk et al., 2010].

These changes in protein conformation result in a soft-solid-like, physical gel with unique adhesive characteristics compared to other bioadhesive systems. Adhesion values ranging from 1 to 1.5 mJ were obtained by the material on steel, acrylic and wood surfaces. Additionally, there was apparent stiffening of the e-gel and increased adhesive force due to dehydration, suggested control of adhesive

properties based on adhesive properties of the hydrogel [Leisk et al., 2010]. Because there are no added chemicals or crosslinkers added into the initial aqueous silk solution, e-gels maintain the biocompatibility and biodegradability of other silk fibroin materials, which supports the application of e-gels as tissue adhesives.

Part I

Clinical Review Study:

Postoperative Hydrodynamic Complications Associated with the Use of DuraSeal Sealant for Dural Repair in Spinal Neurosurgery Cases

Chapter 3: Introduction

As previously described, the incidence of CSF leak can be as high as 42% following neurosurgery procedures [Dolenc et al., 1997]. Due to the numerous tissue sealants and dural replacement materials currently used, clinical reviews have been conducted in order to determine the success of such dural closure techniques in neurosurgery procedures.

3.1 Clinical Reviews of Dural Tissue Sealants

The major material classifications of tissue sealants, as described above, are biologic and synthetic, including both gels and membrane sealant systems. In clinical application, complications have been observed with the use of both types of tissue sealant. In a study of 41 neurosurgery cases including cranial and spinal procedures, the use of DuraSeal for dural closure resulted in a total complication rate of 4.9% [Boogarts et al., 2005]. In another study, Tisseal, a fibrin sealant (Baxter Healthcare Corp., Deerfield, IL), was used in 278 spinal cases and had a total complication rate of 11.9%. The newest tissue sealant technology, adhesive membranes, has also been studied for its clinical success. One such material, TissuePatchDural, had a complication rate of 9.2% out of 119 neurosurgery cases involving both cranial and spinal procedures [Ferroli et al., 2012].

Overall, the leading tissue sealants currently available have been studied in clinical settings and carry significant complication rates.

3.2 Clinical Reviews of Dural Replacement Materials

The majority of clinical review studies regarding the success of dural replacement materials in dural closure procedures have focused on cranial procedures, due to their increased hydrodynamic complication rates. One type in particular is posterior fossa neurosurgery, which is associated with increased hydrodynamic complications compared to other cranial procedures and spinal procedures [Parizek et al., 1998]. This is most likely due to the residual tissue placement after a suboccipital surgical approach coupled with increased CSF pressure in this location [Moskowitz et al., 2009]. Because primary closure is often not possible in these procedures, dural substitutes are generally required for dural closure.

In order to understand the success of dural closure materials in posterior fossa neurosurgery, a single institution study of 128 cases was performed by Moskowitz et al. [2009]. This study looked at the use of acellular dermis, bovine collagen, reformulated bovine collagen, and suturable bovine collagen as dural replacement materials. The complication rates of these materials were high and are shown in Figure 8. Although the risk of hydrodynamic complications associated with posterior fossa neurosurgery is high, the rates remained high when modified with various dural replacement materials.

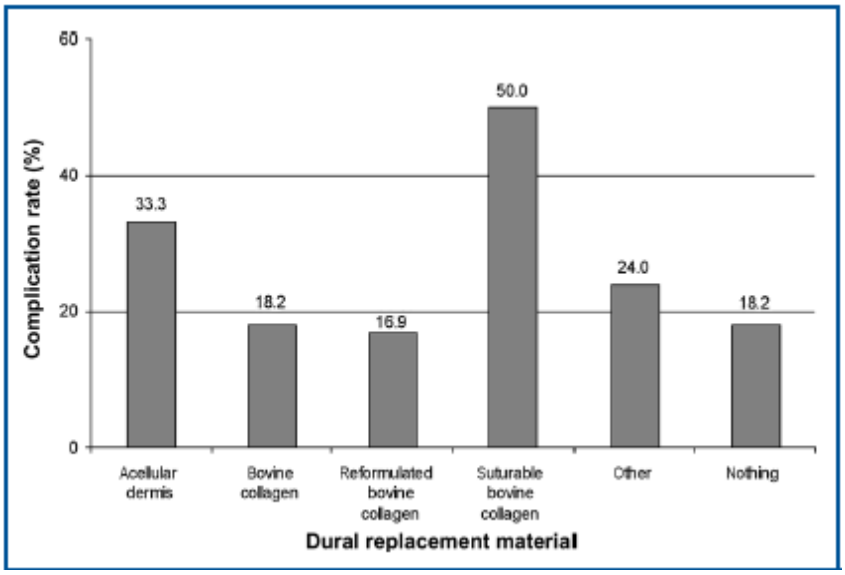

Figure 8: Complication rates of dural replacement materials used in a single institution clinical review of dural closure techniques in 128 posterior fossa neurosurgery cases [Moskowitz et al, 2009].

This study further supports the fact that no dural substitute has been proven to be complication-free in a large clinical trial. However, there have been limited clinical reviews specifically studying spinal procedures and/or the combinatorial effects of tissue sealants and dural replacement materials.

Therefore, we have conducted a single institution study at Tufts Medical Center Department of Neurosurgery to determine the clinical use and success of a specific tissue sealant, DuraSeal, in combination with dural replacement materials.

Chapter 4: Patients and Study Design

A retrospective chart review was performed with approval from the Tufts Health Sciences Campus Institutional Review Board [IRB#:10294 – Clinical

Review of Tissue Sealant in Neurosurgery]. The operating room database was screened for neurosurgery procedures in which DuraSeal™, polyethylene glycol ester and trilysine amine dural sealant system (Covidien, Mansfield, MA), was used for dural closure between March 2005 and January 2011. Spinal procedures, in which dural closure with DuraSeal occurred, both for intentional and unintentional dural openings, were included. Medical records were reviewed for patient demographics, including age, primary diagnosis, and operative procedure. The use of dural closure techniques was identified, including suture use, dural replacement use, and combined techniques. For cases in which dural replacement materials were implanted, the type of material was documented. Postoperative clinical courses were reviewed for complications, specifically hydrodynamic complications. These complications included persistent CSF leakage and pseudomeningoceles. Because postoperative imaging was not routinely performed for each patient, both CSF leakage and pseudomeningoceles were considered only when clinically significant. Specifically, these complications were considered when noted in postoperative clinical notes as including pain, swelling, or requiring such treatments as further surgery procedures and percutaneous CSF aspiration or diversion.

Chapter 5: Results

A total of fifty-five neurosurgery cases in which DuraSeal was used either independently or in addition to other techniques and materials for dural closure were reviewed. From these 55 cases, 43 were identified as spinal procedures and

9 were identified as cranial procedures. Because of the large difference in the anatomy and process of dural closure between spinal and cranial neurosurgery procedures, we decided that these cases should not be grouped in the same analysis further in the study. Therefore, the patient population of this study was limited and identified only as the 43 patients who had undergone spinal procedures. Nine were cervical spine procedures (20.9%), 5 thoracic spine procedures (11.6%), and 29 lumbar spine procedures (69.4% of total 43 patients).

5.1 Dural Closure Materials and Techniques

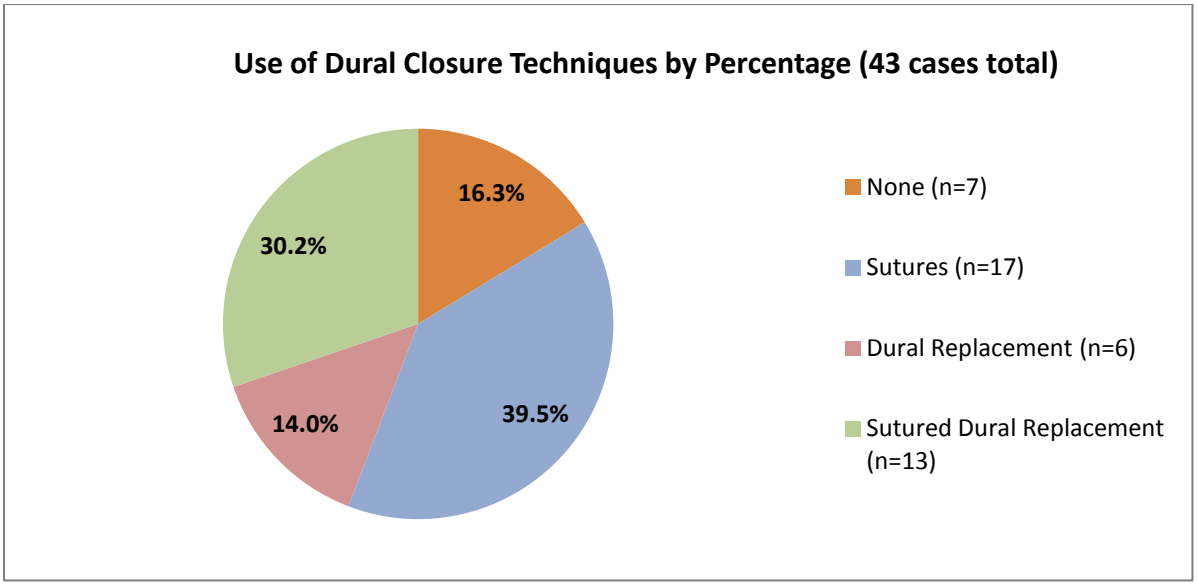

Figure 9: The distribution of dural closure techniques used in the 43 reviewed spinal cases. Percentages were calculated based off of the total number of cases (n=43).

Of the 43 patient cases identified in this study, four different dural closure techniques were used [Figure 9]. All of these techniques included the use of DuraSeal, as this was the criteria of the patient population in the study. In conjunction with DuraSeal, sutures alone were used in 17 patients, sutureless

dural replacement materials were implanted in 6 patients and sutured dural replacements in 13 patients. In 7 patients, no additional sutures or replacement materials were used with the DuraSeal for primary dural closure. In these cases, DuraSeal was applied at areas where CSF leak was evident but the area was too small or the leak too minimal to require a suture.

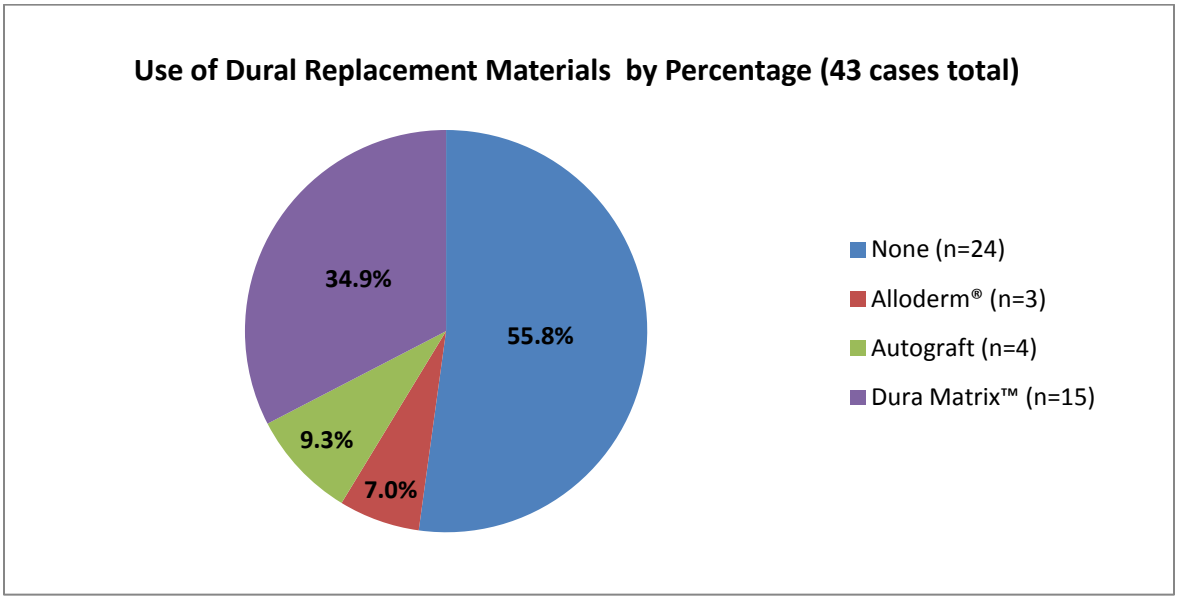

Figure 10: The distribution of dural replacement materials used in the 43 reviewed spinal cases. Percentages were calculated based off of the total number of cases (n=43).

In total, three different types of dural replacement materials were implanted in a total of 19 cases [Figure 10]. A type I collagen matrix, Dura Matrix Collagen Dura Substitute Membrane (Stryker, Kalamazoo, MI), was implanted in 15 patients, including 4 in its sutureless onlay application, and 9 using additional suturing. Acellular human dermis, Alloderm (LifeCell Corp., Branchburg, NJ), was used in 3 patients. Autografts, specifically muscle patches, were used in 4 patients. These muscle patches were primarily used to tamponade CSF fluid,

rather than as a complete dural replacement. There were 3 patients that had both Alloderm and muscle patches implanted for dural closure. All Alloderm and autograft implants were sutured.

5.2 Complication Rates

Complications were seen in 7 of the 43 patients analyzed for a total complication rate of 16.3%. All complications were hydrodynamic in nature. Specifically, CSF leakage was seen in 5 patients, and symptomatic pseudomeningoceles were seen in 2 patients.

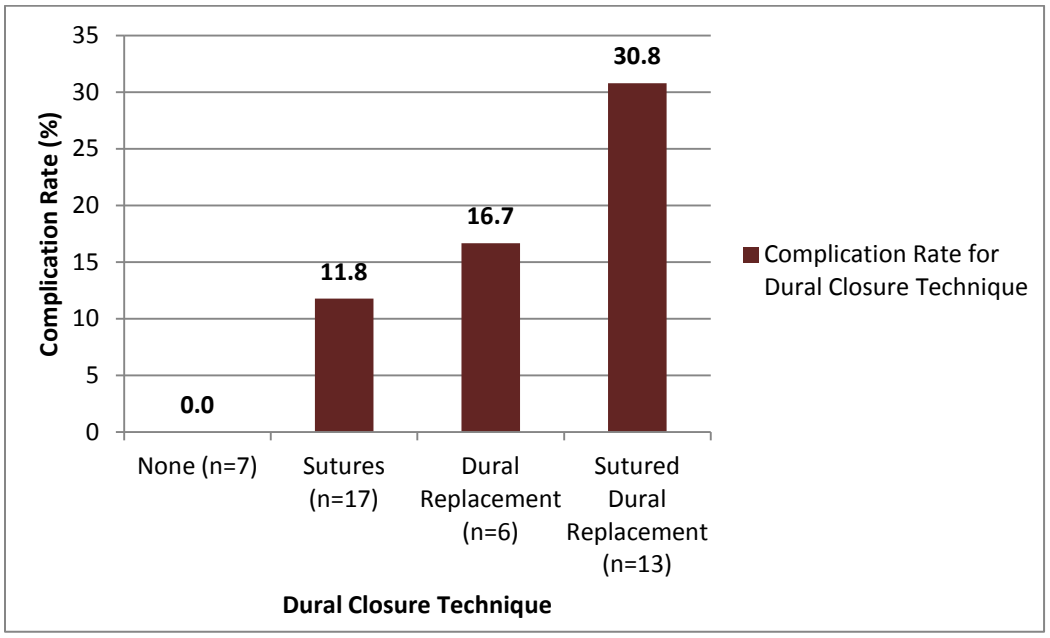

Figure 11: The complication rate of each dural closure technique used in this study. The four different techniques had varying total numbers of cases. The complication rates were calculated using the number of complications in each category compared to the total cases in that dural closure technique category.

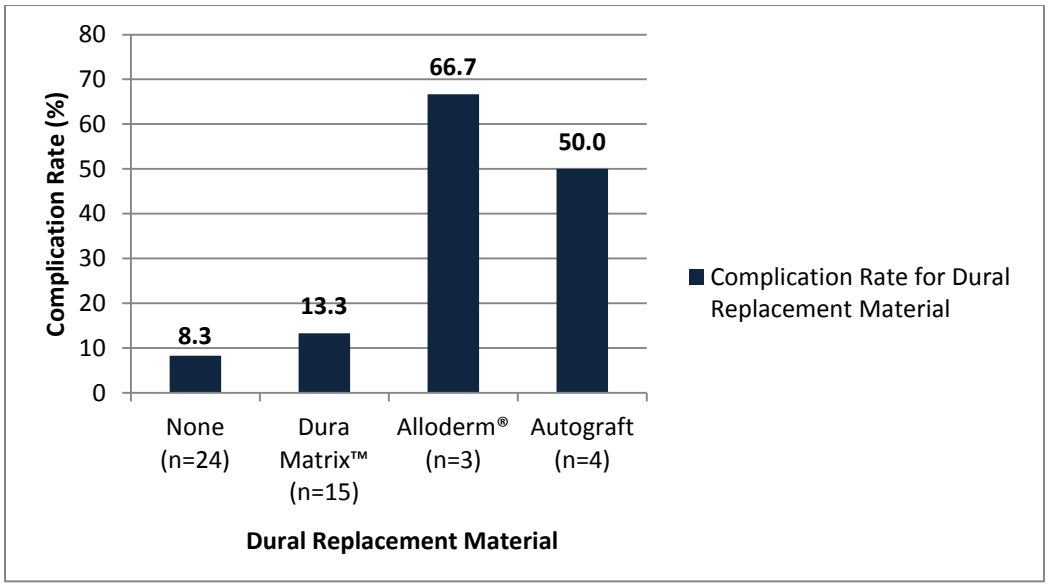

Figure 12: The complication rate of each dural replacement material used in this study. The four different materials (including no dural replacement) had varying total numbers of cases. The complication rates were calculated using the number of complications in each category compared to the total cases in that dural replacement material category.

Complications occurred with all dural closure techniques except those requiring DuraSeal application alone (n=7, 0.0%) [Figure 11]. Complications were seen with only sutured dural closures in 2 of 17 (11.8%), for non-sutured dural replacement material in 1 of 6 (16.7%), and for sutured dural replacement in 4 of 13 cases (30.8%). Complications occurred with the implantation of all used dural replacement materials [Figure 12]. They were seen in 2 of 15 (13.3%) Dura Matrix cases, 2 of 3 (66.7%) Alloderm cases and 1 of 4 (25%) autograft cases. When Dura Matrix was sutured, its complication rate decreased. Complications were not seen (0 of 9, 0.0%) for sutured Dura Matrix and were seen in 2 of 6 (33.3%) cases for Dura Matrix Onlay with no sutures.

Chapter 6: Discussion

Dural tears are sometimes unavoidable during surgical treatment of degenerative spinal conditions, including spinal stenosis and disk herniation. One study showed that the incidence of unintended durotomy during surgical treatments of degenerative spinal conditions had an incidence of 1.8%, with the majority from disk herniation (1.5%) and spinal stenosis (1.7%) treatments [Williams et al., 2011].

Both intended and unintended dural defects require dural closure to recreate the watertight barrier of the native dura and prevent CSF leakage.

6.1 Dural Closure Techniques and Materials

In our small single institution review of spinal neurosurgery cases, numerous dural closure techniques and materials were used. As previously described, DuraSeal was used in all cases either independently or as an adjuvant to dural closure materials and techniques. The use of DuraSeal in all cases occurred due to observed dural defect and/or CSF leak during each surgery.

Within this study, the majority of cases either used no additional methods or only suturing to close dural defects [Figure 9]. This is most likely because the dural defects being treated were small enough to not require the use of dural replacement materials. And during dural closure, reapproximation and suturing of the dural edges can lead to the best seal without exposing the patient to foreign graft materials [Moskowitz et al., 2009] while also limiting surgery time [Islam et al., 2004]. However, when dural replacement materials were needed, the majority

were secured with suturing in order to obtain a water-tight seal around the implanted material.

When a dural substitute material was required, surgeons looked to use autograft materials [Figure 10], specifically muscle patches. In general, both muscle patches and fat grafts are used to plug or tamponade small dural defects against CSF leakage. In fact, this is regularly done for dural defects less than 5 mm in diameter [Ferroli et al., 2012]. The muscle patches used in this study occurred with small dural defects for extra sealing control. The surgeons would look to use these materials rather than dural substitutes due to the small area required and in order to avoid any risks of immune-mediated host response and disease transmission. When larger dural defects required dural replacement materials and autologous tissue did not have the required dimensions or quality, two clinically common materials were used: Alloderm and DuraMatrix.

Overall, neurosurgeons at Tufts Medical Center used a variety of dural closure techniques for the treatment of spinal cases reviewed in this study. While the majority of cases did not required dural replacement materials in addition to DuraSeal application, autografts, Alloderm and DuraMatrix were used when necessary in order to attempt a watertight barrier against CSF leakage and, therefore, a better recovery for the patients.

6.2 Complication Rates

The observed total hydrodynamic complication rate for this study, which was 16.3%, was unexpectedly high, especially for spinal cases in which dural

defects are not as large or prevalent compared to cranial cases. This high complication rate most likely resulted from the patient population, which were patients who required application of DuraSeal. In spinal surgery procedure, DuraSeal is only applied when there is evidence of CSF leakage and, therefore, a demonstrated presence of dural defect or major dural thinning. These patients would have the highest risk of postoperative hydrodynamic complications compared to patients who had spinal procedures but had no decrease in dural mechanical integrity.

Patients who required the implantation of dural replacement materials had the largest dural defects, which could not be closed by sutures or DuraSeal alone. These patients, therefore, would also have higher risk of hydrodynamic complications, but these complications should have been diminished by the extensive dural closure materials. Instead, dural replacements implanted by suturing had the highest complication rates of the observed dural closure techniques [Figure 11]. In fact, the use of sutures with the materials nearly doubled the complication rate from onlay dural replacement materials [Figure 11]. In general, sutures increase risk of dural tearing and CSF leakage through suture holes [Cosgrove et al., 2007]. Although DuraSeal is used as an adjuvant sealant to limit these risks, as shown in this study, the use of sutures with dural replacements results in notably higher rates of hydrodynamic complications. Sutureless dural substitutes, however, have lower rates. Therefore, sutureless dural replacements show potential for limited risk of hydrodynamic complications and, therefore, success as dural closure techniques.

Of all the dural replacement materials used in this study, including the cases in which none were used, DuraMatrix Onlay had the lowest specific complication rate of 8.3% [Figure 12]. The conformable collagen onlay material is flexible and designed to conform to the contours of the defect site and attach to the dural surface by slight adhesion and surface tension. While this is not a watertight dural closure procedure [Ferroli et al., 2012], a previous study showed that such a collagen onlay material in cranial meningioma surgery prevented postoperative CSF leak in 99.6% of patients [Lee et al., 2008]. The success of this type of material stems from its sutureless nature such that the dura does not have additional holes and the resulting risk of further dural tear. Such complications are often seen with Alloderm, which requires suturing and had the highest specific complication rate in this study of 66.7%. This rate is probably unreliable due to the small (n=3) sample size.

Chapter 7: Conclusion

Although DuraSeal is designed as an adjuvant tissue sealant to seal against CSF leakage in dural closure procedures, there was a significant occurrence of hydrodynamic complications in this study of 43 spinal cases in which DuraSeal was used. The complication rate of 16.3% was notably high and could be greatly improved by the development of a novel tissue sealant technology. Additionally, the most successful dural closure technique in this single institution study was the combination of a sutureless dural onlay material and DuraSeal tissue sealant. However, the complication rate for this technique was still 8.3%.

The results of this single institution clinical review of DuraSeal and dural closure procedures in addition to previous studies of cranial procedures show the limitations and high complication rates of the current dural closure technologies. Because no current techniques have been proven to be complication free in large and small clinical studies [Moskowitz et al., 2009], a stronger, adhesive, watertight sutureless dural replacement material has been designed and developed, which is further explained in the scientific sections of this work.

Part II

Design and Characterization of a Silk Dural Tissue Replacement

Chapter 8: Introduction

The ideal dura mater tissue replacement will be biocompatible, prevent CSF leakage and cortical adhesions, be anti-inflammatory, promote regeneration across the dural defect, and biodegrade at the same rate as neo-dura formation [Jackson et al., 2008; Kim et al., 2011].

Silk fibroin is an ideal material for the tissue replacement due to its tunable mechanical properties and biocompatibility. The silk fibroin material has good water vapor and oxygen permeability, blood compatibility, accelerates collagen formation and the proliferation of human skin fibroblasts [Kim et al., 2011]. Previous studies have shown that silk fibroin-based dural replacements inhibited inflammation in dura repair rat models and exhibited no cell toxicity [Kim et al., 2011]. Silk fibroin materials, therefore, show great potential for use as dural tissue replacements. Additionally, these materials can be created with different thicknesses and treatments to control the mechanical properties, such as methanol treatment [Lawrence et al., 2009] and water annealing [Jackson et al., 2008], and with varying surface topographies to promote dural cell migration across the material [Hu et al., 2011].

8.1 Design of Silk Fibroin Dual Layer Composite Dural Replacement

The silk fibroin dual layer composite material has been designed specifically for use as a dural replacement. Its two layers each have their own distinct morphologies and contributing functionalities [Figure 13].

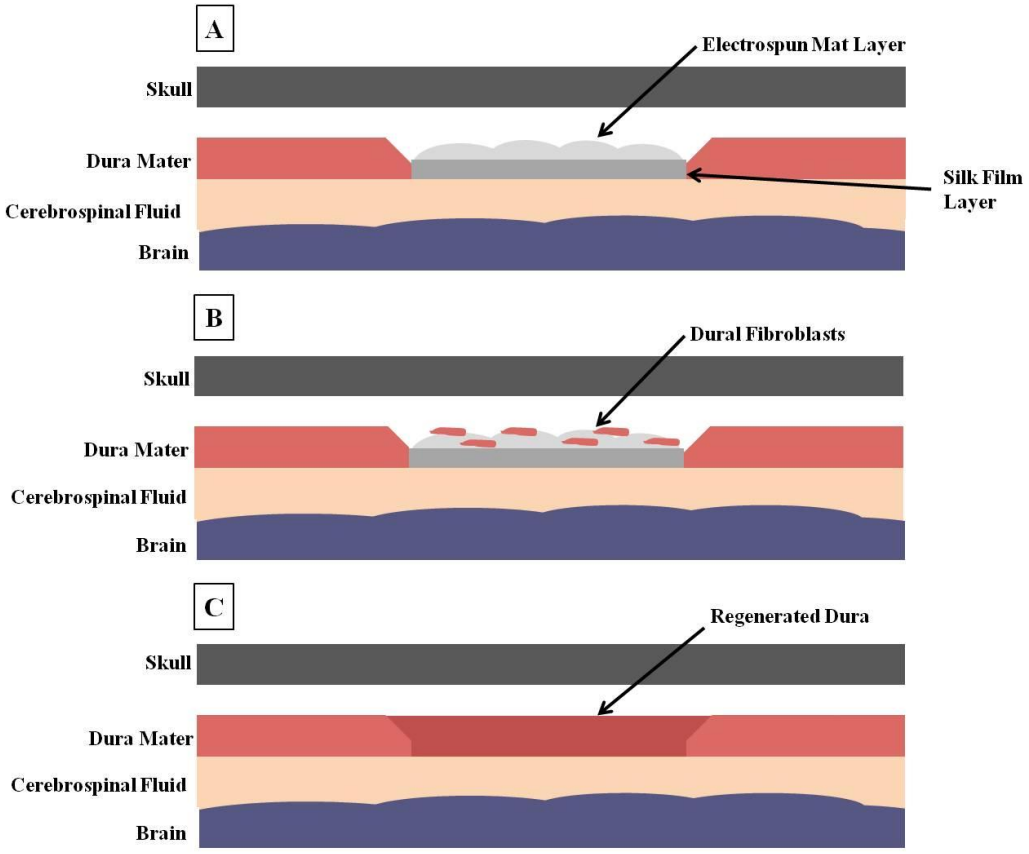

Figure 13: Schematic of silk fibroin dual layer composite material applied as a dural replacement. Once implanted into the durotomy site [A], each layer has its own functionality. The electrospun mesh layer promotes dural fibroblast ingrowth [B] and, therefore, eventual dural regeneration across the material as it biodegrades [C].

8.1.1 Electrospun Mat Layer

The electrospun mat layer of the dual layer composite has been designed to promote dural fibroblast adhesion to the replacement and enhance migration across the durotomy site. The electrospun silk material was chosen for this function because of the microscale mechanical environment it provides for host tissue and cell interaction. The electrospun silk scaffold mimics the structure and biological function of native extracellular matrix (ECM) proteins, which provide

mechanical support and control cell activity. Specifically, nonwoven electrospun scaffolds on the nanometer scale mimic the collagen multi-fibrils that compose the ECM 3D structure [Nishido et al., 1988]. This texture has been shown to control cell adhesion, proliferation, shape and function [Patel et al., 1998], and specifically that of fibroblasts, which are the most common cell type of the dura mater [Min et al., 2004; Xie et al., 2010]. The highly porous structure of the electrospun scaffold layer would allow dural cells to migrate and proliferate throughout its thickness and, therefore, promote dural regeneration. Following implantation of the silk dual layer composite material in the durotomy site, the electrospun mat layer will promote the integration and proliferation of the dural fibroblasts across the wound site and, therefore, promote dural regeneration [Figure 13B].

8.1.2 Silk Film Layer

Because the electrospun mat material is inherently porous, it cannot provide a water tight seal against CSF leak when used as an independent dural replacement material. The nonporous silk film layer is included in the silk dural replacement design for this purpose [Figure 13]. Silk films made from aqueous silk solution have oxygen and water vapor permeability that can be controlled by silk I and silk II protein structures [Minoura et al., 1990]. While this water vapor permeability allows for hydration of the material, it does not permit for liquid to flow through and, therefore, would function as a substitute membrane for CSF leakage prevention. In addition to sealing against CSF leak, the dural substitute must be designed to limit cortical adhesions. The silk film also has this

functionality because it is smooth and non-porous to limit cell attachment and recolonization on its surface. Smooth surface morphologies of substrates limit the speed and success of cell migration across them [Liu et al., 2009] and have been shown to limit tissue adhesion following implantation *in vivo* [Novitsky et al., 2007]. Therefore, the silk film layer would be implanted such that it is the layer closest to the cortical tissue or spinal cord when used for dural closure in neurosurgery [Figure 13]. While the electrospun mat layer promotes dural regeneration across it surface, the silk film seals against CSF leakage, provides mechanical robustness to the composite, and limits unwanted cortical or spinal cord tissue adhesion to the implant.

The dual layer composite silk biomaterial, therefore, has been designed to both mimic the microenvironment of the dura to promote tissue regeneration via the electrospun mat layer while acting as a successful physical barrier to unwanted neural tissue adhesions and CSF leakage via the silk film layer. And because the entire material is made of silk fibroin, it is biocompatible and biodegradable. As the material slowly degrades, dural regeneration will continue across the site until regenerated host dural tissue completely replaces the dural replacement material [Figure 13C].

Chapter 9: Materials and Methods

9.1 Silk Fibroin Processing

Silk fibroin protein was purified from dry *Bombyx mori* silkworm cocoons, resulting in an aqueous silk fibroin solution [Figure 14, Vepari and Kaplan, 2007]. Following removal of silkworms from dried cocoons, the cocoons were cut into small, flat segments. For each 5 g of silk cocoon fragments, a 2 L volume of distilled water was brought to a boil. Once boiling, 4.24 g sodium carbonate (Na_2CO_3) was added for every 2 L of boiling water. Once the sodium carbonate had completely dissolved, the alkaline solution was ready for the addition of the silk cocoons. The silk cocoon fragments were stirred into the boiling alkaline solution for time periods of either 10 minutes or 30 minutes, depending on the desired application of the resulting aqueous silk material. The exposure of the silk cocoon fragments to the boiling alkaline solution results in degumming of the fibers, or purification of sericin from the silk. Following the designated boiling times, the silk material was soaked in distilled water for two 30 minute rinse periods in order to remove any remaining sericin proteins. It was then left to dry overnight.

In order to transform the dry silk fiber material into aqueous silk fibroin solution, the material was solubilized in 9.3M lithium bromide solution at 60°C for 1 to 4 hours. The volume of the lithium bromide solution was calculated as four times the mass of the dried silk material. Following this dissolving step, the resulting silk and lithium bromide solution underwent dialysis to remove the lithium bromide. This was done by injecting the solution into dialysis cassettes or

dialysis tubing and soaking them in distilled water for a total of 48 hours. The dialysis water was changed at designated time points in order to ensure complete removal of lithium bromide via diffusion through the dialysis tubing. Following dialysis, the aqueous silk solution was centrifuged at 4°C and 4000 rpm for two intervals of 20 minutes in order to remove any residual particulate matter.

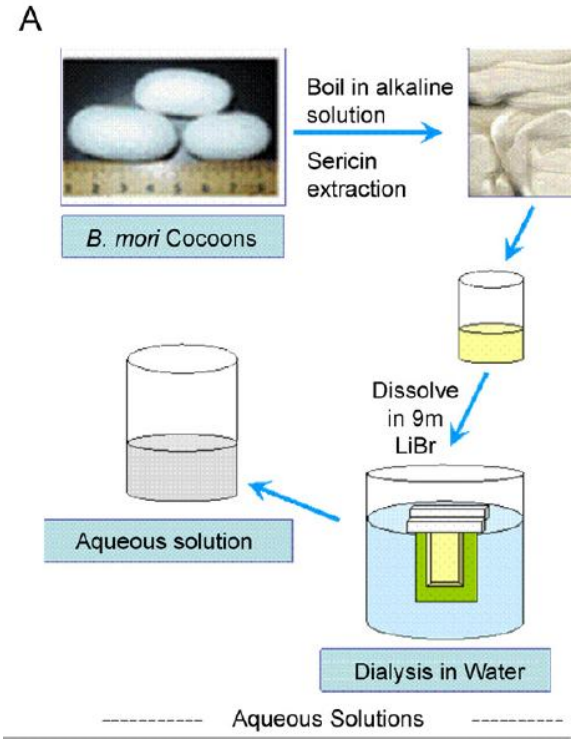

Figure 14: *Bombyx mori* silkworm cocoons were boiled in an alkaline solution to purify the silk fibroin proteins from sericin. This purified material was then processed by dissolving and dialysis techniques to result in an aqueous silk fibroin solution [Vepari and Kaplan, 2007].

In order to determine the final concentration of silk fibroin protein in the resulting aqueous silk solution, small volumes of the solution (0.1-0.5 ml) were weighed. The samples were then left at 60°C overnight or until completely dry. The dry weight was then measured. The final concentration calculation is as follows.

$$conc = \frac{dry}{vol}$$

In this equation, *conc* is the final silk fibroin concentration of the aqueous silk solution, *dry* is the measured mass of the dried sample, and *vol* is the volume of the original wet sample.

9.2 Production of Silk Fibroin Dual Layer Composite Material

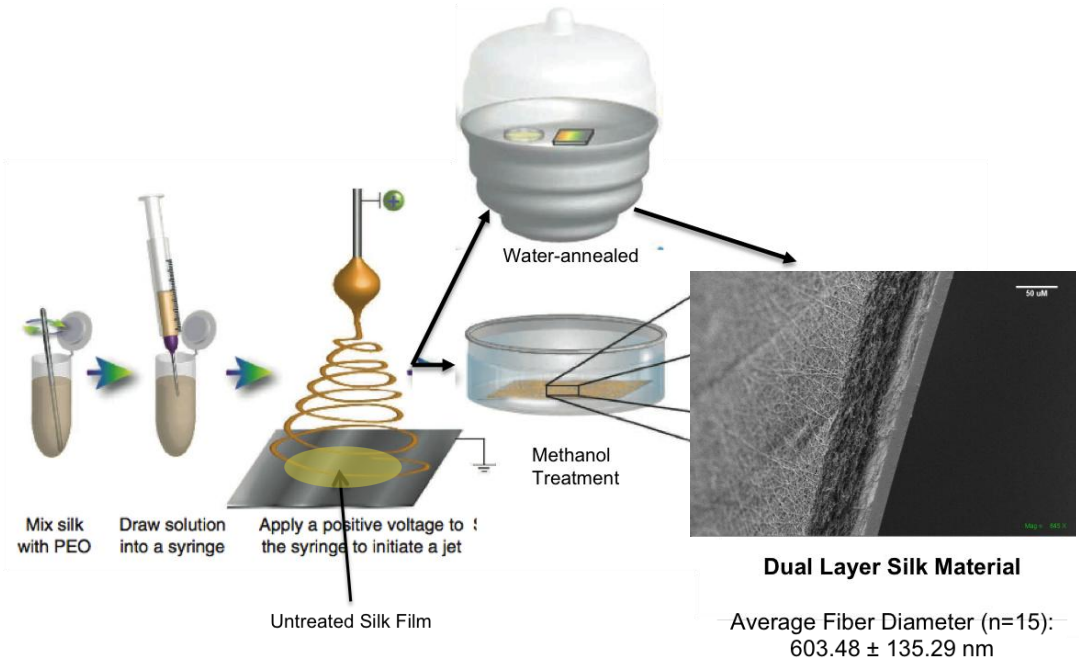

Figure 15: Schematic of the dual layer silk biomaterial fabrication process. Silk and polyethylene oxide mixture is electrospun directly onto an untreated silk film. The resulting dual layer material is then treated either by methanol or water-annealing treatments to produce an insoluble dual layer silk material for in vitro and in vivo testing [Rockwood et al., 2011].

A dual layer silk material, consisting of one layer of nonporous silk film, and one layer of nonwoven electrospun silk mat, is fabricated through a novel procedure that involves both silk film and silk mat production processes [Figure 15].

9.2.1 Silk Film Fabrication

The silk film layer of the dual layer silk material was made by casting silk fibroin solution onto flat surfaces [Figure 16]. Specifically, silk solution, prepared as previously described with a 30-minute boil time and ranging from 5-8% silk fibroin, were cast into 100 mm x 15 mm Petri dishes (Fisher Scientific, Waltham, MA) . Varying volumes were used in order to obtain silk films of varying thicknesses. The silk films were then kept in a dry, ventilated environment overnight in order to perform controlled drying that would avoid any structural changes [Hu et al., 2011]. Once dry, the silk films can be removed from the plastic Petri dishes to be used as the silk film layer of the dual layer silk biomaterial.

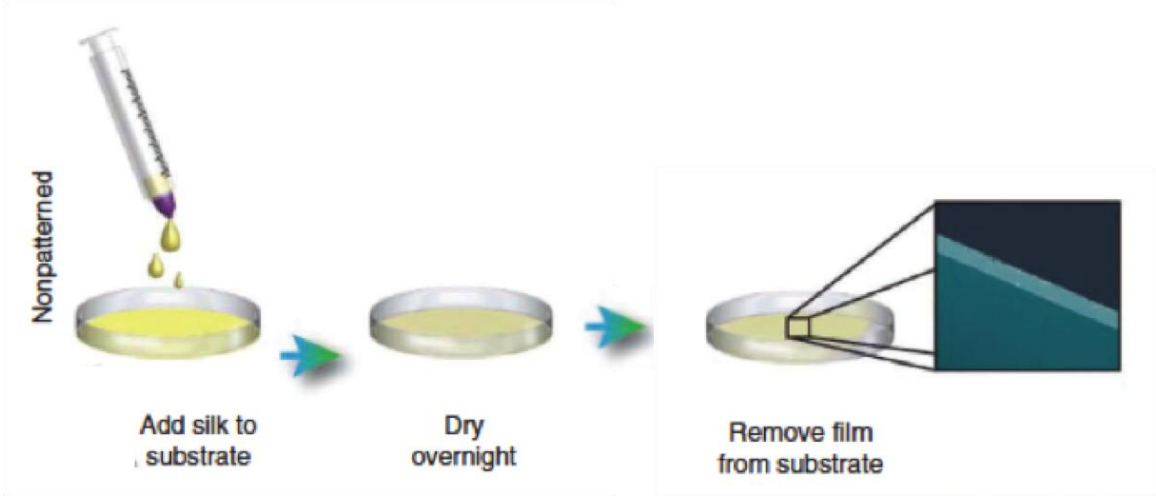

Figure 16: Schematic of nonpatterned silk film production [Rockwood et al., 2011].

9.2.2 Silk Electrospinning

9.2.2.1 Preparation of Spinning Solutions

Silk and polyethylene oxide (PEO) blends in water were prepared by adding 5% Poly(ethylene oxide) (PEO, Sigma-Aldrich Corp., St. Louis, MO) solutions directly into silk aqueous solutions. 5% PEO solutions were prepared by dissolved 5% w/v of PEO into distilled purified water. This was then mixed into silk fibroin solutions in a 1:4 PEO: silk ratio. The silk fibroin solutions used were 6-8% silk fibroin and produced with 30-minute boil times. Mixing was performed by syringing the solutions up and down until the solution appeared homogenous. It was then added into a syringe and left upside down in the refrigerator for approximately 20 minutes. Following this time period, the bubbles that accumulated at the top of syringe were forced out, resulting in a homogeneous silk/PEO mixture containing no air bubbles.

9.2.2.2 Electrospinning

Silk electrospinning was performed by electrospinning the viscous silk/PEO blend directly onto a silk film, which was produced as previously described. Electrospinning was performed with a 1.5 mm steel capillary tube mounted within an electrically insulated base. The capillary tube was maintained at a high electric potential via copper wire connection to a power supply (Gamme High Voltage Research, Ormona Beach, FL) [Jin et al., 2002]. The collection screen was a circular metal plate, which was covered with non-stick aluminum foil and secured on a rotating, grounded magnetic based. The rotating metal platform was positioned 10 cm below the capillary tube. This configuration

allowed for the metal plate to be electrically grounded while rotating in order to produce a random nonwoven electrospun mesh on the plate surface. A silk film was placed in the center of the collection screen such that the electrospun mat formed on its surface. And the capillary tube was connected to a syringe filled with 15-20 ml of silk/PEO spinning solution. A syringe pump (Orion M362-Sage Syringe Pump) was used to control and maintain a constant flow rate. This flow rate was set to keep the solution spinning from the tip of the capillary tube without dripping.

The flow rate and electric potential of the capillary tube were adjusted so that a stable fiber extended from the tip onto the rotating platform. On average, however, the capillary tube was maintained at 10 kV and the flow rate was set in the range of 1/100 X but varied in magnitude to ensure limited dripping.

Following electrospinning, the entire surface of the circular metallic plate is covered in a thin and even layer of electrospun mat. The silk film that is placed in the center of the platform, therefore, is also covered with a layer of electrospun mat. The mesh is able to incorporate with the silk film because the silk film is not treated to be insoluble.

9.2.3 Dual Layer Composite Material Crystallization Treatments

Once the dual layer silk material is produced through the processes described above, it must be treated to remove PEO from the electrospun fibers and to make the entire composite material insoluble and, therefore, usable for *in vitro* and *in vivo* testing.

9.2.3.1 Methanol Treatment

The treatment of silk with low dielecric constant organic solvents, such as methanol and ethanol, is the most common method for converting silk fibroin from random coil to β-sheet organization [Hu et al., 2011]. The dominance of alanine and glycine-rich hydrophobic domains in silk fibroin promotes the tight packing of hydrogen-bonded anti-parallel silk protein chains into the β-sheet organization [Vepari et al., 2007]. The tight organization of hydrophobic components results in insolubility of the material. Therefore, in order to make the dual layer silk material insoluble, it was soaked in 90/10 methanol/water solution for 10 minutes. It was then soaked in distilled water overnight in order to leach any residual methanol and the PEO from the electospun layer.

9.2.3.2 Water-Annealing

Another method to induce β-sheet crystallization of silk materials and, therefore, making them insoluble, is water vapor annealing. This is done by placing the dual layer material sample in a vacuum dessicator at room temperature. The vacuum is set to approximately -20 inHg for 3-6 hours. Following this time period, the sample is removed and left out overnight in air to dry. In order to remove remaining PEO from the electospun mesh layer, the sample is then soaked in distilled water for 12 hours as described above.

9.3 Morphology Characterization: SEM Imaging

Scanning Electron Microscopy (SEM) Imaging was used to qualitatively and quantitatively observe the morphology of produced dual layer silk materials.

The dual layer silk material samples were prepared as described above. Following their treatment and complete drying, samples of the material were mounted onto specimen stages (Electron Microscopy Sciences, Hatfield, PA) using copper tape (Newark Corp., Richfield, OH). The surface of the material to be imaged was face-up on the stages. For those specimens used to image the cross section of the material, additional preparation was needed. In order to obtain a clean cut and, therefore, a cross section with no deformation, liquid nitrogen was used. The samples were exposed to liquid nitrogen for 5-10 seconds. A razor blade was the used to crack the samples and expose the cross section. These samples were then mounted onto the copper tape with cross section exposed for imaging.

Mounted samples were then sputter-coated with gold in order to prepare for imaging. After preparation of the microscope, images were collected at a voltage of 5 V and a resolution of 1024 x 768 (Carl Zeiss Inc., model Supra 55VP. Thornwood, NY). Magnification varied between images.

9.3.1 Analysis of Electrospun Fiber Diameter

ImageJ software was used to determine the fiber diameter of the electrospun mat layer of the dual layer silk material. Images were taken of the electrospun mat surface on the SEM as described above. The scale was set in ImageJ based on the scale bar of the images used. This scale coordinated the value of μm and pixels. Once this scale was set, lines were manually drawn across the cross sections of clearly visible electrospun fibers. The measurement tool was then used to determine their diameters in μm. A total of 15 fibers were measured

this way for each analyzed image of the electrospun mesh layer. The average electrospun fiber diameter and standard deviation of the values were then calculated.

9.4 FTIR Analysis

Beta-sheet content of both layers of the dual layer silk composite material was measured by fourier transform infrared spectroscopy (FTIR) with an attenuated total reflectance accessory (ATR). The silk film and electrospun mat layers were analyzed from composite materials treated with 3 hour and 6 hour water annealing at room temperature, methanol exposure, and untreated composite samples. FTIR measurements were performed with a Bruker Equinox 55/S FTIR spectrometer (Bruker Optics, Billerica, MA).

Each spectrum was acquired in absorption mode on a ZnSe crystal by the accumulation of 10 scans with a resolution of 4 cm^{-1} and a spectral range of 4000-600 cm^{-1}. The spectra were Fourier self-deconvoluted (FSD) with SpectroManager spectroscopy software using the method reported by Hu et al. [2006]. The FSD FTIR spectra were fitted with Gaussian profiles in the amide I region, which occurs between 1595 and 1705 cm^{-1}. The four bands representing beta-sheet content were determined by Hu et al [2006] [Table 3]. The ratio of these bands to the total amide I bands was reported as the percent beta-sheet content in the material.

wavenumber range, cm^{-1}	assignment	reference
1605−1615	(Tyr) side chains/aggregated strands	16, 18, 34, 58
1616−1621	aggregate beta-strand/ beta-sheets (weak)[a]	27, 31, 58
1622−1627	beta-sheets (strong)[a]	15−18, 59
1628−1637	beta-sheets (strong)[b]	15−18, 27, 31, 34, 52, 58
1638−1646	random coils/extended chains	15, 27, 31, 34, 58
1647−1655	random coils	27, 34
1656−1662	alpha-helices	27, 34
1663−1670	turns	16−18, 27, 31, 60
1671−1685	turns	16−18, 27, 31, 60
1686−1696	turns	16−18, 27, 31, 60
1697−1703	beta-sheets (weak)[a]	27, 31, 34, 20, 21

[a] Intermolecular beta-sheets. [b] Intramolecular beta-sheets.

Table 3: Vibrational band assignments in the amide I region for *B. Mori* silk fibroin [Hu et al., 2006].

9.5 Mechanical Analysis

The overall goal of this research was to complete a preliminary study regarding the effect of the layers of the composite material and crystallization treatments on the mechanical properties of dual layer silk composite materials.

Silk fibroin electrospun mats have been previously analyzed for their mechanical properties, specifically for application in tissue regeneration. Adequate mechanical properties are required for successful tissue regeneration and host tissue interaction because any scaffold structure must provide sufficient mechanical properties during the process of tissue regeneration [Jin et al., 2003]. Because the composite material silk material includes both electrospun mat and silk film layers, the mechanical strength of each layer was determined and compared to that of the composite material in order to determine the mechanical

effect of each layer and the overall mechanical properties of the processed composite material.

9.5.1 Sample Preparation

Six silk films were made via solvent casting for use in composite material fabrication. The silk films were made by casting 3.5 ml of 8% aqueous silk solution into 100 mm Petri dishes, and were left to dry overnight. The resulting films were approximately 0.04 mm thick when dry. In order to make the composite material, the silk film was placed in the center of the circular rotating collector and 18 ml of silk/PEO solution was electrospun across its surface per the electrospinning protocol described above. Three of the silk films were electrospun onto and could be processed with different crystallization treatments. The remaining three silk films were used independently for crystallization treatments [Table 4].

Silk Material	Crystallization Treatment	Number of Samples Tested
Electrospun Mat	90% Methanol (10 min Soak)	n=3
	3 hour Water-Anneal	n=3
	6 hour Water-Anneal	n=3
Dual Layer Composite	90% Methanol (10 min Soak)	n=3
	3 hour Water-Anneal	n=3
	6 hour Water-Anneal	n=3
Silk Film	90% Methanol (10 min Soak)	n=3
	3 hour Water-Anneal	n=3
	6 hour Water-Anneal	n=3

Table 4: Samples of silk materials and their crystallization treatments prepared for tensile mechanical testing.

9.5.1.1 Methanol Treatment

One composite material sample was exposed to methanol treatment in order to induce crystallization of the silk material and, therefore, insolubility. The material was soaked in 90/10 (v/v) methanol/water for 10 minutes. The material was then left out to dry and cut into the Instron testing samples (5 mm x 4 cm). These testing samples were then soaked in distilled water overnight in order to leach out any PEO from the electrospun mat and to fully hydrate the material before mechanical testing. The thickness of the methanol-treated composite material was measured with a thickness gage (Mitutoyo, Aurora, IL) both before and after hydration.

9.5.1.2 Water Annealing

The other composite material sample was subjected to two different water annealing processes. After cutting the sample in half, one half was water-annealed for 3 hours and the other for 6 hours. The water annealing process was the same as described above, including annealing at room temperature and at -20 inHg vacuum pressure. Following both annealing procedures, Instron testing rectangular samples (5 mm x 4 cm) were cut from each treated material and soaked in distilled water overnight.

9.5.2 Uniaxial Tensile Testing

All uniaxial tensile tests were performed on an Instron 3366 testing frame (Instron, Norwood, MA) equipped with a 100 N capacity load sensor. The silk materials to be tested were cut into rectangular shape samples, 5 mm in width and 4 cm in length [Figure 17A, Hu et al., 2011]. Prior to mechanical testing, the

samples were hydrated in 0.1 M phosphate-buffered saline (PBS,Sigma-Aldrich Corp., St. Louis, MO) for 24 hours in order to reach a swelling equilibrium. All dimensions were recorded and mechanical analysis performed following PBS hydration in order to mimic the characteristics of the film in an *in vivo* environment. Following this hydration process, the thickness of each sample was measured using a dial thickness gage. Test samples were then submerged in a testing container filled with PBS solution [Figure 17C]. The displacement settings used on the Instron included a crosshead displacement rate of 5 mm min^{-1} and a gauge length of 15 mm. Each sample was secured into the Instron clamps using sandpaper and tape, and the test was run until the silk material failed through tearing. The raw data was recorded through a load vs. elongation graph. This procedure was performed on three replicates for sample group [Table 4].

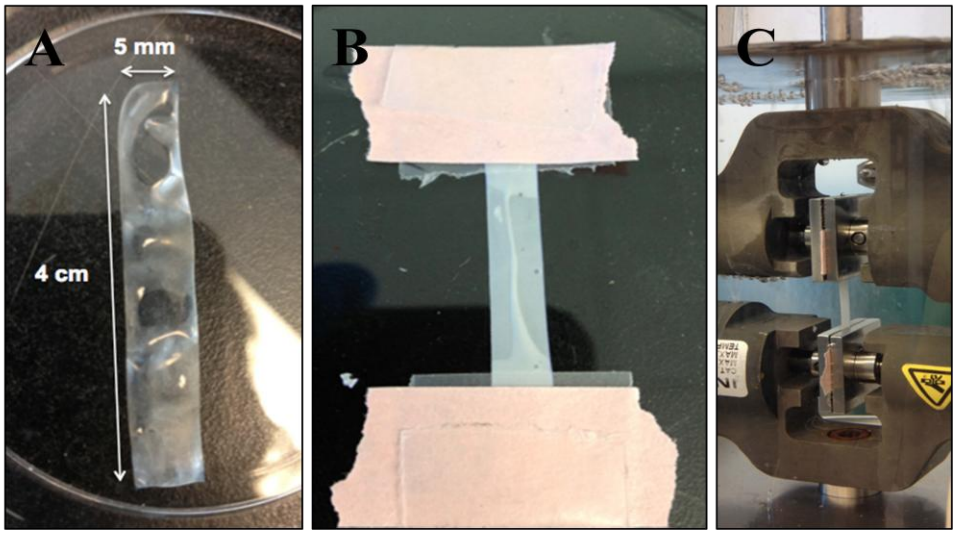

Figure 17: Silk film rectangular sample for Instron mechanical testing with dimensions of 5 mm by 4 cm [A] secured with sand paper and tape pre-testing [B]. Uniaxial tensile testing in PBS hydrated environment was performed on each sample [C].

9.5.2.1 Mechanical Data Analysis and Calculations

Instron uniaxial tensile testing was performed on the silk film samples as described previously. For each treatment group, three replicates were tested for their elastic modulus (MPa), tensile stress at 15% strain (MPa) and ultimate strain (%). These mechanical parameters were calculated from the plots of load (N) vs. elongation (mm), which were first converted into stress vs. strain plots. For each sample, the measured thickness was multiplied by the sample width of 5 mm in order to obtain its cross sectional area. Each load data point was converted to values of stress (MPa) by the calculation below:

$$Stress = \frac{F}{A} = \frac{Load}{A}$$

Strain is defined by force (F) over cross-sectional area (A) so each load data point was divided by the cross sectional area of the corresponding sample. The elongation axis was converted to percent strain by calculating:

$$Strain = \frac{l_f - l_i}{l_i}$$

In this equation, l_f signifies the final elongation of the sample and l_i is the initial elongation, which was the 15 mm gage length unless the sample was loaded with slack. If so, the extension length at which the sample was first pulled taught was determined as the initial elongation.

The initial elastic modulus, tensile strength, and tensile strength at 15% strain (material failure) values were calculated from the stress/strain plots. The initial elastic modulus was calculated by using a linear least-squares fitting between 0.02 N preload and 10% strain past this initial point. The tensile strength

was defined by the tensile stress point observed at the failure strain of each composite sample, which was determined to be 15% strain. The ultimate strain value was determined by the strain corresponding to ultimate failure or breaking of the material. This is a required definition for this study because the composite materials were able to continue elongating after one layer had failed at the ultimate tensile strength. Following one layer failure, the composite material was deemed a failure because the material being tested in the Instron was no longer the entire composite.

9.5.2.2 Statistical Analysis

Following calculations of initial elastic modulus, tensile strength, and ultimate tensile strain, sample sets were statistically compared and analyzed by using a two-tailed, unpaired Student *t* test analysis of means.

9.6 Biocompatibility and Cell Viability Analysis

9.6.1 Cells and Cell Culture

9.6.1.1 Neural Cells

Dissected rat cortices from embryonic day 18 rat pups were kindly provided by the Steven J. Moss Lab in the Tufts University Neuroscience department. Following dissection, the cortices were dissociated in 0.5% trypsin (Invitrogen, Inc., Carlsbad, CA). After additional media was added to the dissociated tissue, the tube was centrifuged to collect all cells in pellet form. After the supernatant was carefully removed, the cells were resuspended in Neurobasal media (Invitrogen, Inc., Carlsbad, CA) by pipetting the pellet up and down. The tube was then left to sit for 2 minutes in order for residual debris to settle to the

bottom. The cell solution was then carefully removed and suspended in a calculated volume of Neurobasal media containing B27 supplement, anti-anti (1%) and Glutamax (1%, Invitrogen, Inc., Carlsbad, CA). This neural cell solution, which primarily consisted of neurons and astrocytes, was then used for neural cell experiments.

9.6.1.2 Human Dermal Papilla Fibroblasts

Dermal papilla fibroblasts isolated from a 37 year old female were provided by Celprogen, Inc. (San Pedro, CA). Specifically, passage 5 cells were used. The cell culture media used previous to and during this experiment was DMEM, 10% FBS, 1% anti/anti (Invitrogen, Inc., Carlsbad, CA) .

Passage 4 human dermal papilla fibroblasts were washed of media and incubated in 0.5% trypsin (Invitrogen, Inc., Carlsbad, CA) for 5 minutes. The unadhered cells were then collected in 50 ml of media and centrifuged at 4°C, 1200 rpm for 10 minutes. After the cell pellet was redistributed in the media, cells were counted using a hemocytometer (Sigma-Aldrich Corp., St. Louis, MO) . The cell concentration of 1.3×10^6 cells/ml was diluted down to the desired seeding density of near 10,000 cells/ml. The passage 5 human dermal papilla fibroblasts were ultimately diluted to a concentration of 9.4×10^4 cells/ml.

9.6.2 Composite Material Sample Preparation and Cell Seeding

The viability of both neural cells and dermal fibroblasts was observed on five different surfaces: silk film, silk electrospun mat, silk film layer of dual layer silk composite, electrospun mat layer of dual layer composite, and a control,

which was tissue culture plastic of a 24-well plate. A dual layer silk composite was made as described above. The areas around the silk film on the electrospinning rotator consisted only of electrospun silk and these were used as electrospun mat samples for this experiment. Additionally, a silk film of the same volume as that used in the composite was cast. All three materials were treated with three hours of water-annealing at room temperature. They were then dried and set overnight.

In order to cast the cells directly onto the four different material types, they had to be converted to a format such that they could cover the bottom of 24-well plates. Therefore, a 15 mm biopsy punch was used to make discs of each material. These samples were then sterilized and adhered to the bottom of the wells in the sterile fume hood. This was done by added 1 ml of 70% reagent ethanol (Sigma-Aldrich Corp., St. Louis, MO) to the wells and dropping the material samples onto the top of the ethanol. As the ethanol vaporated, the samples were sterilized and dried to the bottom of the wells. In order to secure them to the bottom, 15 mm diameter O-rings, which were previously soaked in 70% ethanol, were placed on top of each sample in order to secure its edges to the bottom of the well [Figure 18].

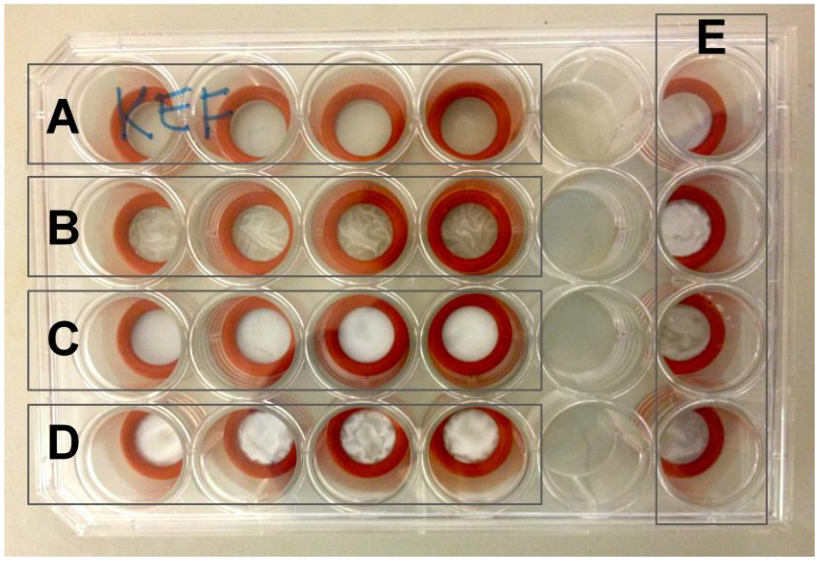

Figure 18: Experimental set up of neural cell viability analysis on silk biomaterials. Wells were covered by silk films (row B), electrospun mats (row C), composites with electrospun mat layers in contact with cells (row D) and composites with silk film layers in contact with cells (column E). All of these samples were compared to a control group of tissue culture plastic (row A). Each condition consisted of 4 sample wells (n=4).

9.6.2.1 Neural Cell Seeding

Before seeding of the rat neural cells onto the silk materials, the samples and wells were pre-treated for neural cell seeding by soaking in 300 μl of 0.01% poly-l-lysine (PLL, Sigma-Aldrich Corp., St. Louis, MO). Poly-L-lysine is the most widely used cell adhesion molecule (CAM) used in neural tissue culture due to its excellent neural cell adhesion capability. Its natural positive charge attracts neurons by electrostatic interactions with their negatively charged cell membranes and promotes neurite outgrowth [Harnett et al., 2007]. Therefore, since the majority of neural cell culture is conducted on lysine-coated surfaces, all culture surfaces were soaked in PLL for this experiment.

After the PLL coating step, neural cells, isolated from the cortical tissue of day 18 embryonic rats as previously described, were seeded at 1 x 10^6 cells per well. This was done by first counting the cell concentration of the cell stock solution resulting from the cell isolation process. This concentration was then diluted down until there were 1 x 10^6 neural cells/ml. Then 1 ml of this solution was added to each well of the 24 well plate. The cells were cultured at 37°C under a humidified atmosphere of 5% CO_2. The supplemented Neurobasal culture media was refreshed every 3 days.

9.6.2.2 Dermal Papilla Fibroblast Seeding

As previously described with neural cells, the viability of human dermal papilla fibroblasts was observed on five different surfaces: silk fibroin film, silk electrospun mat, silk film layer of dual layer silk composite, electrospun mat layer of dual layer composite, and a control, which was tissue culture plastic (TCP) of a 24-well plate. These experimental surface materials were produced and prepared for cell culture in a 24-well plate as described previously [Figure 18]. There were four replicates of each surface, with a total of 20 wells being used. Each surface was soaked in the cell culture media overnight at 37°C and a humidified atmosphere of 5% CO_2.

After the soaking media was aspirated from the materials in a sterile hood, 1 ml of the 9.4 x 10^4 cells/ml solution was added to each of the 20 wells. The cells, therefore, were seeded at 9.4 x 10^4 cells/well. The dermal fibroblast cell cells were cultured at 37°C under a humidified atmosphere of 5% CO_2. The supplemented DMEM culture media was refreshed every 2 days.

9.6.3 AlamarBlue® Cell Viability Assay

AlamarBlue® (Invitrogen Life Sciences, Grand Island, NY) is a cell viability reagent used to monitor nonspecific cell health and proliferation. Resazurin, the active component of alamarBlue® is a non-toxic cell permeable compound, that upon entering living cells, is reduced to resorufin. Therefore, the blue non-fluorescent resazurin is continuously converted to the red, highly fluorescent resorufin by viable cells. This redox reaction allows alamarBlue to indicate the quantitative and qualitative health of cells in culture. In this experiment, alamarBlue was used to determine the viability of neural cells and dermal fibroblasts on the different silk material surfaces of the dual layer composite material.

On day 5 and day 7 of neural cell culture and day 1, day 3, day 5 and day 7 of dermal fibroblast culture, a 10% alamarBlue solution was sterilely prepared (2 ml alamarBlue solution, 18 ml supplemented Neurobasal media). The media component of the solution was warmed in the water bath prior to the 10% alamarBlue solution preparation. In a dark sterile hood, the media was carefully aspirated from each well and 1 ml of the 10% alamarBlue solution was added. The plate was then incubated in a 37°C, 5% CO_2 humidified environment for 2 hours. During this entire process, the plate and alamarBlue solution were kept out of direct light in order to preserve the fluorescent dye.

Following the incubation time period, three 200 μl samples (n=3) were taken from each well and put into a 96-well opaque black plate. This was done for each of the four wells of the four cell-seeding surface conditions [Figure 18] in

addition to three control wells. These control wells (n=3) contained no seeded cells and only the tissue culture plastic surface. The fluorescence was then read by placing the 96-well plate in a plate reader (SpectraMax M2 Multi-Mode Microplate Reader, Molecular Devices, Sunnyvale, CA). The readings were obtained using an excitation wavelenth of 550 nm and emission wavelength of 590 nm.

9.6.3.1 Quantitative Viability Calculations and Statistical Analysis

Fluorescent readings were obtained for each 200 μl sample in the 96-well plate. There were 3 samples per each cell-seeded-well of the 24 well tissue culture plate. The neural cell viability on each silk surface was determined as the average of the four well replicates and normalized to the Day 5 TCP control. The dermal fibroblast viability was determined as the average of the four well replicates and normalized to the Day 1 TCP control [Wray et al., 2011].

All sample sets were performed with four replicates (n=4) and the values expressed as normalized means ± standard deviation (SD). Sample sets were statistically compared and analyzed by using two-tailed, unpaired Student *t* test analyses of means.

9.6.4 LIVE/DEAD® Fluorescence Cell Imaging

In order to determine the relative amounts of living and dead cells and their morphologies on Day 7 of culture, LIVE/DEAD® Cell Imaging Kit (488/570) (Invitrogen Life Technologies, Eugene, OR) and fluorescence microscopy was used. According to the kit, 1 ml of 1 μM Live Green solution was

added to 1 mM lyophilized stock of Dead Red and mixed thoroughly. The functional component of Live Green is green-fluorescent calcein-AM, which indicates intracellular esterase activity. The functional component of Dead Red is red-fluorescent ethidium homodimer-1 to indicate loss of plasma membrane integrity.

On Day 7, media was aspirated and cells were washed twice with PBS. Then, 500 μl of the mixed LIVE/DEAD solution was added to each well. The plate was then incubated for 15 minutes at room temperature out of direct light. Following the incubation period, the dye solution was carefully aspirated in order to avoid fluorescent background levels during imaging, and 1 ml of PBS was added to each well. The cells were then imaged using a fluorescent microscope (Axiovert 40 CFL, Zeiss, Thornwood, NY). Two to three images were taken per well in order to observe the general morphology and distribution of neural cells on the different surfaces.

9.6.5 Scanning Electron Microscopy (SEM) Imaging

Following fluorescence imaging on Day 7, the cell-seeded materials were fixed for scanning electron microscopy (SEM) imaging. Following washing the materials with 1X PBS, 1 ml of 10% formalin (Fisher Scientific, Waltham, MA) was added to each well, and they were fixed for 30 minutes under the fume hood. After this fixing time, the formalin was removed and the materials were washed twice with 1X PBS. In order to dry the samples for SEM imaging, a graded ethanol dehydration process was used [Table 5]. All ethanol solutions were made by diluting 100% ethanol with calculated volumes of deionized water.

% Ethanol Solution	Time Period
50%	20 min
75%	15 min
95%	15 min
100%	15 min
100%	15 min

Table 5: Graded ethanol dehydration process for SEM imaging of cellular scaffolds and wet materials.

After the above process, the cells were completely dried and fixed onto the dry silk materials and, therefore, ready for SEM imaging. Following their treatment and complete drying, samples were mounted onto specimen stages (Electron Microscopy Sciences, Hatfield, PA) using copper tape. The samples were mounted with cell-surfaces up.

Mounted samples were then sputtered with gold for 120 seconds and positioned in the SEM mounting stage. After preparation of the microscope, images were collected at a voltage of 5 kV and a resolution of 1024 x 768 on the Carl Zeiss Inc. Supra 55VP Scanning Electron Microscope. Magnification was varied between images in order to see different levels of cell and silk material surface morphologies.

9.6.6 Confocal Imaging

In order to determine the cell viability and their 3D interactions with the dual layer composite material, confocal imaging of both neural cells and dermal papilla fibroblasts was performed on a Leica DM IRE2 confocal microscope (Leica Microsystems, Buffalo Grove, IL).

Images were obtained when cells were seeded on the silk film layer and on when seeded on the electrospun mat layer of the dual layer silk composite. While the total thickness of each image stack varied based on cell location within the frame, the steps within each image stack were 4 μm/image and two averages were used in order to limit background. The resulting stacked images consist of overlay images with fluorescent settings to obtain live and dead fluorescent objects and bright-field to give dimension to the final stacked image.

9.7 *In vitro* Enzymatic Degradation

9.7.1 Sample Preparation

Dual layer silk composite materials were produced as previously described. The material was treated with one of four crystallization treatments: untreated (control), 3 hour water anneal at room temperature, 6 hour water anneal at room temperature, or 10 minute treatment in 90% methanol. Water-annealed samples were dried in open-air overnight. Methanol treated samples were soaked in de-ionized water for 12 hours in order to remove residual methanol and PEO before being left to dry overnight in open air.

From each type of material, 8 mm biopsy punches were used to obtain discs of 8 mm in diameter. Two of such discs were used together to make up each testing sample. Therefore, the total area of material in each sample was 100.48 mm^2, consisting of 2 disks with areas of 50.24 mm^2 each. Twelve samples (24 discs) were made for each treatment condition: untreated, 3 hr anneal, 6 hr anneal, and methanol treated. The samples were then placed in 25 mm diameter Transwell inserts with 3.0 μm pores that secure within 24-well plates. These

samples were then split between testing in control solution (1X PBS, Sigma-Aldrich Corp., St. Louis, MO) and degradation solution (Protease XIV from Streptomyces griseus, Sigma-Aldrich Corp., St. Louis, MO). One 24-well plate was used for PBS treatment while the other was for Protease XIV treatment.

In order to obtain a baseline initial weight, each sample was soaked in PBS for three hours. After this process, the samples were treated with the drying process that would be used before each weight-loss time point in the 14-day study. This process is explained below. The initial weight was measured after the soaking and drying process rather than as a dry weight of the sample in order to mimic the sequence of events that would within the *in vitro* degradation test and account for any residual moisture present after the drying-process.

9.7.2 In vitro Degradation Test

After measurement of their initial "wet" weight, the dual layer silk composite samples (n=6 per group, n=4 for weight loss, n=2 for imaging at time points) were incubated at 37°C in 1.5 ml solution of 1 U/ml Protease XIV (from Streptomyces griseus, Sigma-Aldrich Corp., St. Louis, MO) in 1X PBS or in PBS as a negative control. The plates were placed on rotating shakers in a 37°C 5% CO_2 incubator in order to create a dynamic environment and to limit the dissolution of the Protease XIV solution. This solution was made and changed daily and the PBS solution was also changed daily. Protease XIV solution was made by added a calculated mass of thawed Protease XIV dry powder to a

calculated volume of 1X PBS and vortexing until the powder was completely dissolved.

On days 1, 3, 5, 7, 11, and 14 of the 14-day degradation study, samples were washed, dried, and weighed for weight-loss calculations. After the solutions were removed from the transwell plates, samples were washed twice with 2 ml of de-ionized water. Following the second wash, the transwell inserts were screwed into the top of 15 ml falcon tubes such that they remained upright with the porous membrane towards the bottom of the falcon tube. The samples were then centrifuged at 37°C at 3000 rpm for 15 minute in this configuration. This was done to remove residual water and small degraded materials from the wells. The transwell inserts were then placed back into the dry 24-well plates. The samples and their transwell inserts were in labeled containers throughout this process in order to maintain their condition identity. The transwell plates were then placed in the 60°C oven for 30 minutes to complete the drying process. Samples were then weighed within their transwell inserts. At the end of the 14 day study, remaining samples were removed from the transwell inserts if able to do so. The transwell inserts were then cleaned by 1.5 hours sonication treatments in warm deionized water. This treatment was used in order to clean the inserts of any silk and/or protease residual mass. After drying overnight at 60°C, the mass of each transwell was measured.

On days 3 and 7, a sample from each sample group was removed from the experiment in order to be used for SEM imaging. Therefore, of the six samples prepared in each condition and each solution treatment, two were used for

imaging, and four were maintained throughout the 14 day experiment for weight loss calculations. All remaining samples were combined for photographs following the study.

Degradation was quantified by determining the percent weight loss of each sample. This calculation appears below.

$$\%weightloss = \frac{w_i - w_c}{w_i} * 100 \quad \%we$$

w_i = Initial "Wet" Weight

w_c = Current "Wet" Weight

The weights are defined as "wet" weights because they follow soaking in either PBS or Protease XIV solutions. Although they are washed and dried through centrifugation and oven-drying, it is possible that residual moisture exists within the material. By using the weight of the samples following this process as the baseline measurement as well (w_i), this residual moisture is taken into account and normalized.

9.7.3 Statistical Analysis

All sample sets were performed with n=4 and the values expressed as normalized means ± standard deviation (SD). Sample sets were statistically compared and analyzed by using two-tailed, unpaired Student *t* test analyses of means.

Chapter 10: Results and Discussion

10.1 Fabrication of Silk Dual Layer Composite Biomaterial

10.1.1 Electrospinning of Silk/PEO Solutions

Aqueous silk solutions (6-8% w/v) without PEO do not electrospin because the viscosity and the surface tension of the solution are not high enough to maintain a stable drop at the end of the capillary tip [Jin et al., 2002]. Because higher concentrations of silk increase viscosity but also result in gelling, PEO was added to the silk to increase viscosity. PEO was added in the ratio of 4:1 silk:PEO (5%) as described in the literature [Jin et al., 2002]. The distance between the tip and the collector was 10-15 cm. In order to maintain a drop at the end of the capillary tip, the field strength was set at 10 kV and the flow rate was around 0.033 ml/min. With these settings, the drop was maintained and had a cone shape with a visible fiber extending from the bottom. Fibers eposited onto the aluminum foil circular rotating collector and eventually became visible on the silk film covered area. The fibers appeared to be randomly distributed in a nonwoven mat and eventually covered the entire surface of the collector.

The morphology and diameters of the electrospun fibers were examined using SEM. The silk/PEO blend resulted in fine uniform fibers that had average diameters of 603.48 ± 135.29 nm [Table 6]. This morphology and diameter mimics that of silk nanofibers documented in literature [Jin et al., 2004] and successfully mimics the structure of the ECM, which consists of crosslinked

networks of multi-fibril collagen proteins with diameters ranging from 15 μm to 5 nm [Xu et al., 2005; Min et al., 2004].

Ratio of silk/PEO blend (wt/wt)	PEO Blend Solution Concentration (%)	Applied Field Strength (kV)	Average fiber diameter (nm)
4/1	5%	10	603.48 ± 135.29

Table 6: Spinning solution composition, applied field strength, and resulting fiber diameter of electrospun silk used in dual layer composite fabrication.

10.1.2 Mechanism of Composite Material Fabrication

As previously described, the dual layer composite material is fabricated by electrospinning directly onto an untreated silk film. Previously, other methods had been used to make the composite material. These methods, including annealing the two materials together and casting a silk film onto a pre-made electrospun mesh, however, resulted in silk materials with varying properties and inconsistent morphologies.

The process of electrospinning directly onto a silk film utilizes the solubility of untreated silk fibroin. Silk fibroin that has not undergone physical or chemical crystallization treatments exists primarily in the turn and random-coil silk protein conformation, which is soluble [Lu et al., 2010]. Therefore, the silk film is a smooth surface of dry but soluble silk fibroin protein. As the silk/PEO solution is electrospun onto this surface, the silk nanofibers are believed to dry as they are spun toward the collector plate [Pham et al., 2006]. Although the electrospinning set up was designed with flow rate and distance between the capillary tube and collector to allow for such drying, the nanofibers do not appear

instantly on the surface of the silk film. Instead, fibers do not appear to significantly cover the film surface until at least 30 minutes of spinning [Figure 19].

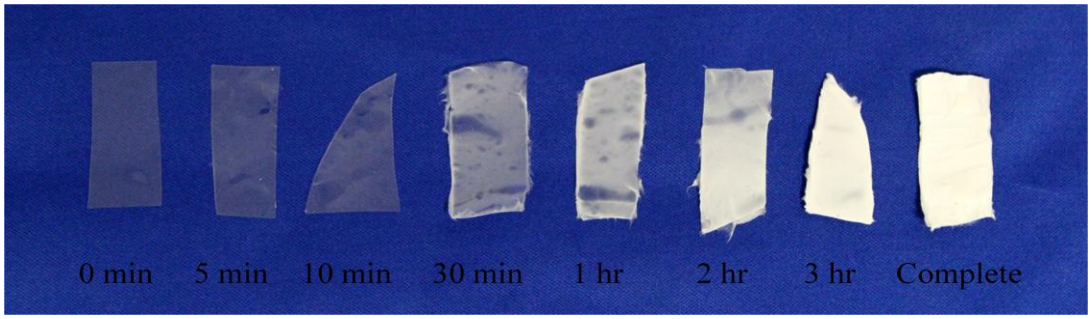

Figure 19: Macroscale image of spinning process onto untreated silk films. Due to the solubility of the untreated silk film, the electrospun fibers do not maintain their fiber morphology and appear on the silk film surface until around 30 minutes of electrospinning.

During this time period, however, there are nanofibers constantly being deposited onto the entire surface of the collector plate. Due to the solubility of both the silk film surface and the silk nanofibers, the nanofibers are dissolving into the silk film surface, which effectively acts as a solvent surface. As this occurs, it is theorized that the dissolved nanofibers build up and create a texturized surface to the silk film [Figure 20]. This texturized surface allows falling fibers to spin across ridges of silk material. And, over these ridges, they do not come in contact with untreated soluble silk and, instead, are able to fully dry and maintain their nanofiber morphology. As this process continues, the silk film grows in texture and a nanofiber mesh is able to build off of the surface [Figure 20].

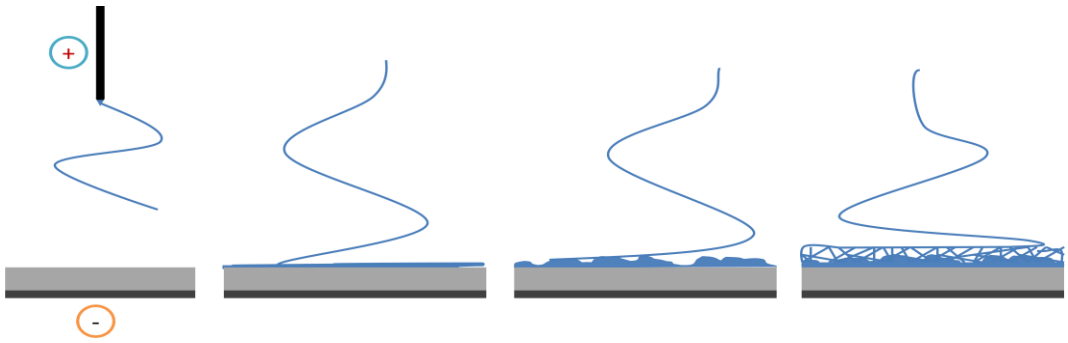

Figure 20: Schematic of silk fibroin dual layer composite fabrication process. The electrospun mat layer builds off of the untreated silk film due to the formation of an intermediate layer of solubilized nanofibers.

The resulting composite, therefore, consists of a silk layer and electrospun mesh layer that are joined by a layer of solubilized nanofibers This is clearly demonstrated in the SEM image of the cross section of the dual layer composite [Figure 21]. In Figure 21A, there are three distinct layers with the nonporous silk film present on the bottom and the silk electrospun mesh on the top. In the middle, there is a mixture of solid silk material and nanofibers, which is more visible in Figure 21B. At this higher magnification, there is clearly a difference between all three layers with the middle layer being a mixture of both film-like and electrospun mesh material. These images support the above theory [Figure 21] regarding the process of this composite fabrication.

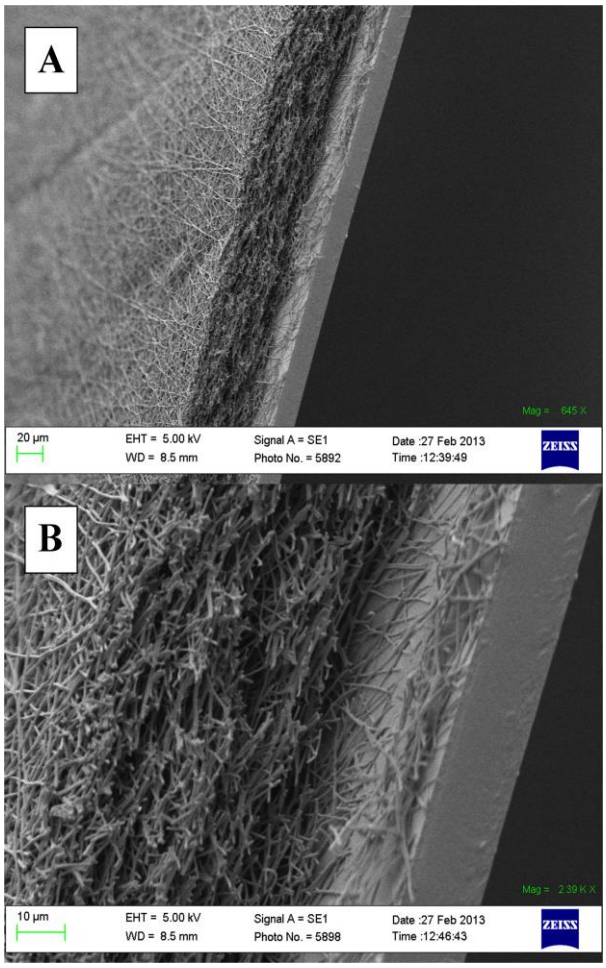

Figure 21: SEM image of cross section of silk fibroin dual layer composite material.

10.1.3 Resulting Silk Dual Layer Composite Biomaterial

The fabrication procedure as described previously results in an all-silk material with two different materials and morphologies on either side: an electrospun mat and a nonporous smooth film [Figure 22]. The two sides have the surface topographies of their respective silk forms, but are combined into a single composite material.

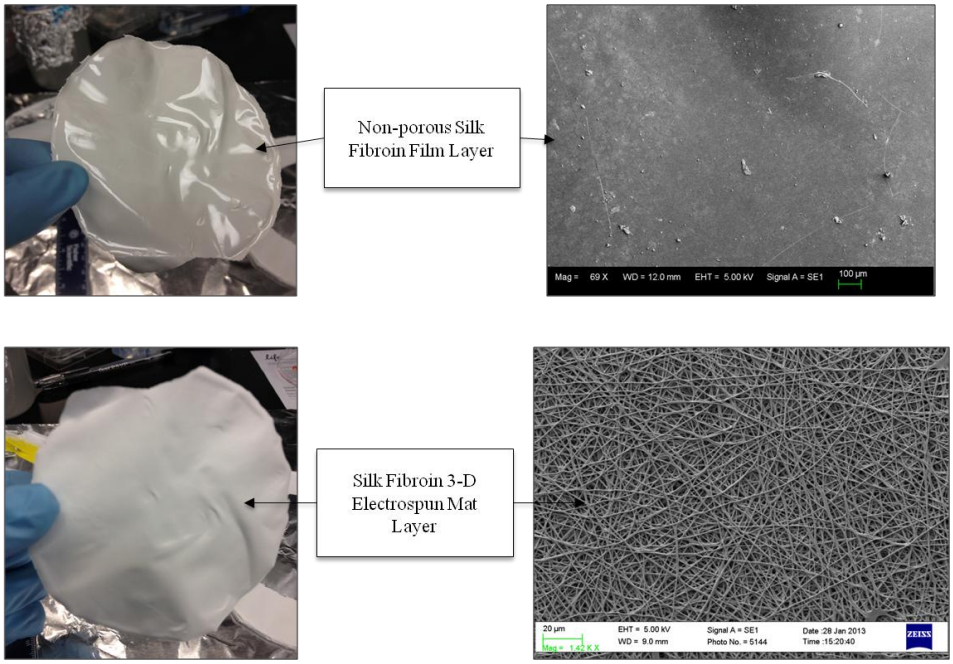

Figure 22: Macroscale and SEM images of the two layers of the silk fibroin composite material: a nonporous silk film layer and a silk electrospun mat layer.

10.1.3.1 Dimensions of Dual Layer Composite Material

The fabricated composite consists of a silk film that was cast as 3.5 ml of 6-8% 30 minute boil silk into a Petri dish. Following overnight drying, these films have an average dry thickness of 35 μm. Approximately 20 ml of silk/PEO solution was then spun onto the entire circular collector, which had a radius of 5 cm. The resulting composite, therefore, had an increased thickness due to the added electrospun mesh layer. The composite had a thickness significantly greater than the thickness of silk films (also 3.5 ml of 6-8% 20-minute boil silk) and of electrospun mat [Figure 23]. The electrospun mat samples were taken from areas of the collector that were not covered by silk film. Therefore, these areas had the same amount of nonwoven random fibers deposits on its surface than the silk film

surface. The trend of a thicker composite was maintained for all crystallization treatments of the biomaterials.

Although the composite is fabricated as a combination of both the silk film and electrospun mat processes, its thickness does not add up to the sum of the two separate silk biomaterials. Figure 23 shows both the theoretical thickness of the silk composite material and the measured thickness. If the electrospun mat spun directly onto the silk film and both materials maintained their original (film) and expected (electrospun mesh) morphologies, neither thickness would be different than when the materials are fabricated independently. However, the thicknesses of the composite materials are significantly lower for the water-annealed materials compared to the sum of the thicknesses of the two layer materials. In fact, there is an **18.7%** and **22.0%** decrease in thickness of the composite material compared to the total thicknesses of the two layer materials for the 3 hour and 6 hour water annealed conditions respectively.

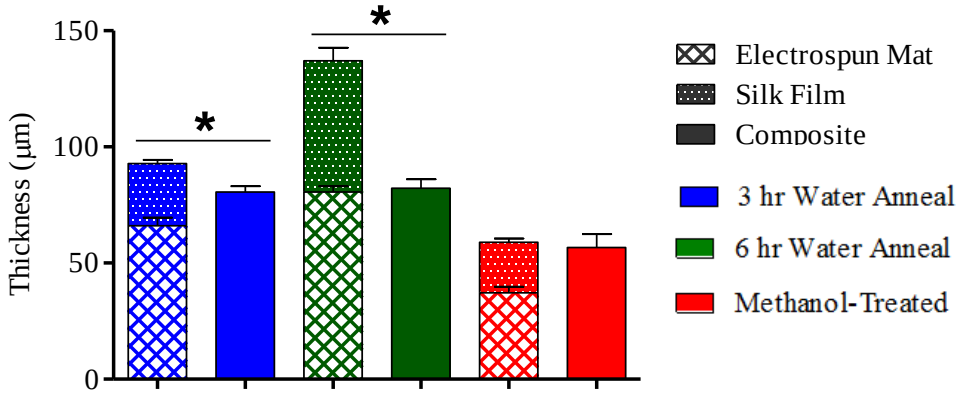

Figure 23: Comparison of theoretical composite thicknesses, as calculated by adding measured thicknesses of electrospun mat and silk film materials with each crystallization treatment, to actual composite thicknesses. The measured composite material thicknesses were significantly lower than the theoretical combined material thicknesses for both water-annealing treatments, but not for methanol treated materials [n=3, $p<0.05$].

The lower thickness of the composite materials also supports the previously described theory of the composite fabrication process. Although the thickness of the pre-made silk film would not be expected to decrease during the electrospinning process, the process of electrospun fibers dissolving onto its surface would decrease the ultimate thickness of the mesh layer and, therefore, the thickness of the composite material. Instead of a nonwoven mesh with large pores and, therefore, large area, the nanofibers condense into a film-nanofiber mixed layer of silk [Figure 20, Figure 21]. This condensing of nanofibers increases the thickness of film-like material in the composite while decreasing the thickness of electrospun mat as compared to that collected on the non-silk collector surface. By attributing the decrease in composite thickness to a decrease in the electrospun mesh layer compared to the thickness of the independent material, the thickness loss in the electrospun mesh layer specifically can be calculated. In fact, for the 3-

hour and 6-hour annealed conditions respectively, there was a 27.6% and a 34.5% decrease in the thickness of the electrospun mat layer as a result of the composite material fabrication process ; specifically, spinning onto an untreated silk film.

10.2 Effects of Crystallization Treatments on Silk Dual Layer Composite

As previously described, in order to render silk fibroin insoluble in aqueous media, crystallization of the protein must be accomplished. Specifically, the naturally occurring random coil of silk I protein conformation, which promotes solubility in water, must be crystallized to predominantly beta-sheet conformation, which is insoluble in water [Wilson et al., 2000]. The dual layer composite materials were treated with both chemical and physical crystallization treatments to eliminate solubility in water. For the chemical crystallization treatment, the composite material was soaked in 90/10 (v/v) methanol/water for 10 minutes [Jin et al., 2002]. The physical treatment was room temperature water vapor annealing for two different time periods: 3 hours and 6 hours. The silk fibroin structural changes after each of the three treatments were observed by FTIR.

10.2.1 FTIR Analysis of Beta-Sheet Content

Infrared spectroscopy with Fourier self-deconvolution is a common method for the quantitative method to study the protein composition of silk materials [Hu et al., 2006]. In this study, the beta-sheet content of the dual layer composite was assessed by Fourier self-deconvolution of the FTIR spectrum in the amide I region (1600 – 1700 cm^{-1}). This method allows the typically indistinct amide I band to be transformed to yield a fitted self-deconvoluted set of bands

from amide I, from which the secondary structural elements of the silk fibroin can be determined [Hu et al., 2006]. The identifiable secondary structural elements are turns, alpha-helices, random coil, beta-sheets, and side chains. The vibrational band assignments for these different elements were obtained from literature. In order to obtain the beta-sheet content of the dual layer composite material, the bands of interest were 1616-1621 cm^{-1}, 1622-1627 cm^{-1}, 1628-1637 cm^{-1}, and 1697-1703 cm^{-1}. These bands are assigned to aggregate intermolecular beta-strand/beta sheets (weak), intermolecular beta-sheets (strong), intramolecular beta-sheets (strong), and intermolecular beta-sheets (weak) respectively [source]. The relative areas of these bands were used to calculate the percentage of beta-sheet content in the silk materials [Figure 24].

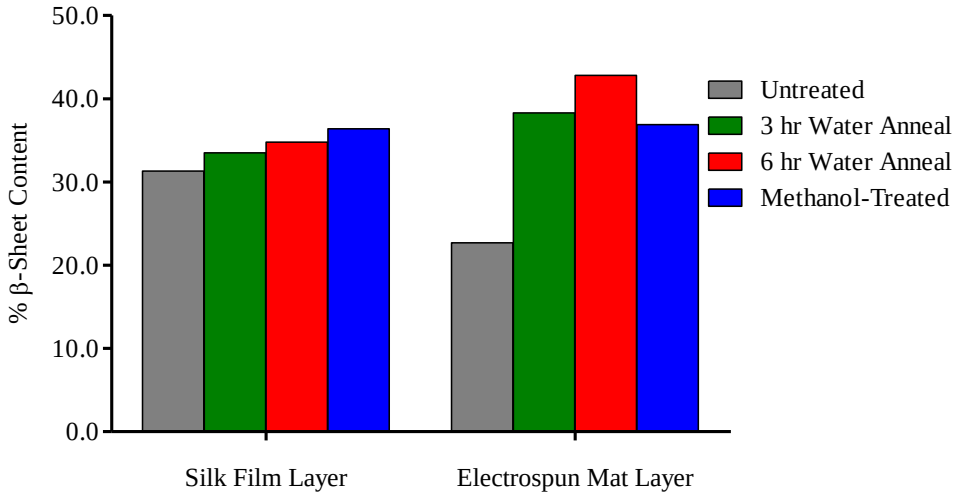

Figure 24: Beta-sheet content of the silk film layer and electrospun mat layers of composite materials with three different crystallization treatments as determined by FTIR (n=1).

As was expected, the beta-sheet content of both the electrospun mat layer and silk film layer within the dual layer composite material increased with

crystallization treatments. The silk film beta-sheet content increased from an untreated value of 31.3% beta-sheets, to 33.1% after 3 hours of water-annealing at room temperature, 33.7% after 6 hours of water-annealing, and 35.5% after methanol treatment. The electrospun mat beta-sheet content increased from 21.75% in the untreated mat to 39.3% after 3 hour water anneal, 41.1% after 6 hour anneal, and 35.35% after methanol treatment [Figure 24]. Although these trends were mostly expected, the beta-sheet content of the untreated materials was higher than seen in literature. This was most likely due to the fact that the material had been made a few days previously and was left at room temperature in an open environment. This exposure to air and mild humidity could have resulted in increased beta-sheet content. Additionally, it would be expected for methanol treatment to result in the greatest crystallization of the silk fibroin in both the mat and film states. In fact, methanol treatment can result in approximately 55% beta sheet content [Hu et al., 2006] while room temperature water-annealing usually results in only around 30% crystalline structure [Lu et al., 2010]. The lower beta-sheet content observed in both layer of the composite materials could have resulted from a short methanol exposure, which was only 10 minutes. This was used only to induce insolubility and not maximize beta-sheet crystalline content.

10.2.2 Effects on Composite Material Morphology

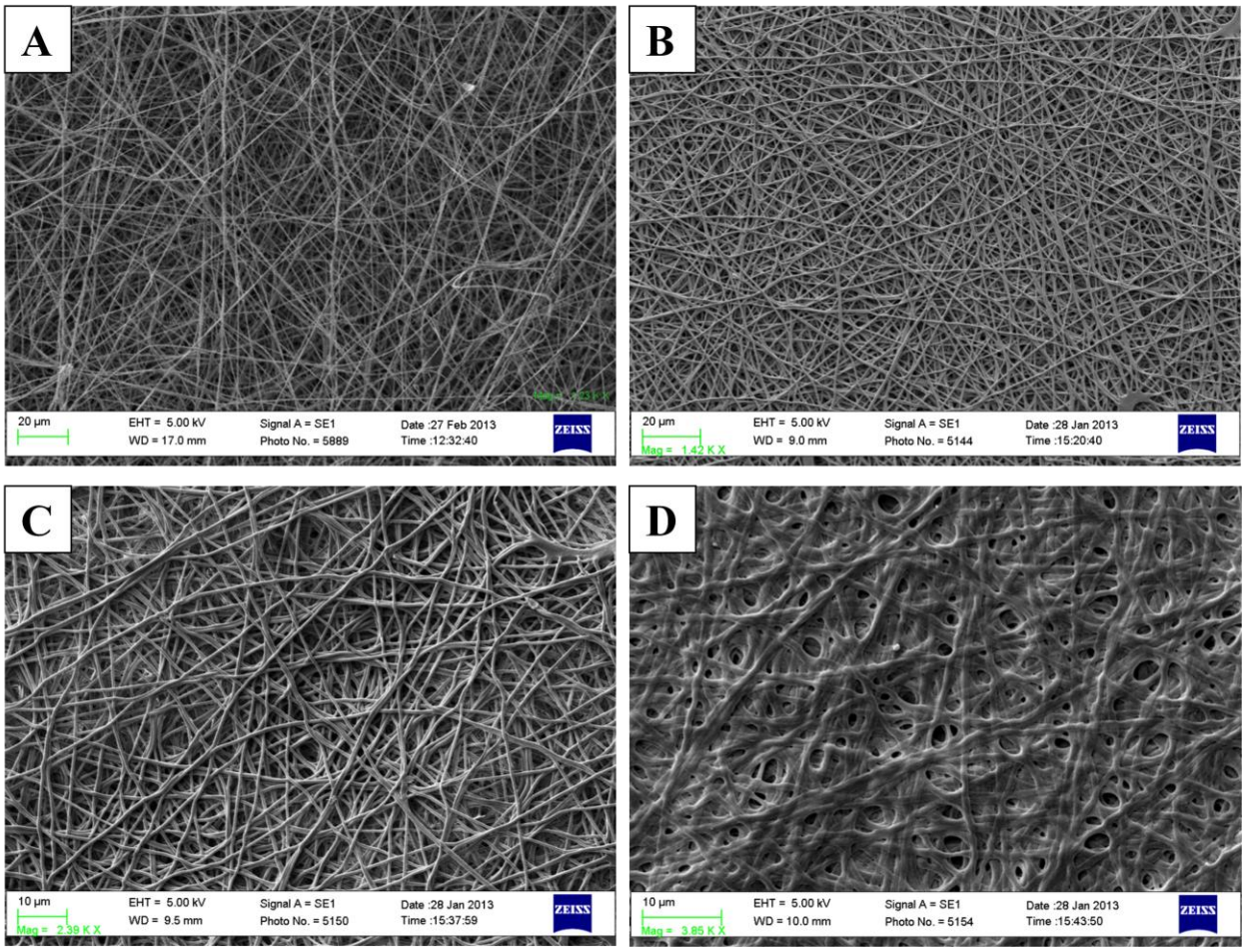

Figure 25: The effect of crystallization treatment on morphology of electrospun mat layer of dual layer silk composite material as compared to the untreated material [A]. The 3 hour water annealed [B] and 6 hour water annealed [C] materials maintained similar fiber morphologies while methanol exposure significantly changed fiber and overall electrospun mat morphologies [D].

The surface texture of the electrospun mat layer of the silk fibroin composite was assessed by SEM [Figure 25]. Fibers treated by water annealing had noticeably different morphologies than those treated by methanol. These fibers exhibited circular cross sections and smooth surfaces compared to the increased surface roughness of methanol treated fibers. Additionally, the packing density of the fibers appears to be affected by the treatments. The untreated mat

layer has thin fibers that appear to have large pores between them both on the horizontal plane and the vertical plane. The water annealed mat layers do not have fibers of different surface morphology than the untreated mat. However, they appear to be more closely packed and, therefore, make a denser mat with smaller pores. The methanol treated fibers, however, look as if they are melded together where they overlap and have a very dense network of interactions. They appear to be very closely packed in both the horizontal and vertical planes. Therefore, the methanol treatment shrinks the mats to form a denser structure and network of fibers [Min et al., 2004]. This process would explain the significant effect of methanol treatment on the thickness of the composite material [Figure 25]. The methanol treatment resulted in thinner materials compared to the water annealed treatments because of the dehydrating effect of methanol resulting in shrinkage and denser packing of fibers in the electrospun mat layer.

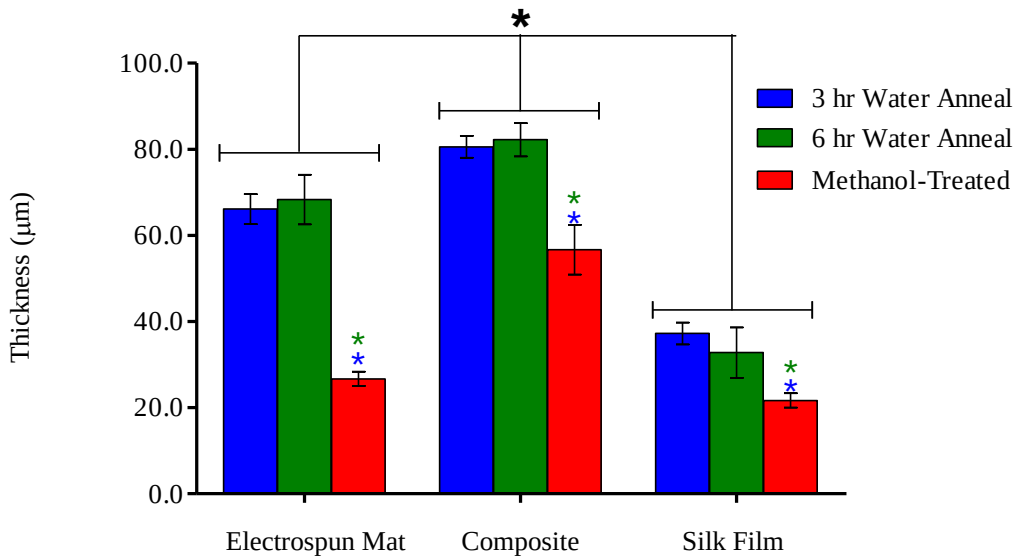

Figure 26: Thickness measurements of silk materials and the effect of crystallization treatments on material thicknesses (n=3). Methanol treatment resulted in significantly thinner thicknesses of all material types [$p<0.05$]. Within each crystallization treatment, there were significant differences in thicknesses between electrospun mat, composite, and silk film treated materials.

It has been previously observed and documented that methanol treatment is significantly harsher to electrospun materials compared to water annealing or controlled drying techniques [Meinel et al., 2009]. This is possibly caused by phase separation between silk fibroin and PEO, possibly due to extraction of the PEO in the methanol during the 10 minute soak [Vandermiers et al., 1998]. Additionally, the dehydrating action of methanol could account for the change in dimensions of methanol treated electrospun mats. In addition to the documented decrease in thickness of the composite material and of electrospun mats alone [Figure 25], previous research has shown that porosity of electrospun materials decreases as a result of methanol treatment. Min et al.[2004] showed that 60 minute treatments in 50% methanol at room temperature resulted in a porosity

decrease from 76.1% to 68.1%. They concluded that the methanol treatment shrunk the electrospun mat material resulting in a denser structure and a higher dimensional stability due to the significant increase in silk fibroin crystallization.

Overall, the silk fibroin crystallization, electrospun fiber morphology, and composite material dimensions were changed by the crystallization treatments. These characteristics of the material independently and in combination affect the mechanical properties and biocompatibility of the material, specifically how cells are able to interact with the material.

10.3 Mechanical Testing

Uniaxial tensile testing was used to determine the mechanical characteristics and tunability of the silk fibroin dual layer dural substitute. The tensile strength at material failure [Figure 27], the elastic modulus [Figure 28], and ultimate strain [Figure 29] of the composite material was calculated.

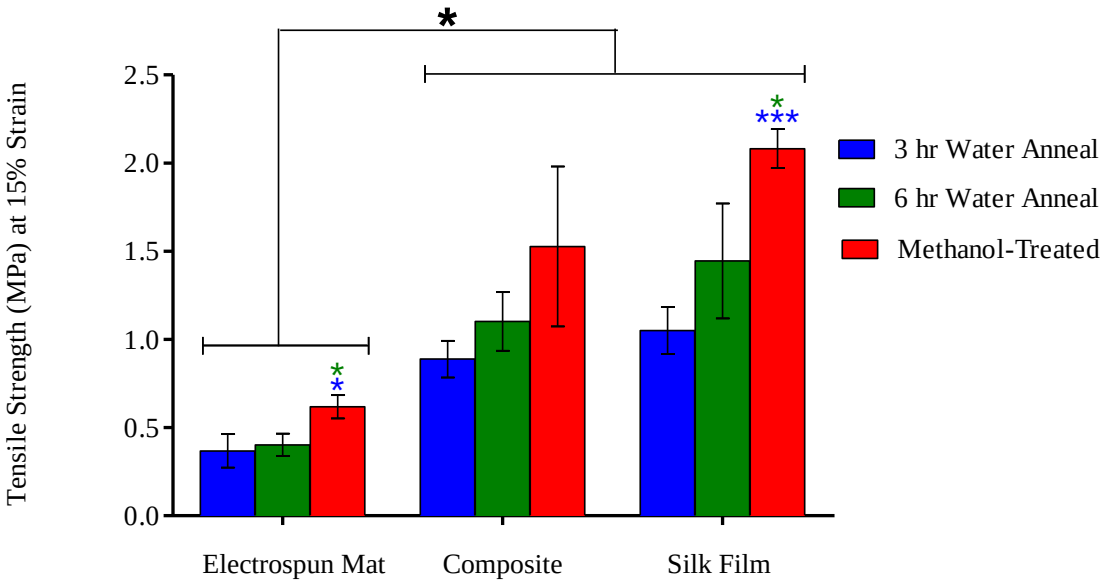

Figure 27: Tensile strength at 15% strain for the dual layer composite material and its individual component materials with three different crystallization treatments. All electrospun mat samples had significantly lower strengths than the composite and silk film samples of coordinating crystallization treatments [n=3, $p<0.05$].

The yield point of a material is defined as the stress at which a material begins to deform plastically. Prior to the yield point the material will deform elastically and will return to its original shape when the applied stress is removed. After the yield point of the three examined silk biomaterials, they are no longer able to regain their original shape and, therefore, were deemed to have irreversible material failure. This material failure was defined to occur at 15% tensile strain for all three forms of silk biomaterial: electrospun mat, dual layer composite, and silk film [Figure 27]. The tensile strength at material failure, therefore, is represented as the tensile strength at 15% strain.

Among the crystallization treatments, methanol-treatment significantly increased the tensile strength of both the electrospun mat and silk film materials [Figure 27]. In terms of biomaterials, the silk electrospun mat biomaterial had a significantly lower tensile strength at the defined failure point compared to the composite and silk film materials for samples of all three crystallization treatments. There was no significant difference, however, between the tensile strength of the dual layer silk composite compared to that of the silk film at 15% strain for all treatments [Figure 27]. This demonstrates that the silk film is the load-bearing element of the composite and defines the tensile strength of the material.

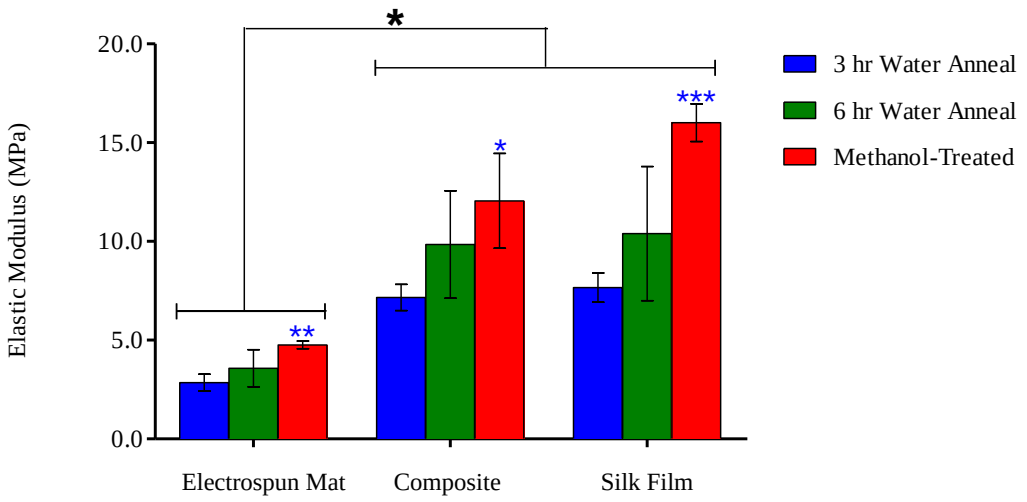

Figure 28: The effect of crystallization treatment on the initial elastic modulus of electrospun mat, silk film, and dual layer composite silk materials. Across all three treatments, the elastic modulus was significantly lower for the electrospun mat samples [n=3, $p<0.05$].

Similar to the tensile strength, the elastic modulus of electrospun mat samples is significantly lower than that of both the composite and silk film

biomaterials for samples at all three treatments. However, there is no significant difference in the initial elastic modulus of the composite and silk film samples [Figure 28]. Additionally, for each biomaterial, the methanol treatment significantly increased the elastic modulus compared to the 3 hr anneal treatment. In fact, methanol treatment increased the average modulus (n=3) from 2.8 to 3.8 MPa for electrospun mats, 7.2 MPa to 12.1 MPa for dual layer composites, and 8.2 for 16.0 MPa for silk film samples.

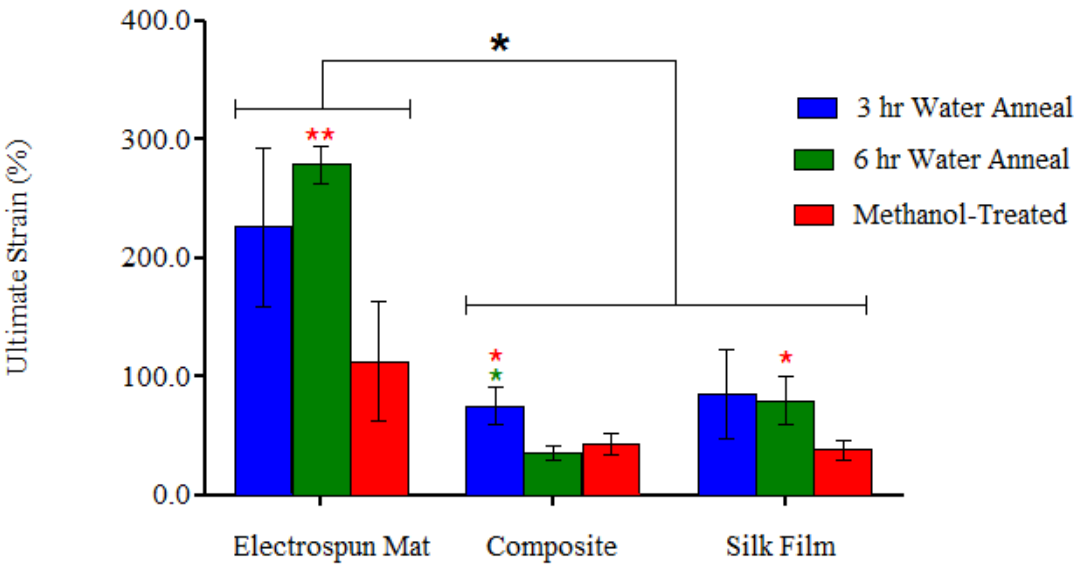

Figure 29: The ultimate strain of the three silk materials with three different crystallization treatments. The electrospun mat samples had significantly larger ultimate stain values for all treatments compared to coordinating composite and silk film samples [n=3, $p<0.05$].

The ultimate strain of three tested biomaterials was defined as the strain at material breaking. The electropsun mat samples were significantly higher than each coordinating sample group of the composite and silk film samples. The composite materials, however, did not have a significantly different ultimate

strain than the silk film samples at each treatment. In terms of each biomaterial, treatment condition did have a significant effect on the ultimate strain of the material. For silk electrospun mats, methanol treatment had a significantly lower ultimate strain that that of the two water-anneal treatments. The methanol treated composite samples had significantly lower ultimate strains that the 3 hour water – annealed samples, and the methanol treated silk film samples broke at a significantly lower strain that the 6 hour water-annealed film samples.

10.3.1 Mechanical Characteristics and Tunability of Silk Dual Layer Composite

The mechanical properties of the silk dual layer composite, specifically the tensile strength at 15% strain, elastic modulus, and ultimate strain, were defined by the silk film layer [Figure 27, Figure 28, Figure 29]. The silk film tested was the same as that used in the composite-fabrication process, specifically 3.5% 6-8% silk cast into a Petri dish at room temperature overnight. And there was no significant difference between the treated silk film samples and the respective treated composite samples. Based on the result that the silk film layer defines the mechanical properties of the overall composite, the composite material can be understood and further mechanically designed.

The mechanical properties of the silk dual layer composite biomaterial can be altered by beta-sheet crystallization of the silk film layer [Figure 27, Figure 28, Figure 29]. Under tensile testing, silk fibroin biomaterials undergo typical extended platform degradation and fibroin chain breaks that define their mechanical activity and which can be directly controlled by their protein structure (silk I vs. silk II) [Hu et al., 2011]. Specifically, increased beta-sheet content has

been shown to result in enhanced stiffness of materials [Lawrence et al, 2011]. As shown in Figure 24, the beta-sheet content of silk films increases with increased length of room temperature water annealing, specifically 3-hour to 6-hour and, and has the greatest percentage of beta-sheet content following methanol treatment. These treatments, therefore, also increase the elastic modulus, tensile strength, and decrease the ultimate strain of the silk films. By understanding the effect of both chemical and physical crystallization treatments, the mechanical properties of silk films can be tuned. And since the mechanical properties of the dual layer silk composite are defined by the silk film layer, the mechanical properties of the composite can also be designed by crystallization treatments.

10.3.2 Mechanical Design for Use as a Dural Substitute

Successful tissue regeneration can occur when the optimal cellular microenvironment is presented to the regenerating host tissue. In addition to physical interactions and signaling molecules from surrounding cells, the stimuli that define this microenvironment include the chemical, physical and mechanical properties of the implanted scaffold. The mechanical properties of the scaffold must mimic those of the host tissue in order to promote regeneration of that tissue. In fact, mechanical properties including the elasticity of the scaffold directly affect cellular function and interaction with the material. The motility [Wong et al., 2003], cytoskeletal organization [Peyton et al., 2007], differentiation [Engler et al., 2006], cell contractile forces, and related cell functions are influenced by the elasticity of the underlying substrate [Kloxen et al., 2010]. Therefore, in order to promote dural fibroblast adhesion, motility, and proliferation across a durotomy

site, the ideal dura substitute would have mechanical properties that mimic those of the natural dura [Table 7].

Graft Material	Thickness (μm)	Tensile Strength (MPa)	Young's Modulus (MPa)	Tearing Strength (MPa)
human dura mater (15 pieces)	626 ± 91.4	8.80 ± 2.37	2.75 ± 1.41	1.9 ± 0.57
Lyodura (5 pieces)	551 ± 121.5	11.93 ± 3.23	12.4 ± 5.76	2.32 ± 0.68
new dural substitute (5 pieces)	220 ± 3.78	11.4 ± 2.84	27.5 ± 8.09	6.42 ± 0.9

* Values are expressed as the mean ± standard deviation.

Table 7: Mechanical properties of human dura mater and two other dural substitute studied by Yamada et al. [1997].

The ideal dural substitute would mimic the mechanical properties of the natural dura in more ways than one. The mechanical microenvironment must be designed to promote successful dural fibroblast growth across the wound site, while the more macroscale mechanical characteristics of the material must allow for successful integration with the host tissue. In fact, the elastomeric dural tissue requires an equally elastomeric scaffold in order to limit mechanical friction between it and the host tissue. Such friction could result in a chronic inflammatory reaction at the durotomy site, resulting in intracapsular hemorrhage [Yamada et al., 1997]. For example, a major complication of a polytetrafluorethylene dura replacement was irritation due to friction resulting from strong surface tension and poor adaptability of the synthetic material [Islam et al., 2004].

Therefore, the goal of the design of elastic properties of the silk dual layer composite biomaterial is to have a dural replacement that successfully mimics the

elasticity of the dura. The elastic modulus of the dura is 2.75 ± 1.41 MPa [Table 7]. Although the composite material has a higher modulus than this for all three crystallization treatments [Figure 29], it falls in the same range as some other leading dural substitutes [Table 7]. Additionally, its modulus is on the lower end of the ranges or lowers than the values completely. Therefore, the dual layer composite material better mimics the modulus of the natural dura compared to these materials [Table 7]. Additionally, as previously described, the silk composite biomaterial can be further designed for mechanical tuning closer to that of the natural dura.

The electrospun mesh layer of the composite has been specifically designed to promote dural cell ingrowth and regeneration across the dural wound site. In addition to its 3D morphology promoting such host cell interaction, the elastic modulus of the mesh layer is consistent with that of the natural dura. The modulus of the nonwoven silk electrospun mat range from approximately 2.5 MPa to 5 MPa based on crystallization treatment [Figure 28], which overlaps with that of the dura [Table 7]. This is exactly in the range of the natural dura and, therefore, mimics the mechanical microenvironment seen by dural fibroblasts. By combining this elasticity and the ECM-mimicking silk fibroin nanofibers, the electrospun mat layer of the composite successfully models the mechanical microenvironment of the natural dura and, therefore, would be expected to promote dural fibroblast adherence, motility, and, therefore, regeneration across the biocompatible silk biomaterial.

10.4 Fibroblast Biocompatibility and Cell Viability on Dual Layer Composite Biomaterial

As previously described, the dual layer silk composite material has been designed as a dural substitute and, therefore, will exist in direct contact with dural fibroblasts when implanted *in vivo*. Additionally, the electrospun mat layer of the composite was designed to promote dural fibroblast adhesion and ingrowth within its 3D structure to more effectively facilitate dural tissue regeneration [Figure 13].

Histologically, the dura mater consists of dural fibroblasts in a rich network of collageneous fibers [Zhou et al., 2006]. Within the connective-tissue family, fibroblasts are the least specialized cell type and are dispersed throughout the body, where they secrete a non-rigid extracellular matrix rich in collagen type I and/or type II [Alberts et al., 2002]. This functionality, in addition to their morphologies, are preserved in locations throughout the body, until they differentiate into other cell types. When their tissue is injured, the nearby fibroblasts proliferate and migrate to the wound site where they produce large amounts of collagenous matrix to induce tissue repair and regeneration [Alberts et al., 2002]. Due to their functionality and high presence in the dura mater, fibroblasts play a key role in the repair of the dura mater. The viability of fibroblasts, therefore, on the dual layer composite silk dural substitute was tested.

Because dural fibroblasts were unable to be obtained from the small mice and rat models, human dermal papilla fibroblasts were cultured on the surfaces of the dual layer silk dural substitute. These cells were specifically chosen because dermal fibroblasts have shown to be easier to handle in culture. They do not show

the same plasticity that fibroblasts from other bodily tissues have and, therefore, would be expected to remain as fibroblasts throughout their culture on the silk dural substitute.

10.4.1 Cell Viability Analysis

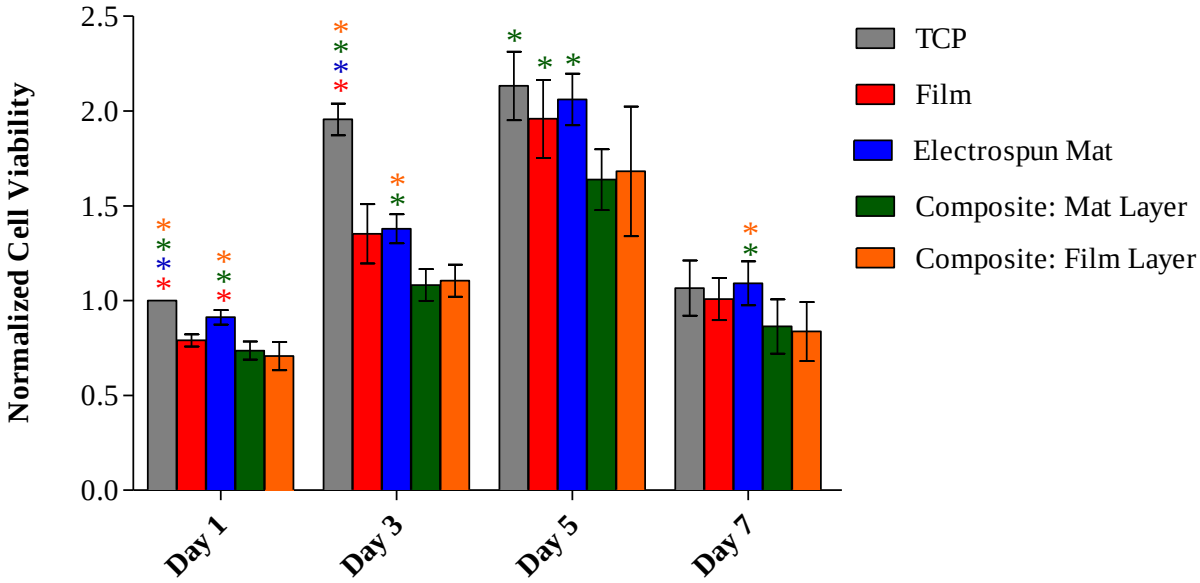

Figure 30: Normalized cell viability of human dermal papilla fibroblasts on layers of dual layer silk composite material as determined by alamarblue analysis. Colored * signifies that that material had significantly higher fibroblast viability on that day than the material of the coordinating color.

Human papilla dermal fibroblast viability and proliferation were studied on days 1, 3, 5 and 7 by alamarBlue assays [Figure 30]. Tissue culture plastic (TCP) was used as a control. The viable cell activity was noted to increase through the first 5 days of the 7 day study, which indicates cell proliferation occurred on the silk material substrates during this time period. From day 5 to day 7, there was a decrease in viability. Because this occurred for all tissue substrates, it is possible that this was a result of a culturing error which resulted in decreased

viability for all cells in culture. This was not indicative of any toxicity of the silk substrates to the dermal fibroblasts. By day 7 of culture, there was no significant difference between cell viability on any of the silk materials compared to the tissue culture plastic control [Figure 30].

For all four cell culture time points, there was significantly higher cell viability on the electrospun mat materials compared to the electrospun mat layer of the dual layer silk composite material [Figure 30]. Because the electrospun mat layer of the composite is thinner than that of the independent electrospun mat [Figure 26], this trend could result from the increased depth of the 3D silk electrospun scaffold. The 3D porous electrospun scaffold has significant void volume, which enables more cells to adhere to the fibrous scaffolds [Yang et al., 2009]. If the cells were able to proliferate through the entire thickness of electrospun mat in both materials, that of the independent electrospun mat would have a greater total depth and overall surface area and, therefore, would facilitate greater cell adhesion and proliferation. Although this would be expected, there was no significant difference between the viability of cells growing on the silk film layer compared to those growing on the electrospun layer of the silk composite. Based on the previous theory of ability for cells to proliferate in three-dimensions, it would not be expected for the solid silk film surface to allow for as much proliferation as the electrospun mat. However, it is possible that the dermal fibroblasts are easier able to spread and reach a healthier morphology for proliferation on the nonporous film surface. Therefore, fibroblasts would be able

to increase dimensions of proliferation in a thicker mat, but also proliferate healthily on the surface of the silk film.

10.4.2 Fluorescent Live/Dead Imaging

Healthy proliferation of the fibroblasts was seen through Live/Dead staining and fluorescent imaging. Figure 31 shows coordinating live and dead stains of fibroblasts on the control substrate (TCP), silk film and the composite material on which cells were seeded onto the electrospun mat layer. For all material conditions, there were significantly more living cells than dead, with only a few fluorescing dead cells on the control material. And, the living cells appear confluent on the control substrate and nearly confluent on both the silk film material and the electrospun mat layer of the composite material [Figure 31A, C, E]. Based on these images, there is no difference in density of living fibroblasts between these two silk materials. Although this shows the ability for fibroblasts to adhere and grow on both types of silk material: silk film and silk electrospun mat, the opaqueness of the composite material resulted in blurriness of the images [Figure 31E,F], which made analysis of cell morphology impossible.

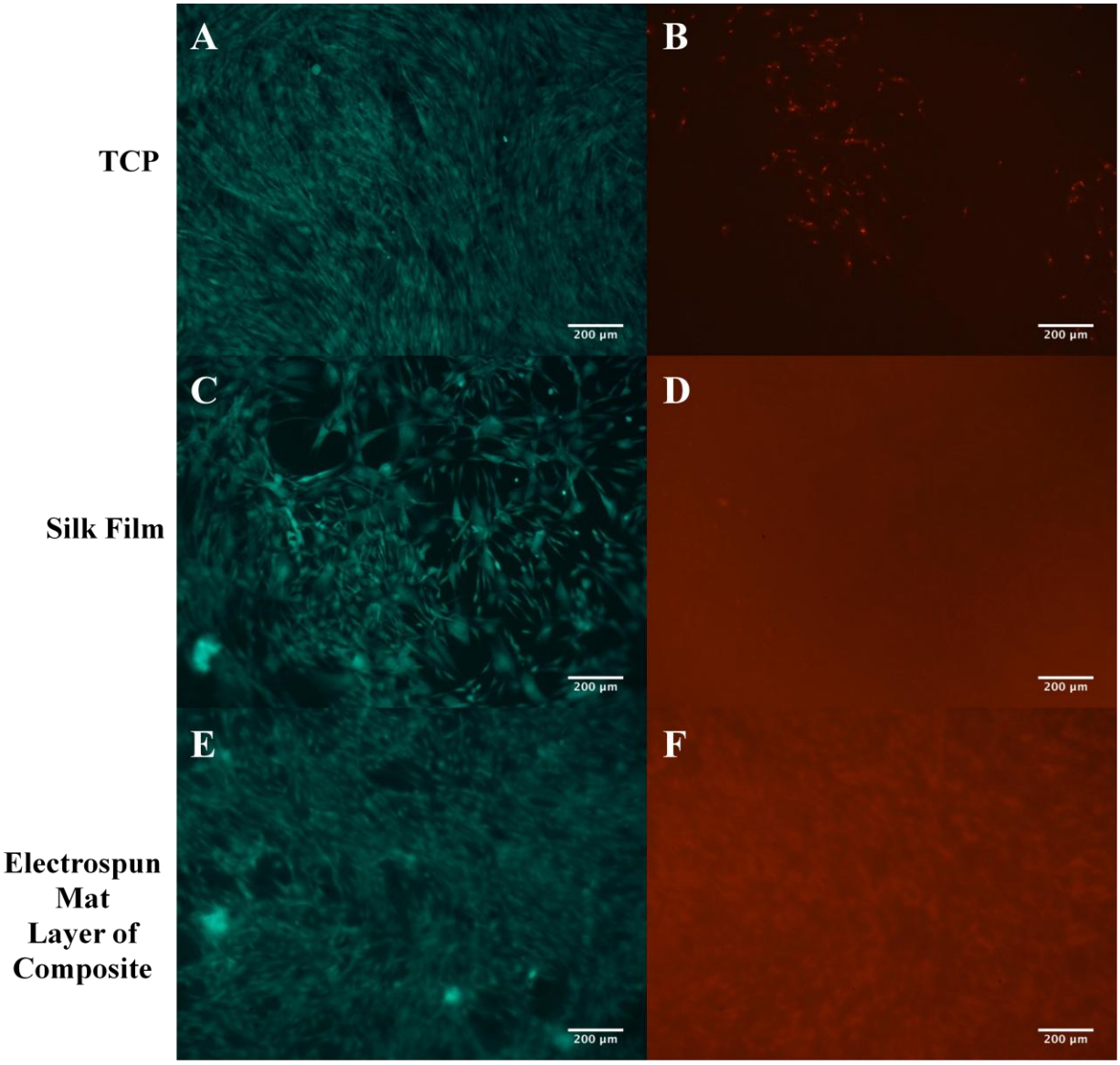

Figure 31: Fluorescence Live/Dead imaging of dural papilla fibroblasts after 7 days of culture. Cells were seeded and imaged on tissue culture plastic control (A,B), silk film (C, D) and the electrospun mat layer of the composite material (E, F). Image pairs show living and dead cells within the same frame.

10.4.3 SEM Imaging

Fibroblast morphology on both layers of the silk dual layer composite was observed through SEM imaging techniques. SEM images of dermal fibroblasts fixed onto either layer following 7 days of cell culture are seen in Figure 32. As

shown the cell attachment and spreading was relatively good for the tested fibroblasts. On the silk film layer, the cells show healthy spindle-shaped morphology indicative of their attachment and spreading on the nonporous silk substrate [Figure 32A,B]. Additionally, the fibroblasts have visibly high density and interactions on the material.

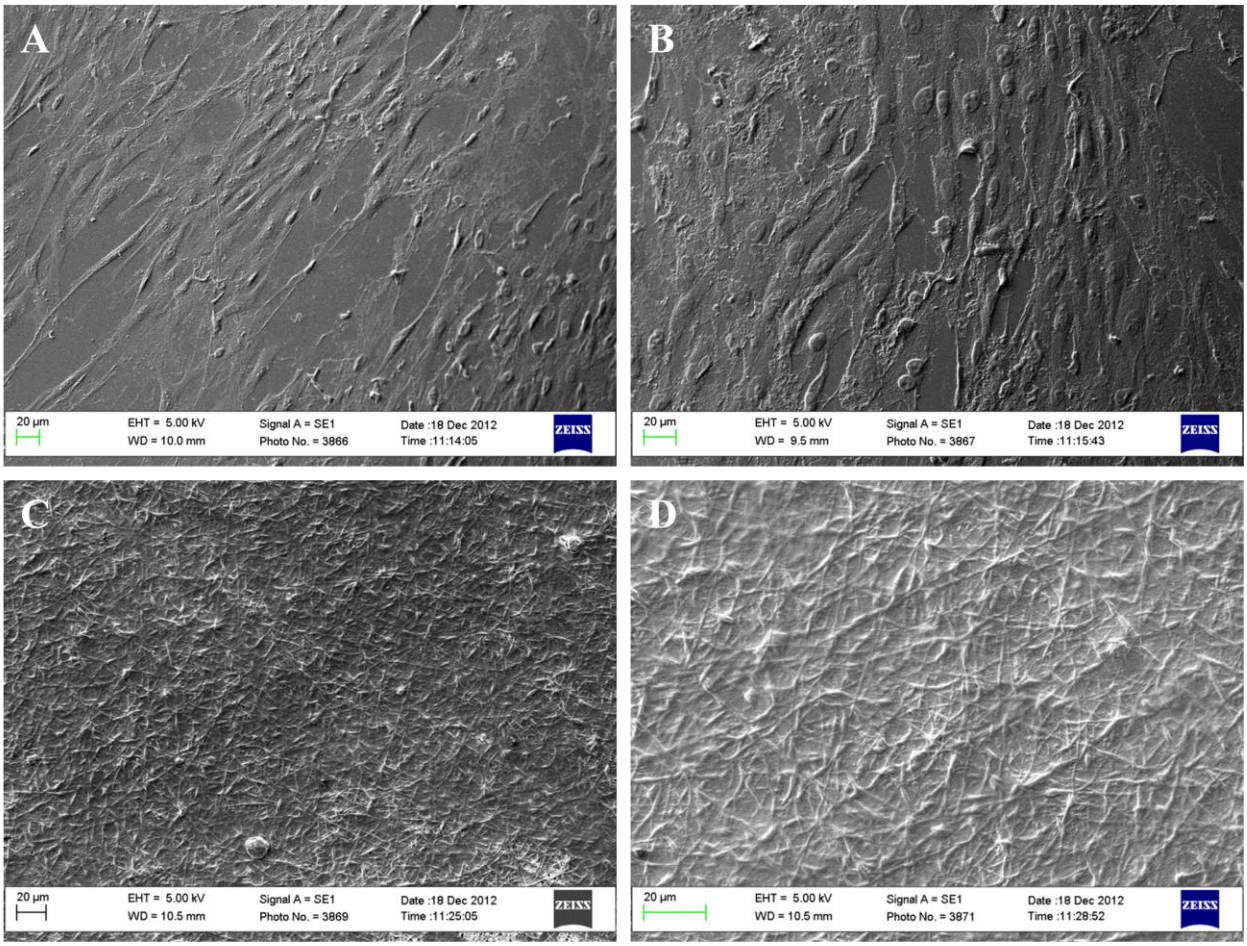

Figure 32: SEM images of dermal papilla fibroblasts cultured for 7 days on the silk film layer (A, B) and the electrospun mat layer (C, D) of the silk dual layer composite material.

On the electrospun mat layer of the composite, fibroblasts had adhered and spread on the surface of the silk fibroin nanofiber network by day 7 of culture

[Figure 32C.D]. The cells appear on the SEM images as areas in which the fibers appear to be covered or filled with solid substrate. By only day 7, they were able to interact with the surface fibers, migrate through the pores and grow under layers of the fibers [Figure 32D]. In some areas, the nanofiber scaffold surface was almost completely covered by multiple layers of fibroblasts and/or deposited extracellular matrix. The cells, ECM and silk fibers formed a visible interconnected network that filled the pores of the material [Figure 32D, E].

Such networks were also observed for human keratinocytes and fibroblasts on silk fibroin electrospun scaffolds [Min et al., 2004], and bone-marrow-derived human mesenchymal stem cells seeded on nonwoven random silk fibroin electrospun mats [Li et al., 2006]and on poly(D,L-lactide-*co*-glycolide) nanofibers [Li et al., 2002]. The ability for these different cell types to interact in a three-dimensional manner with the electrospun fiber network supports the used of the material for tissue regeneration. The high surface area and high porosity of the structures successfully provide a 3D structure for cell interaction and nutrition/gas exchange [Hirano et al., 2004], which was specifically observed for human papilla dermal fibroblasts through SEM imaging.

10.4.4 Confocal Imaging

The morphologies of the human dermal papilla fibroblasts both on the silk film surface and within the 3D network of the electrospun mat were observed through confocal imaging of live/dead stained fibroblast cultures [Figure 33]. For both surfaces, there were no visible dead cells and a relatively high density of living fibroblasts. On the silk film surface [Figure 33A], the fibroblasts were able

to adhere, spread, and maintain the healthy fibroblast spindle-shape [Yang et al., 2009]. On the electrospun mat layer, the fibroblasts appear to have some spindle-shape but also in large clumps of dense cells [Figure 33B]. Additionally, this image is a stack of 11 2-dimentional images with a step size between each image of 4 μm. The image, therefore, documents cells within the electrospun mesh in a 3-dimensional area with a thickness of 44 μm. Based on this image, therefore, the dermal fibroblasts are able to grow within the pores of the electrospun scaffold in a 3-dimensional manner. This scaffold facilitates this growth and also physical interaction and density of cell groups as compared to the more spread out cells on the silk film layer.

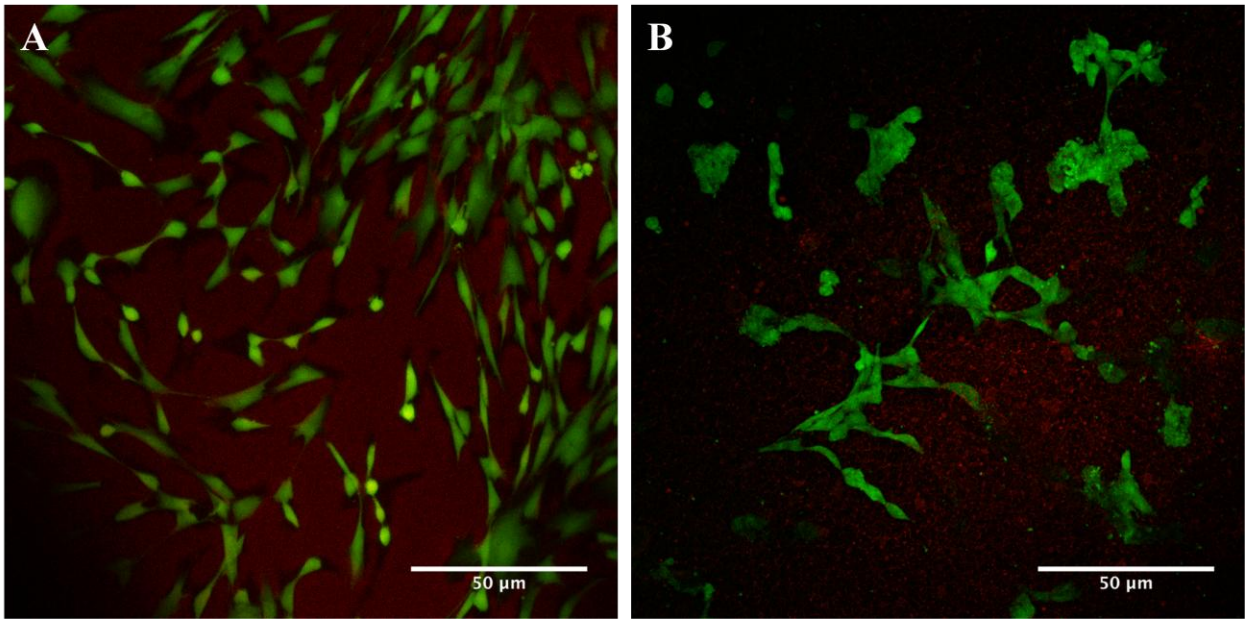

Figure 33: Confocal images of dermal papilla fibroblasts following 7 days of culture on the silk film layer (A) and electrospun mat layer (B) of the silk dual layer composite material.

Overall, dermal fibroblasts are able to grow on both sides of the material but have the 3D capacity on the electrospun mat layer to promote further dural

regeneration. This was documented both by the viability trends observed by alamarlue analysis [Figure 30] and by cell imaging which showed the interaction of the cells with the nanofibers and pores of the electrospun mat and, specifically, the ability of the cells to grow and form networks in a three-dimensional manner. The ability for dermal fibroblasts to behave this way on the material suggests the same behavior for dural fibroblasts after material implantation as a dural substitute *in vivo*. Therefore, it would be expected for biocompatibility of the material with the dural tissue in addition to ingrowth of dural fibroblasts extensively through the electrospun mat layer.

10.5 Neural Cell Biocompatibility and Cell Viability on Silk Composite Biomaterial

While the goal of the design of the dual layer silk fibroin composite material was to promote extensive dural fibroblast ingrowth and dural tissue regeneration, this study was used to determine how neural cells interact with the material and, specifically, if it has any toxicity that would be expected to affect neural tissue, whether brain or spinal cord, when this material was implanted in the dura. Although cortical adhesions would be detrimental to the patient and, therefore, limited neural tissue ingrowth to the material would be desired, it is important to see if the neural tissue, which would be nearly adjacent to the dural substitute, would experience any toxicity or detrimental effects to its health.

10.5.1 Cell Viability Analysis

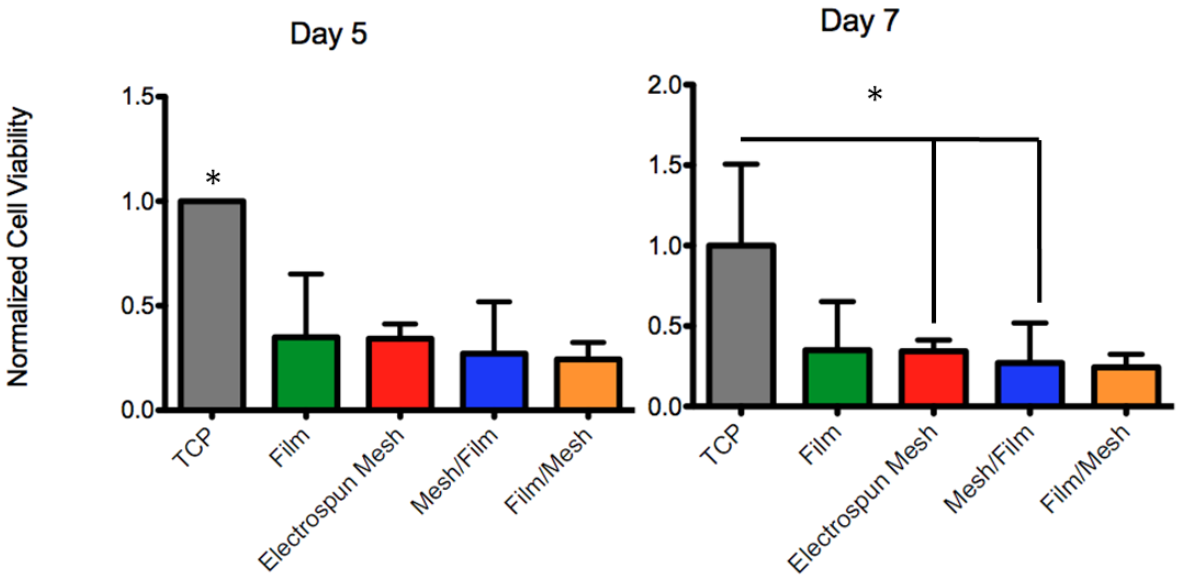

Figured 34: Normalized cell viability of rat neural cells on layers of dual layer silk composite material as determined by alamarblue analysis. There was no significant difference in cell viability between the different silk surfaces [n=3, $p<0.05$].

Rat neural cell viability and proliferation were studied on days 5 and 7 by alamarBlue assays [Figure 34]. The alamarblue assay showed that the neural cells had no significant differences in viability between the silk material conditions after both five days and seven days of cell culture [Figure 34]. On day 7, neural cells cultured on electrospun mesh and on the mesh layer of the silk composite material had significantly lower viability than those cultured on the tissue culture plastic control. However, the neural cells cultured directly on silk film surfaces did not show significant differences in viability as compared to the tissue culture plastic. Based off of this alamarblue data, it appears that neural cells are able to grow more successfully on smooth surfaces, including that of silk films, compared to rougher topographies like that of the electrospun mesh.

10.5.2 Confocal Imaging

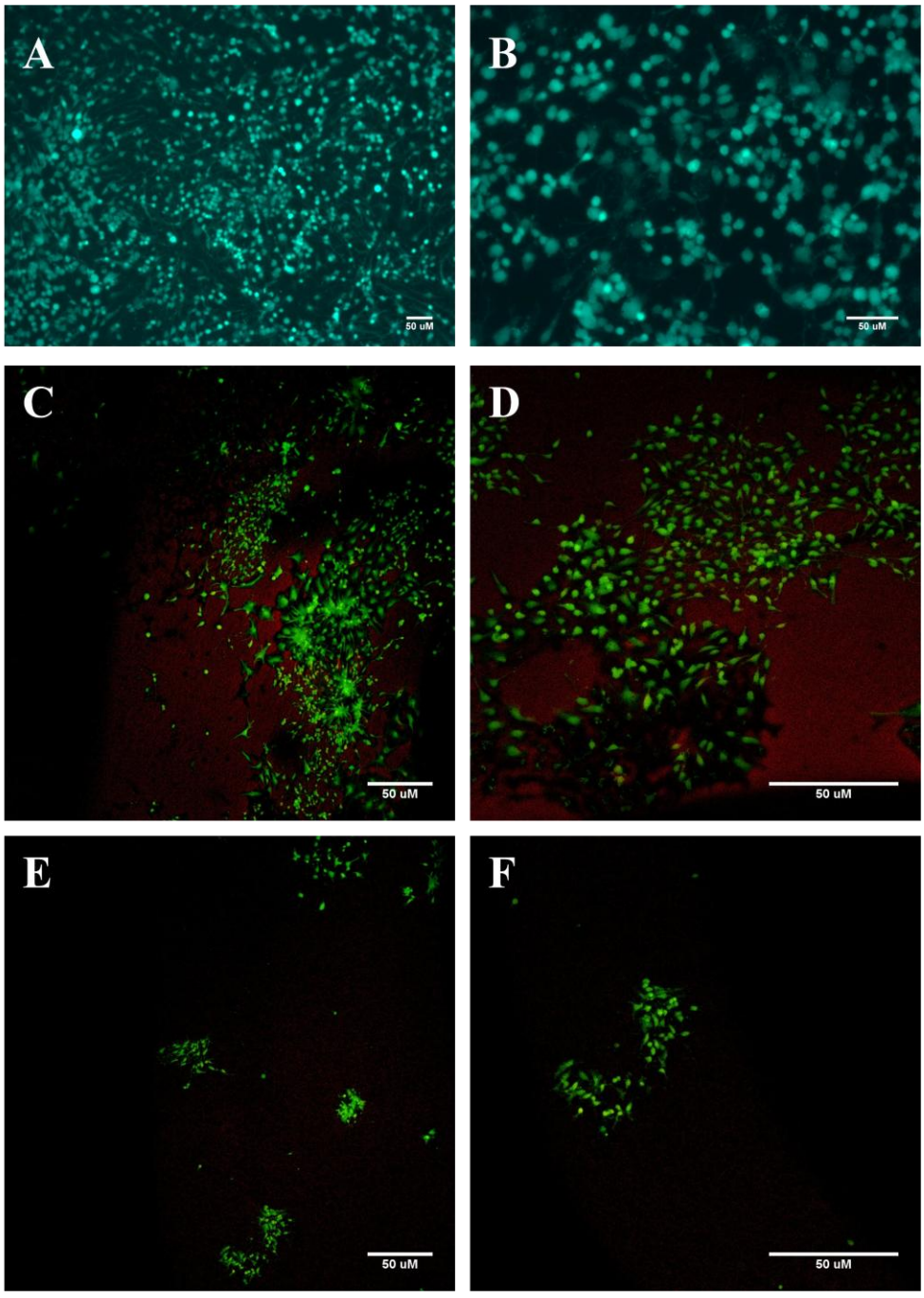

Figure 35: Confocal imaging of rat neural cells following 7 days of culture on silk film layer (C,D) and electrospun mat layer (E,F) of dual layer silk composite material as compared to neural cell viability on tissue culture plastic (A.B).

This trend was also visibly observable through cell imaging. Confocal imaging was used in order to obtain fluorescent images of the cells through the opaque dual layer composite material and to understand how neural cells interact with the 3D electrospun scaffold layer. When seeded directly onto the electrospun mat layer, cells appear as clumps of neural networks [Figure 35A,B]. Although there is not a large density of neural cells spread across the entire mat surface, each imaged clump had at least 50-100 cells, as determined by gross cell counting from images. Additionally, at higher magnification, axons visibly extend between the neurons within the clumps, which signify a healthy network of neural cells.

On the silk film layer of the composite material, the neural cells spread out and cover a much larger area of the material surface [Figure 35C,D]. However, a noticeable difference between cell growth on the film and electrospun mat layers is the presence of astrocytes. Astrocytes are larger and have more cubic bodies as compared to neurons [Nag, 2011]. Due to this difference in morphology, astrocytes can be visibly determined from a cortical tissue cell culture. These larger cells are especially visible in Figure 35C, where the astrocytes incorporate with the neural cells, which have a smaller, round, and uniform morphology. Astrocytes are considered to be supporting cells in the brain, specifically by providing trophic, metabolic, and structural support for neural networks [Nag, 2011]. In fact, neurons are commonly cultured on a layer of astrocytes because astrocytes promote neuron survival, synapse formation, and plasticity [Jones et al, 2012]. Therefore, the higher presence of astrocytes on the silk film layer culture

could contribute to the higher proliferation of neural cells and increased spreading across the surface.

10.5.3 SEM Imaging

SEM imaging was used to better observe the morphologies of the Day 18 embryonic rat neural cells seeded on the dual layer silk composite [Figure 36]. On the smooth silk film layer, the neural cells are spread with high density but without confluence across the material surface [Figure 36A]. At closer magnifications, some large clumps of neural cells were visible [Figure 36B]. Although axons are too fine of structures to be viewed by SEM, the neurons appear healthy and in high numbers. Their small, spherical structures are noticeably different from the astrocytes, which are also present in high density. In fact, in Figure 3B, the spherical neural cells appear to be growing on a layer or dense area of astrocytes, which appear as flatter, larger cells on the silk film surface.

The density of the neural cells on the electrospun mat layer is more difficult to observe from the lower magnification images due to the overall texture of the mesh [Figure 36C]. In Figure 36C, however, the electrospun mat, clearly has neural cells adhered and growing on the surface and possibly the subsurface of the mat layer. At closer magnification, the neural cells can be seen spreading along the surface fibers of the electrospun mat [Figure 36D]. In fact, their cell bodies appear to spread over the fibers and extend along some of the individual fibers.

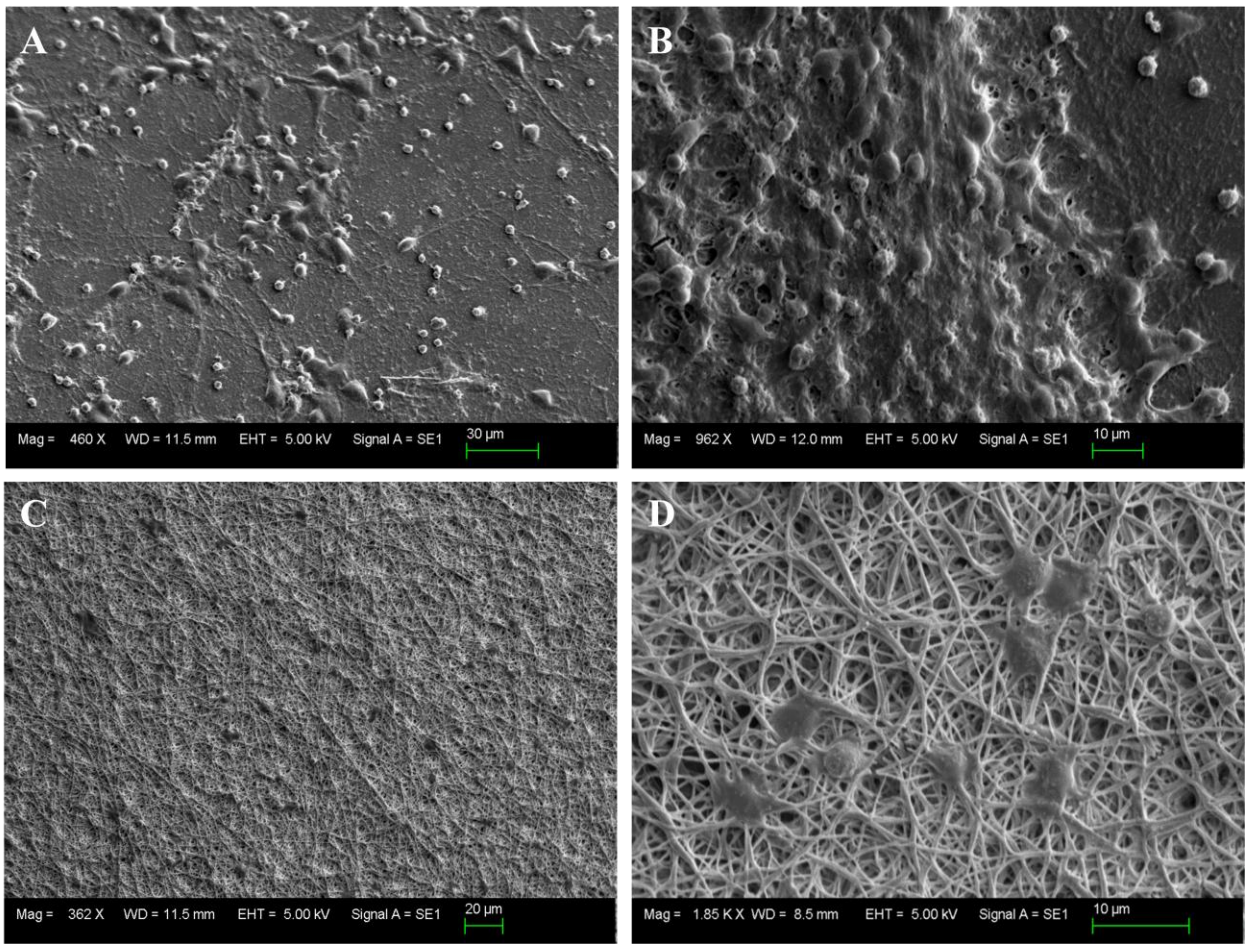

Figure 36: SEM images of rat neural cells cultured for 7 days on the silk film layer (A, B) and the electrospun mat layer (C, D) of the silk dual layer composite material.

On both layers of the dual layer silk composite material, the neural cells from Day 18 embryonic rat cortical tissue were viable with no visible dead cells in confocal images [Figure 35], which would have appeared as fluorescent red, and with healthy morphologies on SEM images [Figure 36]. This seven day preliminary study shows that both layers of the silk dual layer composite are biocompatible with neural cells, specifically from Day 18 embryonic rat cortical tissue.

Although the neural culture experiments were successful in determining the neural biocompatibility of the composite material, as a dural substitute implant, cortical adhesions are unwanted on it. Therefore, neural tissue ingrowth should not be supported by the material. The cell viability data [Figure 1] and cell imaging [Figure 35, Figure 36], however, suggest the ability of successful neural tissue growth on the silk material. Though, as previously described, these materials were treated with poly-L-lysine, which is a commonly used cell adhesion molecule (CAM) specifically for neural cell culture. Therefore, their adhesion was promoted on these materials and the neural cells were provided with the best possible culture conditions. If the materials had not been coated with poly-L-lysine, the neurons would not have successfully attached to and, therefore, grown on the tissue. The uncoated dual layer silk composite material would not be expected to promote neural cell adhesion or ingrowth and, therefore, would be expected to limit neural tissue adhesion. Additionally, nearby neural tissue would not experience any toxic effect from the implanted material due to its proven biocompatibility in this experiment.

10.6 *In vitro* Enzymatic Degradation

As a dural replacement material and dural regeneration scaffold, the dual layer composite silk material should have a degradation rate that matches the rate of new tissue formation. Once the new dural tissue regenerates across the durotomy site, therefore, the scaffold material would be completely degraded and absorbed by the body [Zhou et al., 2010].

Histologically, the dura mater consists of a rich network of collagen fibers with intermingled dural fibroblasts [Zhou et al., 2006]. Although there is limited literature addressing the dural remodeling process across durotomy sites, numerous studies support that dural healing is a result of fibroblastic proliferation and the formation of connective tissue fibers induced by adjacent dural tissues [Collins et al., 1991]. *In vitro* studies have been used to study the cellular healing process of dural defects. In fact, in an *in vitro* dural defect model, the defects were covered by rapidly proliferating dural cells after 13 to 15 days of culture [Zhou et al., 2006]. In an *in vivo* model using a collagen matrix dural replacement in bovine models, histology observations at 1, 3, and 6 months post-implantation showed that dural remodeling is able to occur across dural grafts. In fact, after 1 month, biopsies showed mixed fibroblast and lymphocyte cell population and collagen bilayering across the graft, which was indicative of dural regeneration. After 3 months, the grafts showed increased remodeling with the dural bilayered natural collagen structure. And there was extensive bilayered collagen formation across the dural grafts following six months [Chaplin et al., 1999].

Although the exact mechanism and rate of neodura formation across a dural defect is not completely understood, the results of these studies show that the process occurs over a few months. Therefore, the degradation rate of the silk dural replacement material should be able to match this rate of dural regeneration. In order to determine the degradation rate of the silk dural replacement material *in vivo*, the material degradation was first modeled *in vitro*. The material was incubated in both PBS (negative control) and Protease XIV, which has been

shown to model degradation of regenerated silk fibroin material *in vitro* [Li et al., 2003]. Both quantitative and qualitative degradation effects were observed for the material.

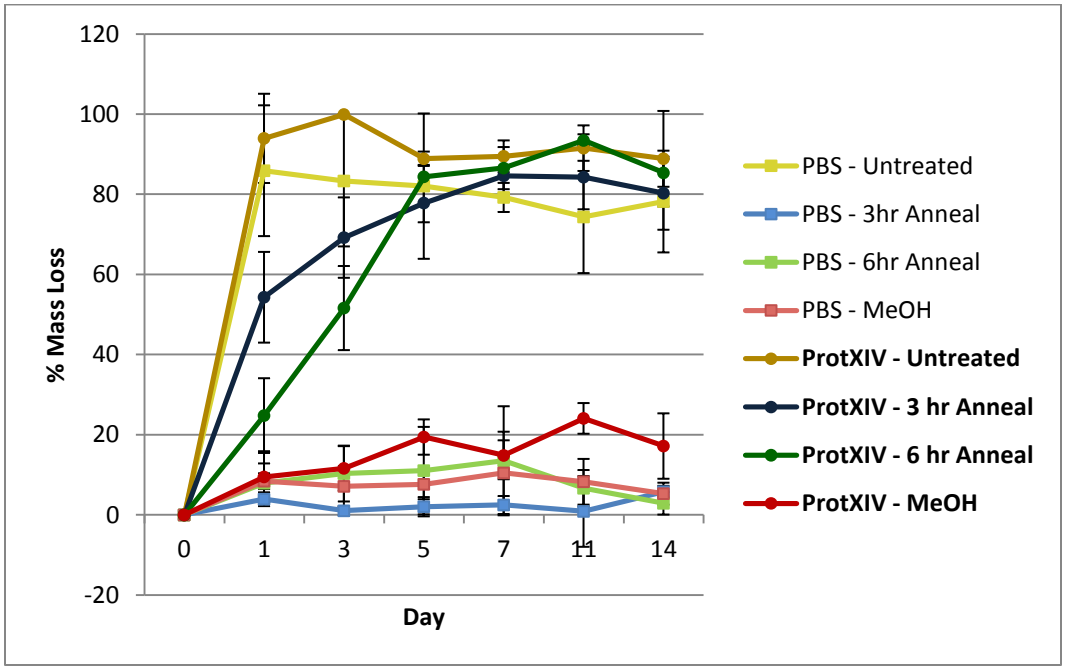

Figure 37: Mass loss of the dual layer composite materials during degradation *in vitro* over 14 days. Data points appear as the average of four replicates of calculate mass loss percentage [n=4].

The degradation profile [Figure 37] and percentage of weight loss of the dual layer silk composite materials over a 14-day degradation period [Figure 37] were calculated. *In vitro* degradation was observed both quantitatively and qualitatively for all samples incubated with Protease XIV. However, crystallization treatments had significant effect on the degradation kinetics of the composite material samples.

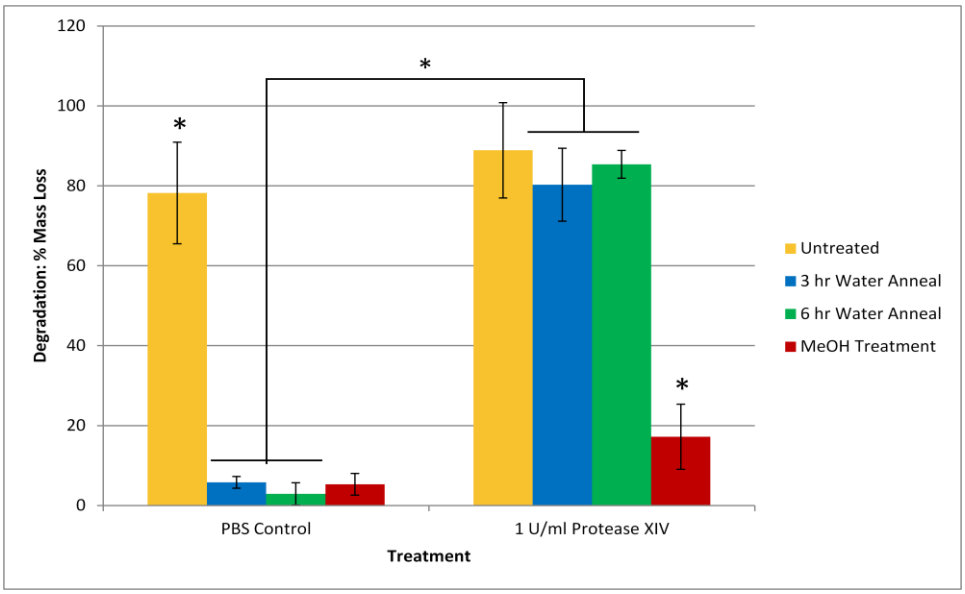

Figure 38: Average percentage mass loss of silk dual layer composite materials after the 14-day *in vitro* degradation study [n=4, $p<0.05$].

Untreated silk dual layer composite samples visible dissolved in the 3 hour PBS soaking step used to obtain the initial "wet" weight of the samples. The mass loss for these samples, therefore, reached between 80 and 100% on Day 1 of the study. This was expected as these materials did not have the beta-sheet crystallization required for solubility in aqueous solutions. The three other sample groups showed no large amounts of mass loss in the PBS solution over the 14-day study. In fact, on day 14, these mass losses ranged from only 2.9 to 5.8% mass loss, with no significant differences between the materials. Therefore, the three different treatments were successful in inducing beta-sheet crystallization in order for the materials to remain insoluble in PBS solution over a prolonged period of time.

The 3 hour water annealed treated materials had the earliest signs of significant mass loss in the Protease XIV solution [Figure 37]. In fact, on day 1,

the 3 hour water-annealed materials had an average weight loss of 54.3%, compared to 24.8% and 9.5% for the 6 hour water-annealed and methanol-treated samples respectively. By day 5, however, both the 3 hour and 6 hour water-annealed samples had an average weight loss of around 80% while the methanol treated samples had only lost 19.4% mass. Therefore, although the 6 hour water-annealed samples degraded at a slower rate than the 3 hour water-annealed samples, there was no significant difference in their average mass losses during the later days in the study.

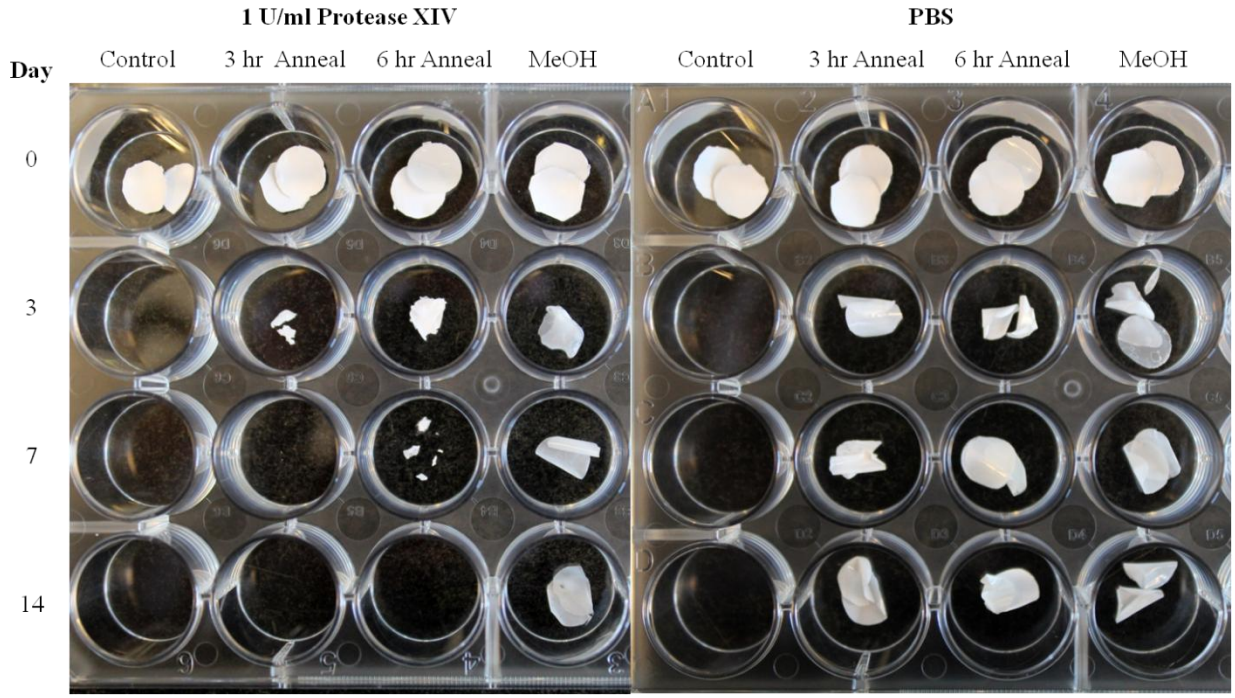

Figure 39: Observed degradation of silk dual layer composite materials on day 0, 3, 5, 7, and 14 of the 14 day *in vitro* degradation study.

This was also visually observed [Figure 39]. By day 7, the only remaining material for the 6 hour water annealed representative sample was small fragments and that of the 3 hour water sample was too small to obtain from the transwells.

The methanol treated samples, however, maintained their solid morphologies through the 14 day study and had a final average mass loss of only 17.2%. The only signs of significant degradation were seen at the microscale [Figure 39]. SEM images show some breaking and buckling and surface erosion of the nanofibers in the electrospun mat layer of the material. The physical integrity of the material, therefore, appears to have been affected by the Protease XIV but not in an excessively deleterious way. The silk film layer was still intact and the electrospun mat would still be able to contribute as a 3D porous scaffold for dural regeneration.

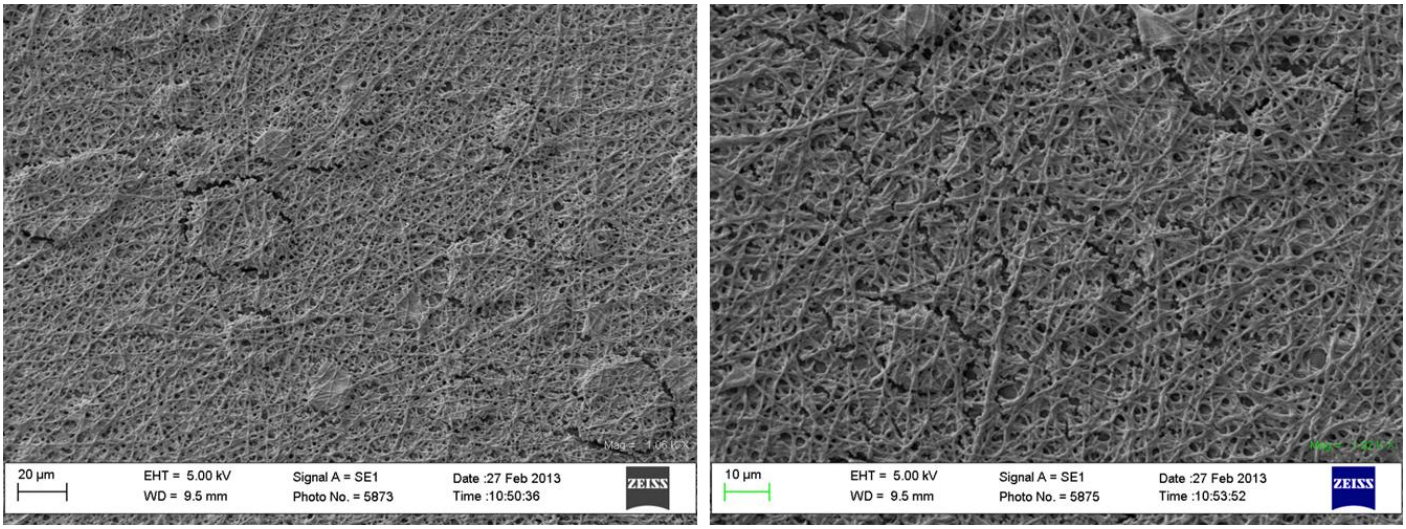

Figure 40: SEM images of electrospun mat layer of methanol-treated composite materials after 7 days in 1U/ml Protease XIV solution.

The observed trends in degradation, both in mass loss and morphology, result from the differences in beta-sheet crystallization previously studied. Methanol treatment results in higher beta-sheet content compared to water-annealing processes [Hu et al., 2011]. Previous studies have shown that the hydrophobic nature of the crystallized silk materials and increased beta-sheet

content in silk materials results in slower biodegradation both *in vitro* and *in vivo* [Jin et al., 2005]. The methanol treated composite material, therefore, has significantly more beta-sheet content that results in its limited degradation by Protease XIV.

The tunable slow biodegradation of the dual layer silk composite material supports its use as a tissue replacement and tissue regeneration scaffold. The ideal scaffold would be completely biodegradable such that a second surgery is not required to remove the implant [Rosso et al., 2005]. However, the rate of degradation should be controllable to mimic the rate of neo-dura formation [Hutmacher, 2000]. The crystallization treatments of the composite silk material allow for the controlled and prolonged degradation of the material to support its use as a dural tissue regeneration scaffold.

Part III

Design and Characterization of a Silk Adhesive and Silk Sutureless Dural Repair System

Chapter 11: Introduction

11. 1 A Silk Fibroin Sutureless Dural Repair System

While the silk dual layer composite material described in Part II shows potential for use as a successful dural replacement material, in order for the material to function as a sutureless dural substitute, an adhesive component must be added. As previously described, conventional suturing techniques have inherent drawbacks: CSF might leak through the suture holes or between the sutures themselves (particularly in older patients or in patients who have undergone radiotherapy), and the sutures carry the risk of foreign body reaction, which can slow tissue healing [Nurata et al., 2009]. While tissue sealants such as DuraSeal are used to seal over sutures, this procedure carries risk of hydrodynamic complications, as documented in the single institution clinical review in Part I. The ideal dural repair system, therefore, would be adhesive, sutureless, biocompatible and biodegradable to facilitate dural regeneration while maintaining a watertight barrier against CSF leak.

11.2 Electrogelated Silk as a Dural Sealant

In order to maintain the biocompatibility and biodegradability of the silk fibroin dual layer in an adhesive system, a silk hydrogel was explored as the adhesive component of the proposed sutureless silk dural repair system. As previously described, electrogelated silk is a unique, bioreversible all-silk adhesive material. It has shown strong adhesion to steel, acrylic, and wood surfaces [Leisk et al. 2010] and has also been explored as a silk hydrogel drug

delivery system. Because it involves no crosslinkers or additional chemistries, the all-silk-fibroin adhesive gel maintains the biocompatibility of other silk fibroin materials, including the dual layer composite material. By applying this all-silk adhesive gel on the silk film layer of the composite material, the dural replacement material becomes an adhesive, sutureless all-silk dural repair system. The design, production, and adhesive testing of this system are explored in Part III.

Chapter 12: Materials and Methods

12.1 Burst Pressure Testing

Burst pressure testing was performed in order to determine the strength of the seal between collagen tissue and the all-silk adhesive dural substitute. The testing was conducted in accordance with ASTM: F 2392-04 Standard Test Method for Burst Pressure Strength of Surgical Sealants.

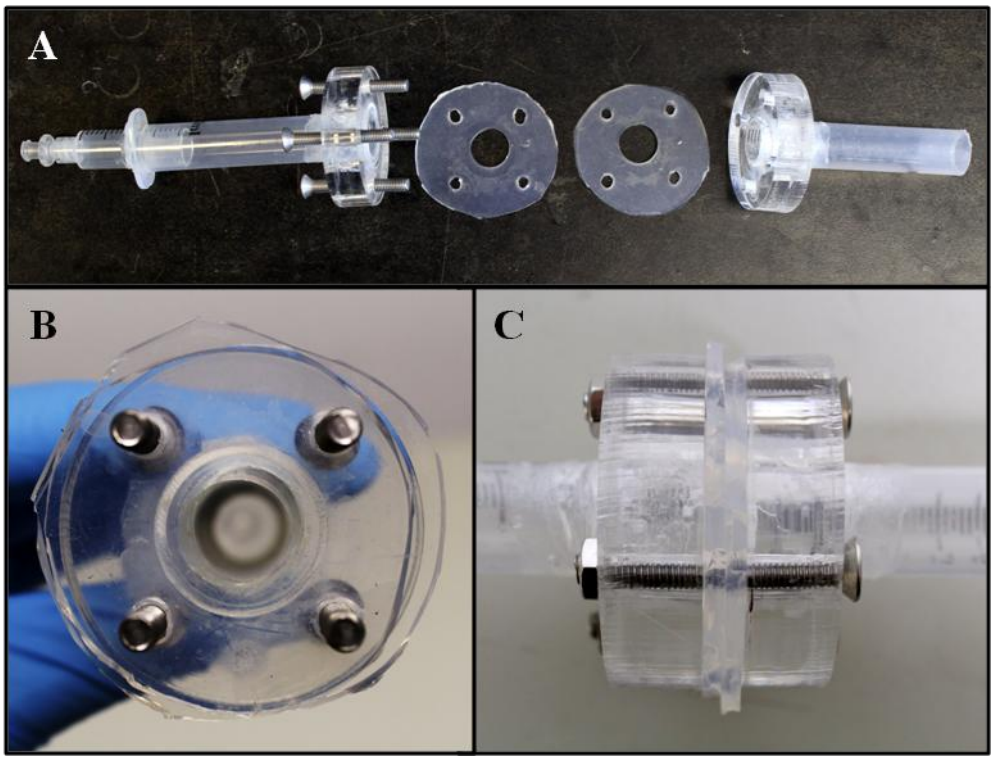

Figure 41: The burst test sample holder [A] uses PDMS gaskets [A,B] and four screws to secure the collagen casing and sample in a watertight seal [C]. The PDMS gasket has a 15 mm central biopsy to connect with both sides of the apparatus tubing and allow exposure of the sample to controlled water flow.

Collagen casing (McKinnon's Meat Market, Somerville, MA) was used as the tissue substrate onto which silk materials were applied and tested for adhesive strength. The casing was first cut in half, in order to be unilayer, and blotted with a Kim-Wipe (Kimberly-Clark, Roswell, GA) to remove excess moisture. It was then secured onto the four securing screws of the sample testing apparatus [Figure 41]. Once secured and the tissue was taught across the 15 mm tube opening, a 3.0 mm biopsy was made in the center of the material [Figure 42]. This biopsy size coordinates with the ASTM: F 2392-04 method and supporting literature [Cambell et al., 2005]. Samples were then placed over the biopsy with centralized alignment. The sample testing apparatus was then closed in order to secure the

collagen case in place in a sealed environment. A watertight seal was produced such that no leaking could occur out of the apparatus or around the collagen casing by two PDMS (Poly(dimethylsiloxane), Sigma Aldrich Corp., St. Louis, MO) gaskets [Figure 41] which were squeezed to seal by tightening of the four securing screws. These gaskets sealed around their 15 mm central openings, which aligned with the 15 mm openings of the tube portion of the sample testing apparatus [Figure 41]. All of these components were designed such that the 12 mm composite material covering the 3 mm defect in the collagen casing was not secured by the PDMS gaskets and was open to water flow through the tube portions of the apparatus.

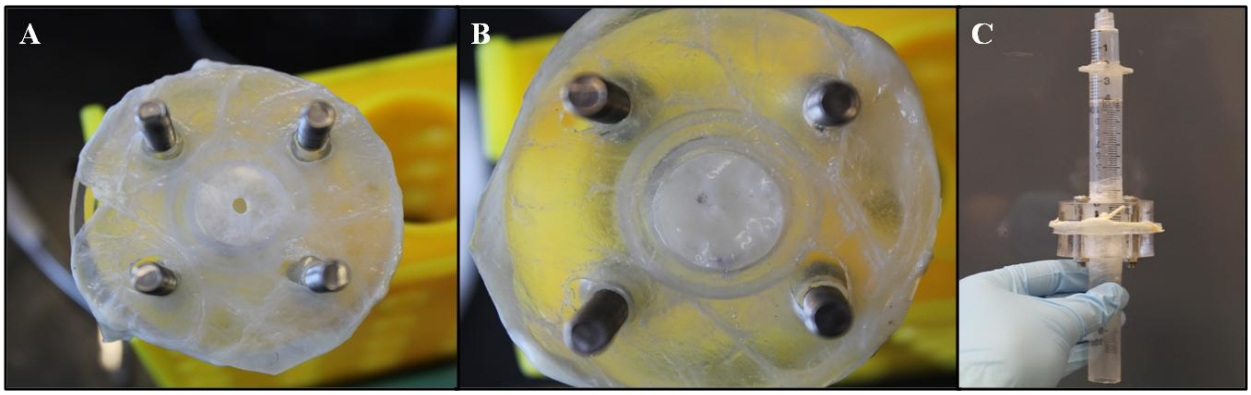

Figure 42: Preparation of burst test sample. Collagen casing was secured in burst test apparatus over a PDMS gasket and a 3 mm biopsy was made in its center [A]. 12 mm silk material samples were prepared and placed over this defect [B]. The sample and tissue were secured in the apparatus with another PDMS gasket and four tightened screws [C].

The sample testing apparatus was then attached to the burst test [Figure 3]. Within the burst test, water was delivered to the sample at a flow rate of 5 ml/min via a syringe pump. A pressure gauge [Ashcroft Inc., Deer Park, NY] and solid state pressure transducer [Omegadyne, Inc., Sudbury, OH] were put in sequence

before connection to the sample testing apparatus. The pressure transducer was connected to a multimeter [Fluke 8846A 6-1/2 Digit Precision Multimeter, Everett, WA], which was able to log changes in voltage through FlukeViewForms software. The sample apparatus was placed in a beaker of water to supply back pressure to the sample. As the water was supplied to the sample at 5 ml/min, voltage change was graphed by the FlukeView software. The maximum pressure reached during the test was deemed the burst pressure of the sample.

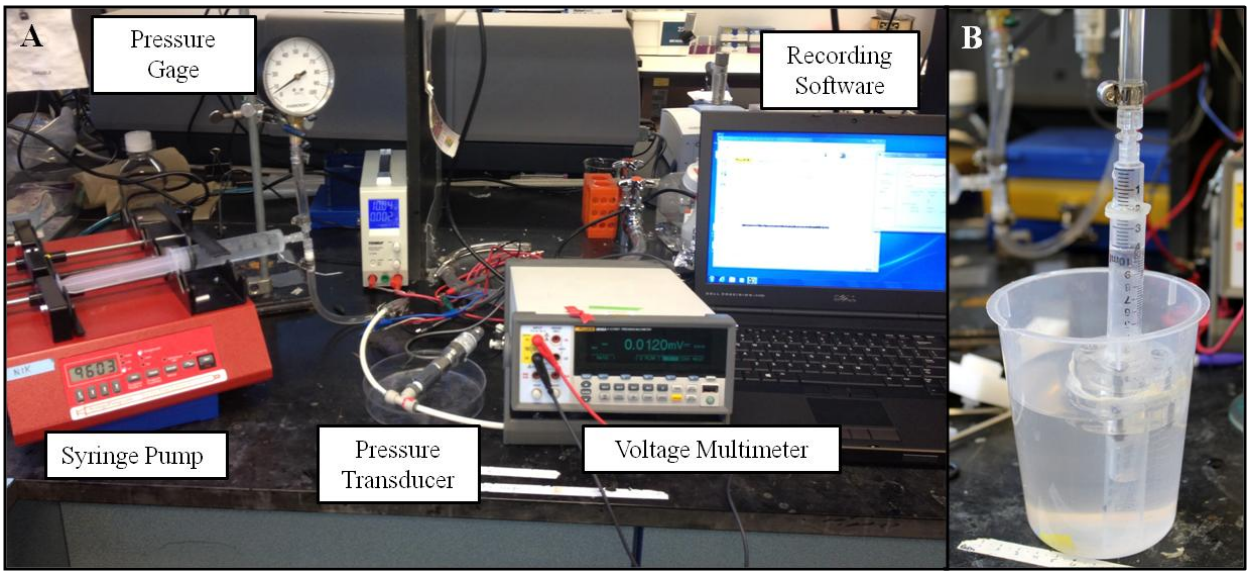

Figure 43: Complete burst test set-up including syringe pump for controlled water flow rate, pressure gage, pressure transducer, voltage multimeter, and voltage recording software. The sample apparatus was attached with tubing after the pressure transducer and was placed in a beaker of water to supply slight back pressure to the sample.

12.1.1 Sample Preparation

All tested samples were prepared by cutting 12 mm circular samples of the silk dual layer composite material. These samples were cut using a 12 mm biopsy punch from dry composite material, which was previously treated with 6

hour water-annealing at room temperature. These samples then received various treatments and tested for adhesive strength to the collagen tissue substrate through burst testing [Table 8]

Sample Group (n=3)	Hydrated Silk Dual Layer Composite (12 mm diameter)	Treatment
1	-	-
2	Yes	-
3	Yes	Ethanol Exposure
4	Yes	Electrogelated Silk Application
5	Yes	Electrogelated Silk Application Ethanol Exposure

Table 8: Burst test sample conditions. Three replicates were performed for each sample group (n=3).

The sample treatments include the 12 mm composite biopsy alone, with ethanol exposure, with electrogelated silk, and with electrogelated silk and ethanol exposure [Table 8]. All samples were applied over the 3 mm biopsy in the collagen casing in their hydrated states. The composites of sample groups 2 and 3 were hydrated for 5 minutes in PBS before being placed on the 3 mm defect in the collagen casing.

Electrogelated silk was produced on the film layer surface of composite samples in sample groups 4 and 5 [Table 8]. This was done by placing the 12 mm composites on non-stick aluminum foil perforating their outer area with a scalpel in order to allow for the conductivity of the foil to extend through the silk composite material. A PDMS mold with a 12 mm circular cut out was placed around the composite in order to secure it in contact with the conductive tin foil and to allow for aqueous silk addition to its surface. 200 µl of aqueous silk (10

minute boil, 6-8% w/v) was then added to the silk film surface of the composite. A weighted electrode was placed onto the PDMS mold such that it was in contact with the silk solution. The foil was connected to a power supply as the positive electrode and the opposite electrode was negative. An e-gel (electrogelated silk) was then formed directly onto the silk film layer of the composite by gelling at 30 V for 5 minutes. The resulting e-gel-coated composite was left to sit for 3 minutes in order for water to evaporate and release a tacky gel surface. This was then placed over the defect in the collagen casing and left to set for 5 minutes before burst testing.

Sample groups 2 and 5 [Table 8] also had 10 seconds of 70% ethanol exposure to the entire surface of the composite sample. This ethanol exposure occurred following the 5 minute set time onto the collagen casing defect and involved an additional 5 minute set time for the ethanol to take effect.

12.1.2 Calculations and Statistical Analysis

Standard curves were performed in order to determine the relationship between logged voltage of the solid state pressure transducer and pressure experienced by the sample. As previously described, the burst pressure of the sample was determined as the maximum pressure reached during the test. Three replicates were performed for each sample group (n=3). Results were displayed as averages with standard deviation.

Sample sets were statistically compared and analyzed by using a two-tailed, unpaired Student *t* test analysis of means.

12.2 Design and Fabrication of Automatic E-gelling Device

12.2.1 Portable Electrogelation (E-gelling) Container

Empty 150 ml IV bags (Thermo Fisher Scientific, Waltham, MA) with two ports were used as the preliminary container. One port was an open tube while the other had a preinstalled septum. The IV bags were cut open along the sides and bottom in order to gain access to the inner surfaces of the bag. To create positive and negative electrodes within the bag, copper wire and aluminum tape was used.

The electrodes were designed such that they had approximately the same area and would not overlap or touch. This was done by cutting and applying sections of aluminum tape (Newark Corp., Richfield, OH). in "E" patterns [Figure 44]. Two oxygen-free insulated 24-gauge copper wires (Newark Corp., Richfield, OH) of approximately 5 inches in length were stripped at each end and threaded through the open port. One wire was secured under the one aluminum "E electrode" simply by placing the stripped area of the wire under the adhesive aluminum tape. The other wire was secured in the same manner to the other aluminum tape electrode. The bag was then sealed along its side and bottom edges [Figure 44].

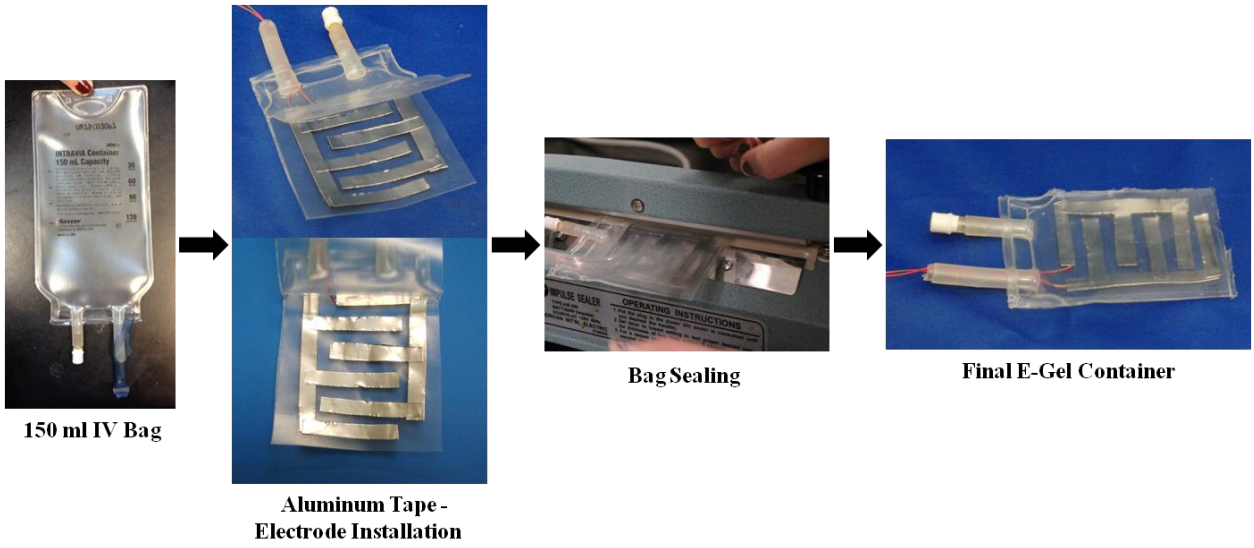

Figure 44: Portable e-gel container production process. Aluminum tape electrodes are installed in a modified 150 ml IV bag and are connected to copper wires exited from an open port. The bag is resealed in order to be filled with silk and used as an e-gelling device.

In order to test the e-gelling ability of this container, 10 minute-boil silk (6-8% w/v) was injected into the sealed container using syringe with an 18-gage needle through the septum port [Figure 45]. The copper wires were then connected to a Tenma Switching Mode Power Supply (Newark Corp., Richfield, OH) to coordinating positive and negative connections. The power supply was turned on to 25 V to induce silk e-gelling on the positive electrode.

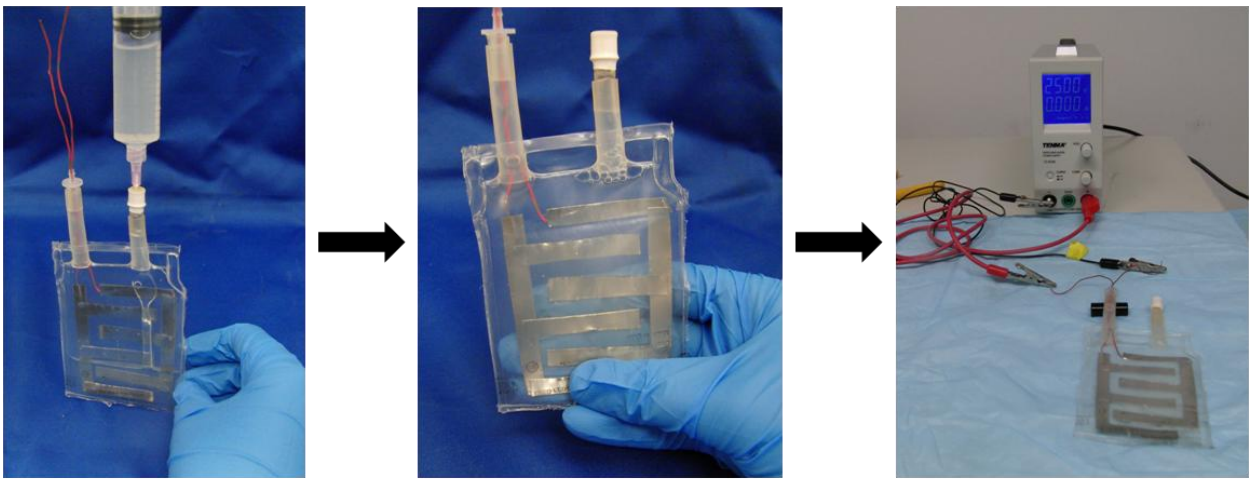

Figure 45: Preparation for silk e-gelling in portable e-gelling container. The container is filled with 10 minute-boil silk (6-8% w/v) and aluminum tape electrodes are connected to 25 V power supply via installed copper wire.

12.2.2 Incorporation of Silk Dural Replacement Material

The above portable electrogelation (e-gelling) container was modified in order to incorporate the silk dual layer composite material and create an e-gel directly on the material. The general procedure for forming a silk e-gel on the silk film layer of the composite material was previously described in the burst testing sample preparation method. In order to create the e-gel directly on the material, the material must be "made conductive." This is done in the modified-IV-bag by creating two electrodes with the silk composite material incorporated into the positive electrode.

Similarly to previously described, the positive and negative electrodes in this design were made with approximately the same surface area. The negative electrode was the same aluminum tape previously used. The positive electrode was made of double-sided copper tape (Newark Corp., Richfield, OH) of the same

area. A slightly smaller sample of the silk composite material was applied to the copper tape. It was then perforated with the point of a scalpel in order to create conductivity on the silk film surface of the material, which was exposed [Figure 46]. The electrodes were connected to two copper wires and the bag edges were sealed as previously described. The bag was then filled with 10-minute boil silk (6-8% w/v) and connected to 25 V of power via the copper wires to induce e-gelling on the silk composite material surface.

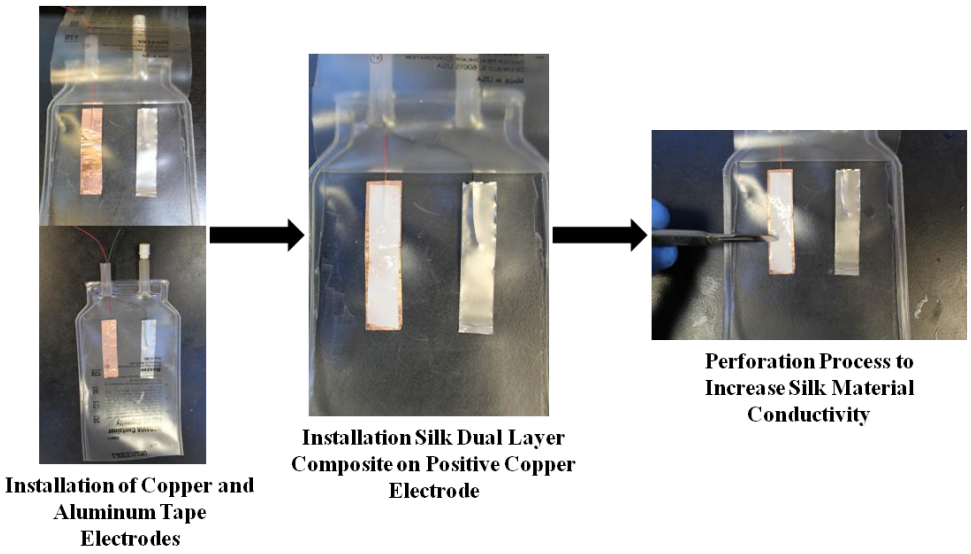

Figure 46: Modification of original electrode design within the portable e-gelling container in order to incorporate the silk composite material. This material was installed on the positive double-sided copper tape electrode and perforated to transfer the tape's conductivity to the silk material surface.

12.2.3 Circuit Design

In order to create an automatic silk electrogelating device for surgical application, a delayed circuit was designed to control the previously described e-gelling portable container.

The preliminary prototype of this circuit was designed and fabricated on a simple breadboard. The electrical components included resistors of varying resistive values, a multicom-BC-107 bipolar transistor, 10 μF capacitors, 5 mm green/yellow LED, red LED, 3 position slide switch, and RCA socket and plug connectors, and copper wire connections between circuit components, which were all obtained from Newark Corp. (Richfield, OH). The design of the circuit is further explained in the next section.

Chapter 13: Results and Discussion

13.1 Burst Testing of Adhesive Strength

13.1.1 Burst Test Set Up

During sample testing, the burst test set up, including the sample testing apparatus, was able to hold all pressures. There were no leaks and pressure was able to build in a constant manner for all tests until the sample burst. Therefore, the sample was secured in a sealed area such that the water flow rate was unable to escape anywhere besides through the 3 mm defect in the collagen casing.

Burst testing was conducted over two days. Standard curves, therefore, were made each day in order to account for all of the current settings, including power supply to the transducer, which ranged from 9.95-10.05 V. Standard curves were made by installing a stopper at the end of the tubing and building pressure to 10, 14, 20, 24, and 30 psi and stalling the pressure at each of these points. This was done three times and the highest voltage at each stop point was calculated and

averaged. From these calculations the relationship was determined between voltage readings and pressure experience within the test.

13.1.2 Burst Test Pressures

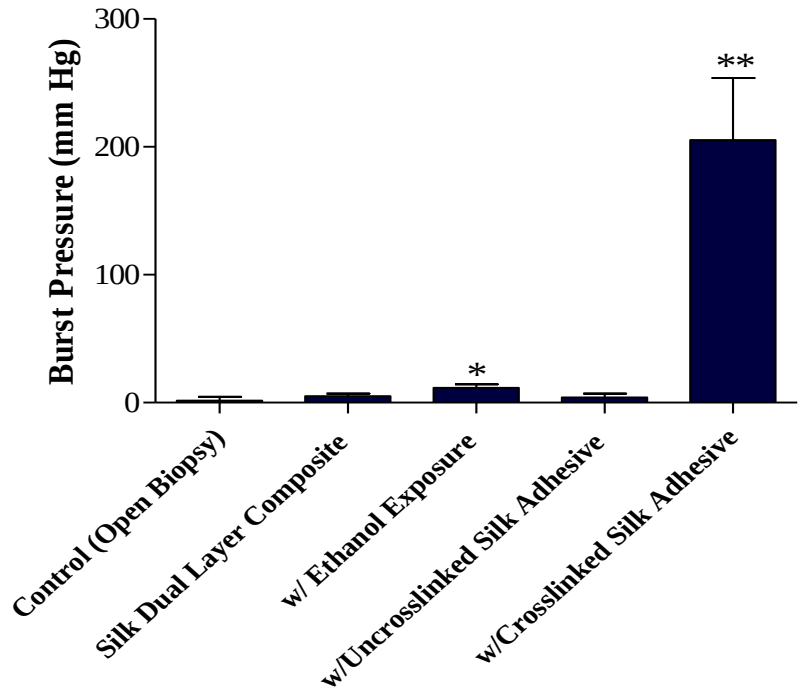

Figure 47: Burst test results of all tested silk material samples as compared to the open biopsy control (n=3). The composite material reached a significantly high pressure than the control and uncrosslinked e-gel silk adhesive (*$p<0.05$). The composite with ethanol-exposed e-gel (crosslinked silk adhesive) had a significantly higher burst pressure than all other samples (**$p<0.01$).

Figure 47 shows the average burst pressure for each sample condition (n=3). The composite with no treatment and with uncrosslinked electrogelated silk (e-gel) had no significant difference from the open biopsy. Therefore, the composite itself or the composite with a layer of untreated e-gel was unable to seal the defect. The ethanol-exposed composite material was able to hold a significantly greater amount of pressure, but this was only an average of 11.7 mm

Hg. This significant but slight increase in burst pressure was most likely due to the drying effect of ethanol, which would increase the time that water would take to saturate the material and leak through the 3 mm defect. The composite with e-gel and ethanol exposure had a significantly higher burst pressure than all other samples. Its average burst pressure was 205.3 mm Hg.

In the original design of the sutureless, and, therefore, adhesive, all-silk dural substitute, the e-gel layer was to be used as the sealing silk adhesive. As demonstrated by the burst testing, however, this layer was not able to hold pressures in the wet environment. When the e-gel, however, was exposed to ethanol before testing, it was able to hold over 200 mm Hg before water leaked through the defect. The untreated e-gel, therefore, was unable to seal against the water while the ethanol-treated gel was able to. Because the only difference between the two sample groups was the ethanol treatment, it is clear that the ethanol had a physical effect on the e-gel adhesive strength resulting in significantly increased sealing ability.

While electrogelated silk has the ability to adhere to steel, wood, and acrylic [Leisk et al., 2010], it has not been thoroughly tested for wet adhesion. It has, however, been shown that dehydrating e-gel samples significantly increases their adhesion strength and mechanical properties [Leisk et al., 2010]. Based on this trend, it would not be expected for e-gels to have increased adhesive strength in wet environments where they are hydrated further.

As previously described, the protein assembly of electrogelated silk involves a decrease in random coil content, increase in helical content, and no change in beta-sheet content compared to aqueous silk [Leisk et al., 2010]. Beta-sheets, however, are the silk fibroin conformation that results in resistance to water solubility [Wilson et al., 2000]. Without increased beta-sheet content, the originally adhesive e-gel layer on the silk composite material dissolves around its edges where it is first exposed to the water flow. At these areas, the water is able to dissolve away some of the gel and/or hydrate it to saturation. These processes would result in the ability for water to pass under or through the gel, respectively, and through the 3 mm defect in the collagen casing, which was observed in the inability of the e-gel to seal against the slow 5 ml/min water flow [Figure 47].

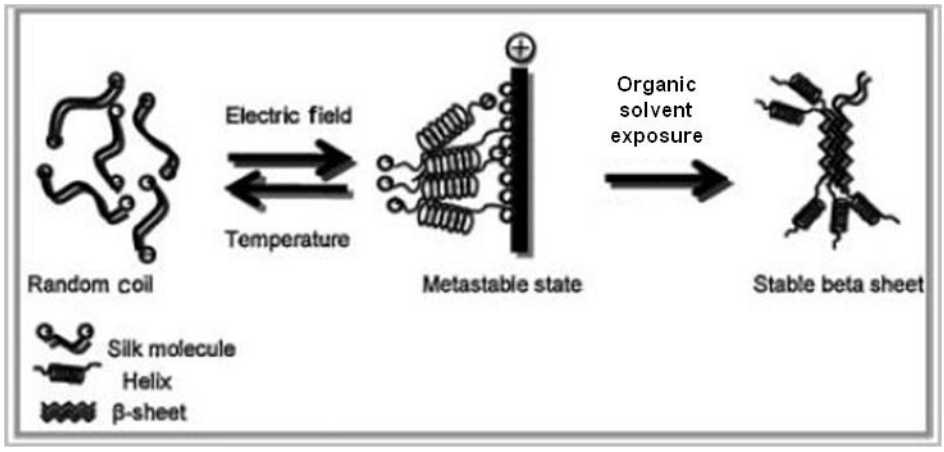

Figure 48: Silk fibroin conformational changes from random coil to the helical state during the electrogelation process [Leisk et al., 2010]. Additional organic solvent exposure is proposed to result in further protein conformational changes to water-stable beta-sheet structures.

The treatment of silk fibroin with low dielectric constant organic solvents, including ethanol is the most common method for converting the protein to beta-sheet organization [Noguerira et al, 2010; Ishida et al., 1990; Venyaminov et al., 1990]. When the silk materials on the 3 mm defect were exposed to ethanol, all areas of the e-gel in contact with the organic solvent were facilitated to beta-sheet. Therefore, a layer of beta-sheeted silk was then present at the exposed e-gel surfaces, which effectively were the edges of the e-gel and the composite material [Figure 48]. This crystallization or crosslinking treatment, therefore, effectively sealed the composite material over the defect by allowing the adhesive strength of the e-gel to be maintained on the surface of the collagen casing while the beta-sheeted silk areas sealed any water from solubilizing the e-gel and reaching the defect.

13.1.3 Comparison to Dural Sealant Clinical Standards

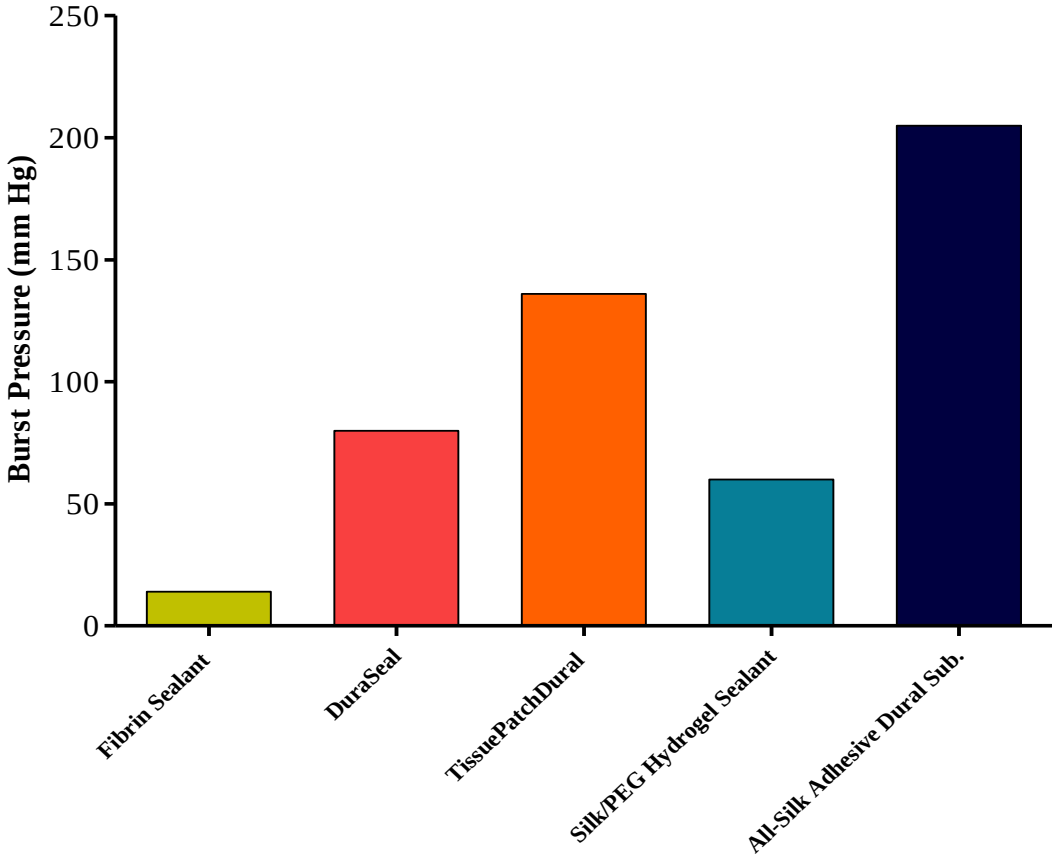

Figure 49: Burst pressure comparison of the all-silk adhesive material with clinically leading dural sealant systems. All burst pressures shown were obtained through burst pressure testing adapted from ASTM: F 2392-04 [Cambell et al., 2005; TissueMed Ltd., 2011].

The all-silk adhesive dural substitute was able to hold a higher burst pressure than its clinically used dural sealant competitors [Figure 49]. Figure 49 compares the all-silk adhesive composite material to its clinical tissue sealant competitors including: biologic sealants, synthetic sealants, and the newly designed film or membrane-type sealants. All of these sealants have been primarily designed to reinforce sutured closure of the dura. Fibrin sealant, which

is primarily used for haemostatic effect and biodegradation [Emilia et al., 2011], had a documented average burst pressure of 14 mm Hg [Cambell et al., 2005]. The most commonly used synthetic sealant, DuraSeal, had an average burst pressure of 80 mm Hg and that of TissuePatchDural (TPD) had a burst pressure of 136 mmHg [Cambell et al., 2005, Tissuemed Ltd, 2011]. With an average burst pressure of 205 mm Hg, the adhesive silk composite had a 1364%, 156%, and 51% increase in burst pressure compared to fibrin sealant, DuraSeal and TPD respectively.

Because the purpose of these sealant technologies is to prevent CSF leak following intracranial and spinal neurosurgeries, they must be able to seal against the CSF pressures seen within the body. The normal value of intracranial pressures is approximately 5 mm Hg. But this value can increase to 50 mm Hg with illness, coughing and sneezing [Yamada et al., 1997; Marchbanks et al., 1990]. The pressures seen lower in the spine are slightly larger due to the spinal column, which effectively acts as a hydrostatic CSF column [Marchbanks et al., 1990]. Fibrin sealant cannot sustain the 50 mm Hg maximum pressure seen within the body and, therefore, is generally used to support sutures but not as its own sealing mechanism [Thavarajah et al., 2009]. Additionally, the previously researched silk-PEG sealant was only able to maintain 60 mm Hg of burst pressure. While DuraSeal has a documented burst pressure of 80 mm Hg, it has shown high hydrodynamic complication rates in our clinical review and in others.

Based on the above comparative study, adhesive solid materials rather than liquid or gel sealants are able to maintain higher burst pressures, and,

therefore would be more successful as dural closure and sealant systems following neurosurgery. TissuePatchDural, which is a multilayered device with alternating layers of poly(lactide-*co*-glycolide) and a proprietary adhesive, is a resorbable adhesive membrane marketed for temporary wound support [Puppa et al., 2010]. The adhesive layer functions by nucleophilic substitution reactions between *N*-hydroxysuccinimide and amine/thiol groups [Ferroli et al, 2012]. It was designed to covalently adhere to the dural surface and, therefore, create an impermeable sealed membrane across the dural defect.

While TPD has improved burst pressures compared to liquid and gel sealants, this material requires the initial closure of the defect with autologous or synthetic dural substitutes and/or sutures before it can be applied. This is necessary in order to avoid adhesion of the material to the cerebral tissue [Ferroli et al., 2012]. The covalent bonding system is not specific to dural tissue and, instead, could result in bonding to any tissue once activated by water or CSF. This material, therefore, must be used in addition to numerous other dural tissue closure techniques, which inherently carry their own risks, and the material increases the general risk of cortical and cerebral tissue adhesions. Additionally, a documented risk of TPD is an allergic reaction to the device and local, mild inflammatory response *in vivo* leading to encapsulation and fibrosis [Ferroli et al., 2012].

The all-silk sutureless dural substitute has a similar design to TPD, but with clear advantages. The e-gel layer of the silk substitute acts as an adhesive layer while the dual layer composite material is an impermeable barrier to CSF

leak. Although this general design is similar to TPD, the dual layer composite material has also been designed to function as a complete dural substitute and has the surface topography and 3D structure to facilitate dural regeneration while also limiting cortical adhesions. TPD, on the other hand, requires additional dural substitutes because it cannot come in contact with cerebral or spinal tissue. Additionally, all layers of the adhesive silk dural substitute consist of only silk fibroin protein, which is biocompatible and, therefore, would not be expected to induce an immune response [Kaplan et al., 2006]. The adhesive dual layer silk composite material, therefore, is able to hold greater burst pressure compared to TPD while also working as a fully functional dural substitute requiring no additional materials and with no risk of immunogenic response.

13.2 Design and Production of Automatic E-gelling Device

13.2.1 Portable Electrogelation (E-gelling) Container

In order to test the e-gelling ability of the modified-IV-bag e-gel container, 10-minute boil silk (6-8% w/v) was injected into the sealed container using syringe through the septum port [Figure 45]. The wires were then connected to a 25 V power supply.

Within 30 second of power supply to the electrodes, bubbles were visible on both the positive and negative aluminum tape electrodes. The bubbles, however, congregated first on the upper area of the electrodes, closest to the copper wire connection locations. Within 15 minutes, opaque e-gel was visibly forming on the top area of the aluminum tape positive electrode []. The e-gel

formed in a similar manner to its formation on platinum wires within silk solution as previously documented [Leisk et al., 2010]. The thick layer of e-gel continued to gradually form down the positive aluminum electrode. Within 1 hour, it extended towards the bottom of the electrode and after approximately 4 hours, a thick layer of e-gel covered the entire positive electrode [Figure 50]. Also at this time, there was notable brown coloration around the gel of the electrode, which most likely resulted from corrosion of the copper wire.

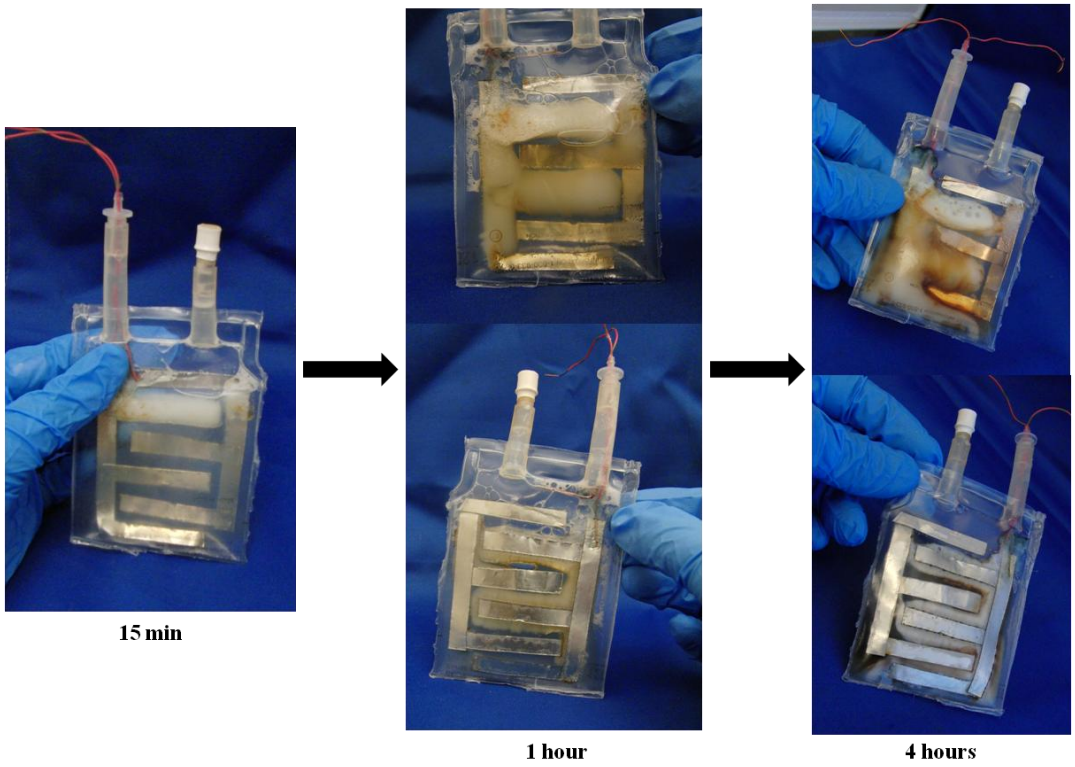

Figure 50: E-gelling process within portable e-gelling container. Gel begins to form on areas closest to copper wire connection but gradually builds over entire positive electrode.

Once the residual silk solution was drained, the resulting e-gel was removable from the positive electrode and had the same adhesive quality and mechanical robustness of traditionally produced e-gels. This portable

electrogelation container, therefore, shows the success and potential of this preliminary device design to be used for the portable formation and application of e-gels. This device could be further developed in a sterile manner such that e-gels could be produced in clinical settings to be used as tissue sealant and/or tissue regeneration scaffolds.

13.2.2 Incorporation of Silk Dural Replacement Material

The above portable electrogelation container was modified in order to incorporate the silk dual layer composite material and to create an e-gel directly on the material. This was done by installing the composite material on a copper tape positive electrode and perforating it in order to expose the conductive surface [Figure 46].

When 25 V was supplied to this set-up, bubbles visibly formed on both the negative electrode and surface of the dual layer composite material. This demonstrated the occurrence of electrolysis within the silk and the successful use of the composite material as a positive electrode. After 3 minutes, e-gel was visibly forming on the silk film surface of the composite material. And after a total gelation time of 5 minutes, the residual aqueous silk solution was drained from the bag. An e-gel layer was visible on the composite material, which was easily removed from its copper tape backing due to the hydrated silk environment. The resulting material was, therefore, the dual layer composite silk material with a thin layer of e-gel on the silk film side of the material.

An adhesive, all-silk dual layer composite material can be successfully produced in the designed portable electrogelation device. The successful prototype of this device supports the use of e-gels as tissue adhesives because they can be produced in a portable manner and, therefore, could be made in clinical and, more specifically, surgical settings. Additionally, the resulting e-gelled composite material would be able to maintain adhesive strength and burst pressures as high as 205 mm Hg while also being a biocompatible implant to the patient.

13.2.3 Circuit Design and Complete Device Preliminary Design

In order to create an automatic silk electrogelating device for surgical application, a delayed circuit was designed to control the previously described electrogelating portable container.

The audio jack component connects to the positive and negative electrodes within the IV-bag-modified electrogelation container. This audio jack connects into the audio plug of the circuit, and this plug connects the container to a delayed circuit. The delayed circuit consists of a network of capacitors, resistors, and a single transistor. The design was modified from the circuit below, which programs a delayed LED [Figure 51]. This delayed circuit allows for power supply to the positive and negative electrodes within the electrogelation container for only a short time. At the end of this time period, the power supply is terminated to the electrodes and instead passes to a green LED. Therefore, the surgeon would be able to turn on the device, allow the e-gel to form, and then would be notified that the gel was done by the green LED.

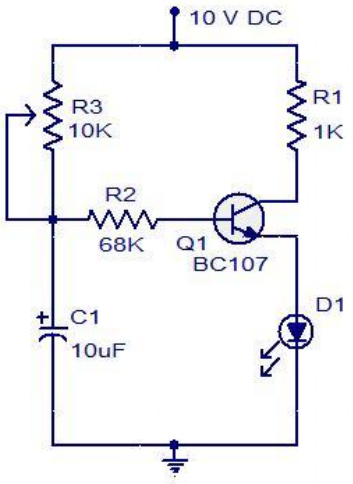

Figure 51: Delayed LED circuit. The circuit design in this work was modified from this delayed LED circuit's sequence of resistors, 10 uF capacitors, and the BC107 transistor [Image: http://www.circuitstoday.com/delayed-on-led].

Our preliminarily designed circuit allows for a delay of approximately 10 seconds before this green LED turns on. Because this time period is not long enough to produce a significant e-gel, the circuit must be further designed and optimized to allow for longer time intervals. Additionally, a future design to this circuit would allow for programmable time delays depending on the type or amount of e-gel being formed.

At this point, our preliminary circuit and device design shows the potential for portable and automated silk electrogelation, both on its own and onto a silk composite material. Such an optimized device would make the adhesive silk composite dural system, which has showed burst pressures and, therefore, sealing ability exceeding those of the current leading dural sealant systems, usable by neurosurgeons for sutureless dural closure. The ultimate goal of this device and circuit design is to allow for a surgeon to turn on the device for a predetermined

length of time during which power would be supplied to the container's positive and negative electrodes. During this time, therefore, e-gel would be produced within the container. Once this gel was produced, the automatic system would turn off this power and the surgeon could remove the container from its electronic "dock," drain the residual silk solution, and use the produced e-gel and/or adhesive silk composite dural replacement. A schematic of this proposed system is shown in Figure 52.

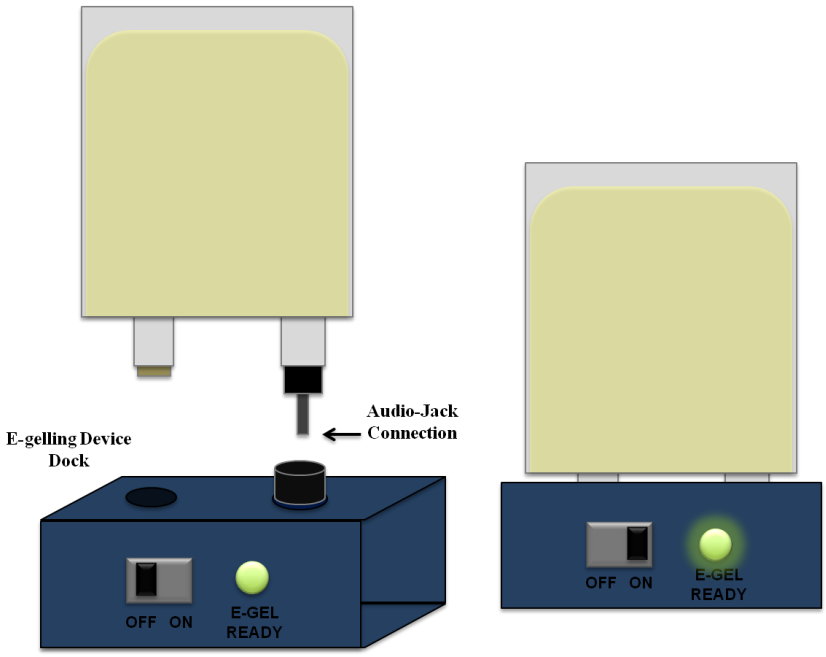

Figure 52: Schematic of proposed automatic e-gelling device including the electronic e-gelling "dock." After connecting the audio jack of the e-gelling container to the electronic dock and turning the device on, the dock's internal circuit will have a specific time delay such that an e-gel of predetermined size is formed. When gelling is done, the green LED turns on signaling to the surgeon that the silk adhesive is ready for use.

Chapter 14: Research Conclusions

14.1 Silk Fibroin Dual Layer Composite Material as a Dural Replacement

A novel silk fibroin dual layer composite material was created, which consists of a silk film layer and silk electrospun mat layer. This composite of materials had not previously been done and a successful protocol was developed involving no added chemicals or crosslinkers to join the two materials. The procedure employs an untreated and, therefore, soluble silk film surface onto which an silk electrospun mat is able to form and result in a single composite material with layers of two completely different morphologies.

This material was specifically designed for application as a dural replacement material. The morphologies of the two layers contribute two different and required functionalities for this type of material. The nonporous silk film layer acts as an impermeable barrier to CSF leakage and also limits unwanted adhesion of cortical or spinal tissue. The nanofiber network of the electrospun mesh layer mimics the ECM, acts as a three-dimensional scaffold and, therefore, promotes dural fibroblast migration and ingrowth. Such interaction with dural cells facilitates dural regeneration across the material and wound site.

The mechanical characteristics of this composite material were examined and determined to be defined by the silk film layer. Therefore, the elastic modulus, tensile strength, and ultimate strain of the material can be further designed to match those of the natural dura specifically by manipulation of the silk film layer. In terms of biocompatibility, both layers of the composite material

proved to be nontoxic to fibroblast and neural cells. Therefore, when implanted into the dura mater, this material would be expected to be completely biocompatible with all surrounding tissues, including dural fibroblasts and neural tissue. The biodegradability of the material was also shown to be tunable by crystallization treatments. One such crystallization treatment, methanol treatment, resulted in unchanged mass of the material over a 14-day degradation study. Such results demonstrate the potential of the controlled degradability of the material to match the rate of neo-dura formation and, therefore, facilitate successful and complete dural regeneration across the scaffold.

14.2 Adhesive Sutureless Silk Fibroin Dural Replacement

The previously described silk fibroin dural replacement material was successfully made adhesive by the addition of an electrogelated silk layer. This system showed to be able to seal against a water burst pressure of 205 mm Hg, which is significantly higher than the maximum expected intracranial pressures [Yamada et al., 1997] and higher than burst pressures of the clinically leading dural sealant systems [Cambell et al., 2005]. An applicator system was also developed to create the electrogelated layer on the composite material in a portable manner such that it could be used in a clinical and, specifically, neurosurgical setting.

Such an optimized device would make the adhesive silk dural repair system usable by neurosurgeons for sutureless dural closure. This novel dural

closure system is completely silk fibroin and, therefore, entirely biocompatible and biodegradable.

Based on the design and results of this research, the novel silk dual layer composite material in combination with electrogelated silk shows potential as a sutureless dural repair system that would improve on the limitations and induced postoperative complications of current dural closure materials and techniques.

Chapter 15: Future Directions

15.1 *In Vivo* Testing

Although the dual layer silk composite material has been designed for a tissue engineering application and shows the biocompatibility and degradability to be successful in this application, *in vivo* studies must be conducted in order to see host tissue interaction and success as a dural substitute.

In order to first determine how the silk composite material reacts with host tissue, samples could be implanted in a subcutaneous or intramuscular study in rat models. This has previously been done with silk materials including silk films [Meinel et al., 2005] and electrospun mats [Kim et al., 2012]. The materials could be treated with different crystallization treatments, including water-annealing and methanol treatment, in order to determine if these have effect on biocompatibility and biodegradation *in vivo*. Postoperative time points of 2, 4, and 8 weeks could be used to assess the materials histologically and observe any biodegradation. An antigenic effect of the silk composite material would not be expected *in vivo* due

to the silk purification process that results in silk fibroin with no sericins and, therefore, no antigenic effects [Sofia et al., 2001].

For testing of the material as an adhesive sutureless dural replacement, rat models could also be used. Kim et al. [2005] used rat models to test silk fibroin films as dura mater substitutes. This was done by performing craniotomies and incising the dura mater with controlled dimensions. The silk film was then placed over the exposed cortical tissue with the edges of the dura mater placed below the margins of the silk film. This surgical set up and animal model could be used to test for effective CSF sealing ability and dural tissue regeneration facilitated by the silk composite material described in this work. Specifically, analysis of CSF leakage or infection could be completed through animal observation and histology. Histology at postoperative time points would also be used to determine how the host tissue is able to interact with the material, specifically looking for dural regeneration and integration of the material.

Once shown successful in the smaller animal models, an additional animal model for this application could be used: the larger canine model. This model has more adequate brain volume, measurable intracranial pressures and approachable post-surgical care to be used as a model for human dura closure with the adhesive silk composite material.

15.2 Drug Delivery

As a tissue replacement, the dual layer silk composite is specifically designed for implantation *in vivo*. Due to this application, it also has the potential

to act as a localized drug delivery system. Additionally, it is an all-silk material, including silk film, electrospun mat, and adhesive e-gel components. Silk fibroin has been thoroughly studied as a drug delivery vehicle due to its biocompatibility, slow biodegradability, excellent mechanical properties, and novel manufacturing techniques, including mild all-aqueous processes. In fact, silk fibroin matrices have been demonstrated to successfully deliver and preserve the potency of protein drugs including sensitive protein and nucleic acid therapeutics [Wenk et al., 2011]. These matrices have been produced in the forms of silk fibroin including films, hydrogels and electrospun scaffolds. Previously, electrospun mats loaded with BMP-2 have promoted bone formation [Li et al., 2006], biofunctionalized electrospun fibers containing epidermal growth factor (EGF) accelerated wound healing when applied topically [Schneider et al, 2008], silk films loaded with nerve growth factor (NGF) promoted *in vitro* nerve regeneration [Uebersax et al., 2007], and numerous silk fibroin drug delivery devices have been fabricated for *in vitro* and *in vivo* bone, cartilage, and vascular regeneration [Wang et al., 2008].

All silk fibroin forms within the silk composite material and tissue adhesive described in this work result from processing of aqueous silk fibroin solutions. These solutions can be directly loaded with drugs either by dissolution or colloidal dispersion and then cast into films, gelled or electrospun [Li et al., 2006]. Therefore, each layer of the dual layer silk composite in addition to the silk adhesive gel have the potential to act as drug delivery systems to the wound site. Growth factor loading could be used to promote dural regeneration and, therefore,

quicker natural repair of the durotomy. Additionally, antibiotics could be released to fight any risk of infection or chemotherapy active molecules could be release to sites of removed meningiomas or cranial tumors. The different layers of the composite material allows for numerous vehicles of different growth factor and therapeutic protein release with varying rates of release within the single implantable material.

15.2.1 Chemotherapy

As previously described, the silk fibroin dural replacement would be implanted in direct contact with surrounding native dura and in close proximity to cortical tissue or the spinal cord. Due to the location of the implanted silk dural replacement material, it could be used to deliver chemotherapy drugs to resected tumor sites, including meningiomas and cranial tumors.

For the treatment of cranial tumors, including malignant glioma and glioblastoma multiforme, a common treatment adjunt to surgery and radiation includes the implantation of Gliadel® wafers. These wafers consist of polifeprosan 20 with carmustine (BCNU), which is a commonly used chemotherapy drug for the treatment of several types of brain cancer. When placed in the tumor resection cavity, the controlled release of BCNU decreases the chance of tumor reoccurrence, which most commonly occurs within 2 cm of the original lesion [Hochburg and Pruitt, 1980]. The slow local release of BCNU has shown to efficiently limit reoccurrence of glioma multiforme (GBM) and increase survival time in patients undergoing surgery for recurrent GBM [Brem et al., 1995]. During the resection of a cranial tumor, the dural replacement material

is in direct contact with the tumor resection site. Therefore, loading the silk dural replacement with BCNU would allow for controlled release of BCNU through the flexible material and would limit the need for additional wafer implants.

Meningiomas require different treatment compared to cranial tumors. Most commonly, meningiomas are treated by full resection of the involved dura tissue and bone, which generally requires dural closure techniques including the use of dural replacement materials. Full resection, however, is possible in only 30-40% of cases depending on the degree of resection [Mason et al., 2002]. And even after full resection, the recurrence rate of benign meningiomas after 10 years is at least 9% and after subtotal resection without adjuvant radiotherapy it is approximately 40% [Marks et al., 1986; Miramanoff et al., 2010]. Treatment options for patients with recurrent meningiomas include hormone therapy, immunotherapy, or chemotherapy [Mason et al., 2002]. One such chemotherapy drug that has shown potential for meningioma treatment is hydroxyurea. In a study to evaluate the efficacy of hydroxyurea to treat patients with recurrent or unresectable and enlarging meningiomas, it was able to arrest the progression of the meningiomas when administered over a prolonged time period [Mason et al., 2002].

The implanted silk dural replacement material would be in direct contact with the native dural tissue, which would be surrounding the area of the resected meningioma. By loading the material with chemotherapy drugs such as hydroxyurea, it would expose the native tissue to controlled levels of the drug

over a prolonged period of time in order to arrest any new or continuing meningioma growth.

15.2.2 Antibiotics

Antibiotics can be encapsulated into the electrospun nanofiber network, film layer, and/or silk adhesive component of the silk dural repair system. The embedding of antibiotics in the silk material would limit infection, reduce inflammation, improve wound healing, and prevent post-surgery adhesion [Bolgen et al., 2007].

Antibiotic-loaded implant materials have been previously evaluated for neurosurgery applications. In fact, a cranioplasty synthetic implant loaded with gentamicin was produced and tested to assess its neurotoxicity as well as the efficacy of the material to lessen the infectious morbity of cranioplasty procedures. The results showed no evidence of neurotoxicity and, therefore potential clinical efficacy of the gentamicin-loaded material [Ronderos et al., 1992]. In another study, antibiotic-impregnated DuraGen was tested *in vitro* for its efficacy in preventing infection. In this study, DuraGen was loaded with vancomycin, which resulted in the inhibition of microorganism growth on the dural replacement material [Kaplan et al., 2011]. By making the DuraGen a vancomycin-delivery system, therefore, the dural replacement material showed the potential to limit infection when implanted *in vivo*.

Loading the silk dural repair system described in this work with such antibiotics as gentamicin and vancomycin would allow the material to not only

create a successful dural repair, but also limit the risk of infection at the wound site and promote wound healing.

15.3 Additional Tissue Applications

While the dual layer silk composite material was specifically designed as a dural replacement in this work, its biocompatibility, tunable mechanical strength, characteristics, and physical dimensions, and nature as a 3D scaffold for tissue engineering, support its use in other tissue replacement and regeneration applications. Specifically, the composite material shows potential for further soft tissue applications, including abdominal wall reconstruction, plastic surgery support procedures, oral procedures, and replacement of damaged or inadequate integumental tissue.

Another potential application of the all-silk adhesive composite material would be for enhanced dermal wound healing. The silk materials, especially the electrospun morphology, exhibit absorption, water vapor transmission, oxygen permeation and enzymatic biodegradation that makes it suitable for application in full-thickness wound sites [Wharram et al., 2010]. Additionally, the ability to biofunctionalize the silk material would increase its success as a wound dressing by accelerating wound healing [Schneider et al., 2009]. During our study, we created a proof-of-concept wound dressing from our silk composite material and e-gel adhesive [Figure 53].

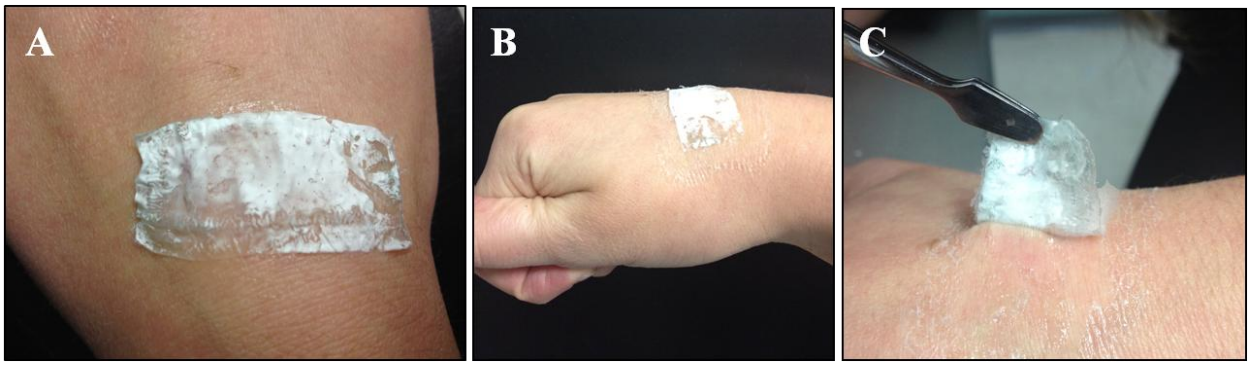

Figure 53: Proof-of-concept design of silk dual layer composite material with e-gel adhesive layer for dermal application. The all silk material showed ability to adhere and conform to the skin (A, B) and required mechanical force to be removed from the skin (C).

This material adhered very well to the skin and conformed well to the tissue surface. While the electrospun mat layer maintained contact with the dermal tissue and could be designed to release beneficial drugs and growth factors, the silk film layer provided a nonporous layer to protect the wound site from the outside environment while still allowing for oxygen and water vapor permeability. The adhesive dual layer silk composite material, therefore, showed preliminary success and great potential as a dermal wound dressing to enhance wound healing. And, this material could be further designed and mechanically tuned to meet requirements of other soft tissue applications.

References

ASTM: F 2392—04. "Standard Test Method for Burst Strength of Surgical Sealants."

Ahmed TAE, Giulivi A, Griffith M, and Hincke M. 2011. Fibrin glues in combination with mesenchymal stem cells to develop a tissue-engineered cartilage substitute. Tissue Engineering, Part A 2011; 17(3,4): 323-335.

Alberts B, Johnson A, Lewis J et al. 2002. Fibroblasts and their transformations: the connective-tissue cell family. Molecular Biology of the Cell, 4th edition.

Alleyene CH, Cawley CM, Barrow DL, et al. Efficacy and biocompatibility of a photopolymerized, synthetic, absorbable hydrogel as a dural sealant in a canine craniotomy model. J Neurosurg 1998;88: 308-313.

Bolgen N, Vargel I, Korkusuz P, Menceloglu YZ, and Piskin E. *In Vivo* performance of antibiotic embedded electrospun PCL membranes for prevention of abdominal adhesions. J Biomed Mater Res Part B 2007; 81B: 530-543.

Boogaarts JD, Grotenhuis JA, Bartels RH, Beems T. Use of a novel absorbable hydrogel for augmentation of dural repair: results of a preliminary clinical study. Neurosurgery 2005; 62(3): 146-151.

Brem H, Piantadosi S, Burger PC, Walker M, Selker R, Vick NA, Black K, Sisti M, Brem S, Mohr G, Morawetz R, and Schold SC. Placebo-controlled trial of safety and efficacy of intraoperative controlled delivery by biodegradable polymers of chemotherapy for recurrent gliomas. Lancet 1995; 345: 1008–1012.

Campbell PK, Bennet SL, Driscoll A, Sawhney A. 2005. Evaluation of absorbable surgical sealants: In vitro testing. Confluent Surgical Inc. 1-4.

Carmouche JJ, Molinari RW. Epidural abscess and discitis complicating instrumented posterior lumbar interbody fusion: a case report. Spine. 2004;29(23):E542–E546.

Caroli E, Rocchi G, Salvati M, Delfini R. Duraplasty: Our Current Experience. Surgical Neurology 2004; 61(1):55–59.

Chaplin JM, Costantino PD, Wolpoe ME, Bederson JB, Griffey E, Zanh WX. Use of Acellular dermal allograft for dural replacement: an experimental study. Neurosurgery 1999; 45(2):320–327.

Collins RL, Chirstiansen D, Zazanis GA, Silver FH. Use of collagen film as a dural substitute: Preliminary animal studies. J Biomed Mater Res 1991; 25: 267-276.

Cosgrove GR, Delashaw JB, Grotenhuis JA, Tew JM, Van Loveren H, Spetzler RF, Payner T, Rosseau G, Shaffrey ME, Hopkins N, Byenw R, Norbash A. Safety and

efficacy of a novel polyethylene glycol hydrogel sealant for watertight dural repair. Journal of Neurosurgery 2007; 106:52-58.

Couture D, Branch CL Jr. Spinal pseudomeningoceles and cerebrospinal fluid fistulas. Neurosurg Focus. 2003;15(6):E6.

deFreitas DJ, McCabe JP. Acinetobacter baumanii meningitis: a rare complication; of incidental durotomy. J Spinal Disord Tech. 2004;17(2):115-116.

Della Puppa, A, Rossetto, M, Scienza, R. Use of a new absorbable sealing film for preventing postoperative cerebrospinal fluid leaks: remarks on a new approach. J Neurosurg Sci 2010; (18): 609-611.

Dolenc VV: Comment in Yoshimoto T, Sawamura Y, Houkin K, Abe H: Effectiveness of fibrin glue for preventing postoperative extradural fluid leakage. Neurol Med Chir 1997; 37: 889.

Duarte AP, Coelho JF, Bordado JC, Cidade MT, Gil MH. 2011. Surgical adhesives: Systematic review of the main types and development forecast. Progress in Polymer Science 2011; online.

Eismont FJ, Wiesel SW, Rothman RH. Treatment of dural tears associated with spinal surgery. J Bone Joint Surg Am. 1981;63(7):1132-1136.

Emilia M, Luca S, Francesca B, Luca B, Paolo S, Giuseppe F, Gianbattista B, Carmela M, Luigi M and Mauro L. Topical hemostatic agents in surgical practice. Transfusion and Apheresis Science 2011; (45):305-311.

Epstein N. Dural repair with four spinal sealants: focused review of the manufacturers' inserts and the current literature. The Spine Journal 2010; (10):1065-1068.

Fattahi T, Mohan M, and Caldwell G. Clinical applications of fibrin sealants. Journal of Oral and Maxillifacial Surgeons 2004; (62):218-224.

Ferroli P, Acerbi F, Broggi M, Schiariti M, Albanese E, Tringali G, Franzini A, and Broggi G. A novel impermeable adhesive membrane to reinforce dural closure: A preliminary retrospective study on 119 consecutive high risk patients. World Neurosurg. 2012: 1-7.

Fu Y, Kao WJ. In situ forming poly(ethylene glycol)-based hydrogels via thiol-maleimide Michael-type addition. Journal of Biomedical Materials Research A 2011;(98A):201-2011.

Groteinuis JA. Costs of postoperative cerebrospinal fluid leakage: 1-year retrospective analysis of 412 consecutive nontrauma cases. Surg Neurol 2005;(64): 490-494.

Harnett EM, Alderman J, and Wood T. The surface energy of various biomaterials coated with adhesion molecules used in cell culture. Colloid Surf B 2007;(55):90-97.

Hino M, Ishiko O, Honda K-I, Yamane T, Ohta K, Tabuko T, Tatsumi N. Transmission of symptomatic parvovirus B19 infection by fibrin sealant used during surgery. Br J Haematol 2000;108: 194–5.

Hochberg F, and Pruitt A. Assumptions in the radiotherapy of glioblastoma. Neurology 1980; 30: 907–911.

Horan RL, A.K., Collette AL, Wang Y, Huang J, Moreau JE, Volloch V, Kaplan DL, Altman GH. In vitro degradation of silk fibroin. Biomaterials 2005; (25): 3385-3393.

Hu X, Kaplan DL, and Cebe P. Determining beta-sheet crystallinity in fibrous proteins by thermal analysis and infrared spectroscopy. Macromolecules 2006; 39: 6161-6170.

Hu X, Shmelev K, Sun L, Gui E-K, Park S-H, Cebe P, and Kaplan DL. Regulation of Silk Material Structure by Temperature-Controlled Water Vapor Annealing. Biomacromolecules 2011; (12): 1686-1696.

Hutmacher DW. Scaffolds in tissue engineering bone and cartilage. Biomaterials 2000; (21): 2529, 2000.

Ishida M, Asakura T, Yokoi M and Saito H. Solvent-and-Mechanical-Treatment-Induced Conformational Transition of Silk Fibroins Studied by High-Resolution Solid State ^{13}C NMR Spectroscopy. Macromolecules 1990; (23): 88-94.

Islam S, Ogane K, Ohkuma H, Suzuki S. Usefulness of acellular dermal graft as a dural substitute in experimental model. Surg Neurol 2004; (61): 297–302.

Jackson N, Muthuswamy J. Artificial dural sealant that allows multiple penetrations of implantable brain probes. Journal of Neuroscience Methods 2008; (171): 147-152.

Jankowitz BT, Atteberry DS, Gerszten PC, Karausky P, Cheng BC, Faugh R, Welch WC. Effect of fibrin glue on the prevention of persistent cerebral spinal fluid leakage after incidental durotomy during lumbar spinal surgery. Eur Spine J 2009; (18): 1169-1174.

Jin H-J, Chen J, Karageorgious V, Altman G, and Kaplan DL. Human bone marrow stromal cell responses on electrospun silk fibroin mats. Biomaterials 2003; (25): 1039-1047.

Jin HJ, Park J, Karageorgiou V, Kim UJ, Valluzzi R, Cebe P and Kaplan DL. Water-Stable Silk Films with Reduced β-Sheet Content. Adv. Funct. Mater. 2005;(15): 1241–1247.

Jin HJ. Fridrikh SV, Rutledge GC, and Kaplan DL. Electrospinning Bombyx mori Silk with Poly(ethylene oxide). Biomacromolecules 2002; (3): 1233-1239.

Jones E, Cook D, Murai KK. A neuron-astrocyte co-culture system to investigate astrocyte-secreted factors in mouse neuronal development. Methods Mol Biol 2012; (814): 341-352.

Kaplan M, Akgun B, Demirdag K, Akpolat N, Kozan SK, Cagasar O, and Yakar H. Use of antibiotic-impregnated DuraGen® to reduce the risk of infection in dura repair: An in vitro study. Cen Eur Neurosurg 2011; 72(2): 75-77.

Kaptain GJ, Vincent DA, Laws ER. Cranial base reconstruction after transsphenoidal surgery with bioabsorbable implants: Technical note. Neurosurgery 2001;48(1): 232-234.

Karageorgiou V, Meinel L, Hofmann S, Malhotra A, Volloch V, Kaplan D. Bone morphogenetic protein-2 decorated silk fibroin films induce osteogenic differentiation of human bone marrow stromal cells. J Biomed Mater Res A 2004;71(3):528–37.

Kaufman BA, Matthews AE, Kwienenberg-Lee M, and Lew SM. Spinal dural closure with nonpenetrating titanium clips in pediatric neurosurgery. J Neurosurg Pediatrics 2010;(6): 359-363.

Kim D, Eum W, Jang S, Park J, Heo DH, Sheen SH, Lee HR, Kweon H, Kang, SW, Lee KG, Cho S, Jin HJ, Cho YJ, and Choi S. A transparent aritifucal dura mater made of silk fibroin as an inhibitor of inflammation in craniotomized rats. J Neurosurg 2011; (114): 485-490.

Kim KH, Park HN, Shin SY, Park WH, Lee SC, Kim TI, Park YJ, Seol YJ, Lee YM, Ku Y, Rhyu IC, Han SB, Chung CP, Biological efficacy of silk fibroin nanofiber membranes for guided bone regeneration. J Biotechnol 2005; 120(3): 327-339.

Kim UJ, Park J, Li C, Jin HJ, Valluzzi R, Kaplan DL. Structure and properties of silk hydrogels. Biomacromolecules 2004; 5(3): 786–92.

Lawrence, BD, Omenetto, F, Chui, K and Kaplan, DL. 2008. Processing methods to control silk fibroin film biomaterial features. J Mater Sci 2008; (43): 6967-6985.

Li C, Vepari C, Jin H-J, Kim HJ, Kaplan DL. Electrospun silk-BMP-2 scaffolds for bone tissue engineering. Biomaterials 2006; (27): 3115-3124.

Li M, Ogiso M, Minoura N. Enzymatic degradation behavior of porous silk fibroin sheets. Biomaterials 2009; (24): 357-365.

Li W, Laurencin CT, Caterson EJ, Tuan RS, Ko FKElectrospun nanofibrous structure: a novel scaffold for tissue engineering. J Biomed Mater Res 2002; 60: 613-621.

Lin CC, Anseth KS. PEG hydrogels for the controlled release of biomolecules in regenerative medicine. Pharmaceutical Research 2009; (26): 631-643.

LiuY, Franco A, Huang L, Gersappe D, Clark RAF, Rafailovich MH. Control of cell migration in two and three dimensions using substrate morphology. Exp Cell Res 2009; (36): 333-368.

Lu CH, Ho ST, Kong SS, Cherng CH, Wong CS. Intracranial subdural hematoma after unintended durotomy during spine surgery. Can J Anaesth. 2002; 49(1): 100-102.

Lu Q, Hu X, Wang X, Kluge JA, Lu S, Cebe P, and Kaplan DL. Water-insoluble silk films with silk I structure. Acta Biomaterials 2010; (6); 1380-1387.

Macchiarini P, Wain J, Almy S, et al. Experimental and clinical evaluation of a synthetic, absorbable sealant to reduce airleaks in thoracic operations. J Thorac Cardiovasc Surg 1999;117: 751-758.

Marchbanks RJ, Reid A. Cochlear and cerebrospinal fluid pressure: their inter-relationship and control mechanisms. British Journal of Audiology 1990; 24(3): 179-187.

Marks SM, Whitewell HL, and Lye RH. Recurrence of meningiomas after operation. Surg Neurol 1986; 25: 436-440.

Mason WP, Gentili F, Macdonald DR, Hariharan S, Cruz CR, and Abrey LE. Stabilization of disease progression by hydroxyurea in patients with recurrent or unresectable meningioma. J Neurosurg 2002; 97: 341-346.

McCallum J, Maroon JC, Jannetta PJ. Treatment of postoperative cerebrospinal fluid fistulas by subarachnoid drainage. J Neurosurg. 1975;42(4):434-437.

Meinel, AJ, Kubow, KE, Klotzsch, E, Garcia-Fuentes, M, Smith, ML, Vogel V, Merkle, HP, and Meinel, L.Optimization strategies for electrospun silk fibroin tissue engineering scaffolds. Biomaterials 2009; 30: 3058-3067.

Meinel L, Hofmann S, Karageorgioue V, Kirker-Head C, McCool J, Gronowicz G, Zichner L, Langer R, Vunjak-Novakovic G, Kaplan DL. The inflammatory responses to silk films in vitro and in vivo. Biomaterials 2005; 26: 147-155.

Michael A. On the addition of sodium acetacetic ether and analogous sodium compounds to unsaturated organic ethers. Am Chem J 1887; 9:115.

Mikawa Y, Watanabe R, Hino Y, Ishii R, Hirano K. Cerebellar hemorrhage complicating cervical durotomy and revision C1-C2 fusion. Spine 1994; 19(10): 1169-1171.

Min B-M, Lee G, Kim SH, Nam YK, Lee TS, Park WH. Electrospinning of silk fibroin nanofibers and its effect on the adhesion and spreading of normal human keratinocytes and fibroblasts in vitro. Biomaterials 2004; 25: 1289-1297.

Minoura N, Aiba S, Higuchi M, Gotoh Y, Tsukada M, Imai Y. Attachment and growth of fibroblast cells on silk fibroin. Biochem Biophys Res Commun 1995; 208(2): 511–6.

Minoura, N, Tsukada M, Nagura M. Physico-chemical properties of silk fibroin membrane as a biomaterial. Biomaterials 1990;11(6): 430-434.

Mirimanoff R, Dosoretz DE, Linggood RM, Ojemann RG, and Martuza RL. Meningioma: analysis of recurrence and progression following neurosurgical resection. J Neurosurg 2010; 112(2): 18-24.

Moskowitz SI, Liu J, Krishnaney AA. Postoperative complications associated with dural substitutes in suboccipital craniotomies. Operative Neurosurgery 2009; 1: ons28-ons34.

Nag S. Morphology and properties of astrocytes. Methods Mol Biol 2011; 689: 69-100.

Nakayama Y, Matsuda T. Photocurable surgical tissue glues composed of photoreactive gelatin and poly(ethylene glycol) diacrylate. J Biomed Mater Res (Appl Biomater) 1999; 48: 511–521.

Narotam PK, Reddy K, Fewer D, Qiao F and Nathoo N. Collagen matrix duraplasty for cranial and spinal surgery: a clinical and imaging study. Journal of Neurosurgery 2007; 106(1): 45–51.

Narotam PK, Qiao F and Nathoo N. Collagen matrix duraplasty for posterior fossa surgery: evaluation of surgical technique in 52 adult patients. Journal of Neurosurgery 2009; 111(2): 380–386.

Nguyen KT, West JL. Photopolymerizable hydrogels for tissue engineering applications. Biomaterials 2002; 23: 4307–4314.

Nishido T, Yasamoto K, Otori T, Desaki J. The network structure of corneal fibroblasts in the rat as revealed by scanning electron microscopy. Invest Opthalmol Vis Sci 1988; 29: 1887-1890.

Nurata H, Cemil B, Kurt G, Ucankus NL, Dogulu F, and Omeroglu S. The role of fibroblast growth factor-2 in healing the dura mater after inducing cerebrospinal fluid leakage in rats. Journal of Clinical Neuroscience 2009; (16): 542-544.

Nuttelman CR, Rice MA, Rydholm AE, Salinas CN, Shah DN, and Anseth KS. Macromolecular monomers for the synthesis of hydrogel niches and their application in cell encapsulation and tissue engineering. Prog. Polym. Sci. 2008; 33:167– 179.

O'Connor D, Maskery N, Griffiths WE. Pseudomeningocele nerve root entrapment after lumbar discectomy. Spine 1998; 23(13): 1501-1502.

Omenetto FG, and Kaplan DL. A new route for silk. Nature 2008; (2): 641-643.

Parizek J, Mericka P, Spacek J, Nemecek S, Nemeckova J, Spacek J, Suba P, Sercl M. Posterior cranial fossa surgery in 454 children: Comparison of results obtained in pre-CT and CT era and after various types of management of dura mater. Childs Nerv Syst 1998; 14: 426-439.

Parlato C, di Nuzzo G, Luongo M, Stegano R, Accardo M, Cuccurullo L, and Moraci A. Use of a collagen biomatrix (TissueDura®) for dura repair: a long-term neuroradiological and neuropathological evaluation. Acta Neurochir 2011; (153): 142-147.

Parlato C, Granata R, Moraci A, and Accardo M. (2012). Dural Reconstruction in Meningioma Surgery, Meningiomas - Management and Surgery, Dr. Daniel Monleon (Ed.), ISBN: 978-953-51-0175-8, InTech.

Pham QP, Sharma U, and Mikos AG. Electrospinning of polymeric nanofibers for tissue engineering applications: A review. Tissue Engineering 2006; 12(5): 1197-1211.

Phelps EA, Enemchukwu NO, Fiore VF, Sy JC, Murthy N, Sulchek TA, Barker TH, Garcia A. Maleimide cross-linked bioactive PEG hydrogel exhibits improved reaction kinetics and cross-linking for cell encapsulation and in situ delivery. Adv. Mater. 2012; (24): 64-70.

Polikov VS, Hong J-S, Reichert WM. Soluble factor effects on glial cell reactivity at the surface of gel-coated microwires. Journal of Neuroscience Methods 2010; (190): 180-187.

Reece TB, Maxey TS, Kron IL. A prospectus on tissue adhesives. American Journal of Surgery 2011; (182): 40S-44S.

Reneker DH, and Chun I. Nanometre diameter fibres of polymer, produced by electrospinning. Nanotechnology 1996; (7): 216.

Rockwood DN, Preda RC, Yucel T, Wang X, Lovett ML, Kaplan DL. Materials fabrication from Bombyx mori silk fibroin. Nat Protoc. 201; 6(10): 1612-31.

Ronderos JF, Wiles DA, Ragan FA, Dempesy CW, Culicchia FC, Fontana CJ, and Richardson DE. Cranioplasty using gentamicin-loaded acrylic cement: A test of neurotoxicity. Surgical Neurology 1992; 37(5): 356-360.

Rosso F, Marino G, Giordano A, Barbarisi M, Parmeggiani D, and Barbarisi A. Smart materials as scaffolds for tissue engineering. J. Cell Physiol. 2005; 203**:** 465.

Scheider A, Wang XY, Kaplan DL, Garlick JA, Egles C. Biofunctionalized electrospun silk mats as a topical bioactive dressing for accelerated wound healing. Acta Biomaterailia 2008; 5: 2570-2578.

Serban M, Panilaitis B, and Kaplan D. Silk fibroin and polyethylene glycol-based biocompatible tissue adhesives. Journal of Biomedical Materials Research 2010; (00A).

Sierra DH, Feldman DS, Saltz R, Huang S. A method to determine shear adhesive strength of fibrin sealants. J Appl Biomater 1992; 3: 147–51.

Sofia S, McCarthy MB, Gronowicz G, Kaplan DL. Functionalized silk-based biomaterials for bone formation. J Biomed Mater Res 2001; 54(1): 139–48.

Spicer P. and A. Mikos. Fibrin glue as a drug delivery system. Journal of Controlled Release 2010; (148): 49-55.

Stendel R, Danne M, Fiss I, Klein I, Schilling A, Hammersen S, Pietilae T, Janisch W and Hopfenmuller W. Efficacy and safety of a collagen matrix for cranial and spinal dural reconstruction using different fixation techniques. Journal of Neurosurgery 2008; 109(2): 215–221.

Terasaka S, Iwasaki Y, Shinya N, Uchida T. Fibrin glue and polyglycolic acid nonwoven fabric as a biocompatible dural substitute. Neurosurgery 2005; (58): 134-139.

Thavarajah D, De Lacy P, Hussain R, and Redfern, R. Postoperative cervical cord compression induced by hydrogel (DuraSeal). Spine 2009; (35): E25-E26.

TissueMed, Inc. TissuePatchDural Brochure – Data on file at TissueMed.

Torchiana DF. Polyethylene Glycol Based Synthetic Sealants:. Journal of Cardiac Surgery 2003; 18: 504–506.

Uebersax L, Mattotti M, Papaloizos M, Merkle HP, Gander B, Meinel L. Silk fibroin matrices for the controlled release of nerve growth factor (NGF), Biomaterials 2007; 28(30): 4449–4460.

Vanaclocha V, Saiz-Sapena N: Duraplasty with freeze-dried cadaveric dura versus occipital pericranium for Chiari type I malformation: comparative study. Acta Neurochir (Wien) 1997; 139: 112–119.

Vandermiers C, Damman P, Dosier M. Static and quasielastic light scattering from solutions of poly(ethylene oxide in methanol). Polymer 1998; 39: 5627-5631.

Venyaminov SY, Kalnin NN Quantitative IR spectrophotometry of peptide compounds in water (H2O) solutions. II. Amide absorption bands of polypeptides and fibrous proteins in alpha-, beta-, and random coil conformations. Biopolymer 1990; 30: 1259-1271.

Vepari C and Kaplan DL. Silk as a biomaterial. Prog. Polym. Sci. 2007; (32): 991-1007.

Wallace DG, Cruise GM, Rhee WM, Schroeder JA, Prior JJ, Ju J, Maroney M, Duronio J, Ngo MH, Estridge T, Coker GC. A tissue sealant based on reactive multifunctional polyethylene glycol. J Biomed Mater Res (Appl Biomater) 2001; 58: 545–555.

Wang X, Kim HJ, Xu P, Matsumoto A, Kaplan DL. Biomaterial coatings by stepwise deposition of silk fibroin. Langmuir 2005; 21(24): 11335–41.

X. Wang X, E. Wenk E, X. Zhang X, L. Meinel L, G. Vunjak-Novakovic G, Kaplan DL, Growth factor gradients via microsphere delivery in biopolymer scaffolds for osteochondral tissue engineering. J. Control. Release 2008; 134 (2): 81–90.

X. Wang X, X. Zhang X, J. Castellot J, I. Herman I, M. Iafrati M, Kaplan DL. Controlled release from multilayer silk biomaterial coatings to modulate vascular cell responses. Biomaterials 2008; 29(7): 894–903.

Warren WL, Medary MB, Dureza CD, Bellotte JB, Flannagan PP, Oh MY and Fukushima T. Dural repair using acellular human dermis: experience with 200 cases: technique assessment. Neurosurgery 2000; 46(6): 1391–1396.

Wharram SE, Zhang X, Kaplan, DL, McCarthy SP. Electrospun silk material systems for wound healing. Macromol. Biosci. 2010; 10: 246-257.

Weber PC, Lambert PR, Cunningham CD, Richardson MS, Genao RB. Use of Alloderm in the neurotologic setting. American Journal of Otolaryngolgoy 2002; 23(3): 148-152.

Wenk E, Merkle HP, Meinel L. Silk fibroin as a vehicle for drug delivery applications. Journal of Controlled Release 2011; (150): 128-141.

Williams BJ, Sansur CA, Smith JS, Berven SH, Broadstone PA, Choma TJ, Goytan MJ, Noordeen HH, Knapp DR, Hart RA, Zeller RD, Donaldson WF, Polly DW, Perra JH, Boachie-Adjei O, Shaffrey CI. Incidence of unintended durotomy in spine surgery based on 108,478 cases. Neurosurgery 2011; 68(1): 117-124.

Wilson D, Valluzi R, Kaplan D. Conformational Transitions in Model Silk Peptides. Biophys J 2000; 78: 2690-2701.

White JK, Titus JS, Tanabe H, et al. The use of a novel tissue sealant as a hemostatic adjunct in cardiac surgery. The Heart Surg Forum 2000; 3: 56-61.

White MJ, DiCaprio MJ, Greenburg DA. Assessment of neuronal viability with Alamar blue in cortical and granule cell cultures. Journal of Neuroscience Methods 1996; (70): 195-200.

Wong C, Bini E, Hensman J, Knight DP, Lewis RV, Kaplan DL. Role of pH and charge on silk protein assembly in insects and spiders. Applied Physics A 2006; 82(2): 223-233.

Wray LS, Hu X, Gallego J, Georgakoudi I, Omenetto FG, Schmidt D, Kaplan DL. Effect of processing on silk-based biomaterials: Reproducibility and biocompatibility. J Biomed Mater Res Part B 2011; 99B: 89–101.

Xie J, MacEwan MR, Ray WZ, Liu W, Siewe DY, Xia Y. Radially aligned, electrospun nanofibers as dural substitutes for wound closure and tissue regeneration applications. ACS Nano 2010; 4(9): 5027-5036.

Xu CY, Inai R, Kotaki M, et al. Aligned biodegradable nanofibrous structure: a potential scaffold for blood vessel engineering. Biomaterials. 2004; 25: 877–86.

Yamada K, Miyamoto S, Nagata I, Kikuchi H, Ikada Y, Iwata H, and Yamamoto K. Development of a dural substitute from synthetic bioabsorbabe polymers. J Neurosurg 1997; (86): 1012-1017.

Yang Y, Zhu, X, Cui W, Li X, Jin Y. Electrospun composite mats of poly[(D,L-lactide)-co-glycolide] and collagen with high porosity as potential scaffolds for skin tissue engineering. Macromolecular Materials and Engineering 2009; 294: 611-619.

Zhou F, Chen G, Zhang JM, and Huang ZS. An in vitro culturing model for rabbit dural cells. Ann Clin Lab Sci 2006; 36(3): 341-344.

Zhou J, Cao C, Ma X, Hu L, Chen L, and Wang C. In vitro and in vivo degradation behavior of aqueous-derived electrospun silk fibroin scaffolds. Polymer Degradation and Stability 2010; 95: 1697-1685.